IJEST

ISSN: 0973-6255
Vol. 3 No. 1
January - June 2009

Indian Journal of Engineering, Science, and Technology

A Refereed Research Journal









BANNARI AMMAN
INSTITUTE OF TECHNOLOGY
Stay Ahead

BANNARI AMMAN INSTITUTE OF TECHNOLOGY
Sathyamangalam - 638 401 Erode District Tamil Nadu India

Indian Journal of Engineering, Science, and Technology

IJEST is a refereed research journal published half-yearly by Bannari Amman Institute of Technology. Responsibility for the contents rests upon the authors and not upon the IJEST. For copying or reprint permission, write to Copyright Department, IJEST, Bannari Amman Institute of Technology, Sathyamanagalam, Erode District - 638 401, Tamil Nadu, India.

From the Editor-in-Chief's Desk

IJEST welcomes Dr.Seshadri Ramkumar to its Editorial Board.

The Indian Journal of Engineering, Science, and Technology, a peer-reviewed journal welcomes Dr.Seshadri Ramkumar, Associate Professor, Texas Tech University to its Editorial Advisory Board.

Dr.Ramkumar's expertise in materials science and textiles will be very valuable towards expanding the scope of the journal. Dr.Ramkumar wishes the journal to be of international scope and would endeavor to enhance the quality and the outreach of the journal.

The journal looks forward to Dr.Ramkumar's contribution.

Dr.Ramkumar
seen with his latest
military fabric technology

(Dr.A.Shanmugam)
Editor -in-Chief

Indian Journal of Engineering, Science, and Technology

Volume 3 Number 1 **January - June 2009**

CONTENTS

HYDRAZINIUM METAL 1-HYDROXY 2-NAPHTHOATES - NEW PRECURSORS FOR METAL OXIDES

N. Arunadevi, S. Devipriya and S. Vairam
Department of Chemistry, Government College of Technology, Coimbatore - 641 013, Tamil Nadu
E-mail: vamshen @ yahoo.com,arunadevi_chem@yahoo.co.in
(Received on 26 October 2008 and accepted on 04 December 2008)

Abstract

Aromatic metal carboxylates are now-a-days used as precursors for the preparation of metal oxides. In this work, we have presented the formation of metal oxides of nano size by the thermal decomposition of the complexes of 1- hydroxy -2-naphthoates of divalent transition metals, Ni, Co, Cd, Zn and Cu with hydrazinium cation, prepared as crystalline compounds with the general formula, $(N_2H_5)_2[M\{C_{10}H_6(O)(COO)\}_2.(H_2O)_2$ and characterized by spectroscopic techniques (electronic & IR Spectra, powder XRD method, magnetic moment measurements and thermal analytical (TG-DTA)). The reaction of the acid and hydrazine gives crystalline monohydrazinium salt with formula $(N_2H_5)(C_{10}H_6(O)(COO).3H_2O$. The study of thermal degradation of the complexes indicate that they undergo dehydration in the range of 120-200°C and an oxidative decomposition in the range of 261-700°C showing strong exothermic peaks at 315-493°C resulting in the formation of metal oxides as decomposition residues. The metal oxides obtained by the incineration of these precursors in the muffle furnace at their decomposition temperatures, followed by sintering the metal oxides at the same temperature for about 30 minutes, were found to have the particle size in the range of 17-25 nm.

Key Words: *Complex Precursors, Hydrazinium Complexes, 1-Hydroxy 2-Naphthoic Acid, IR, Thermal Analysis*

1. INTRODUCTION

Thermal decomposition of hydrazinium metal carboxylates is interesting due to their easier combustibility. Simultaneous DTA-TG-DTG study of metal hydrazine formate [1], acetate [2], glycinate and glycolate [3] and oxalate [4], malonate, succinate [5], hydroxybenzoate [6] indicate that these complexes undergo decomposition at lower temperature than their non-carboxylate counter parts. This behaviour has been used for the preparation of fine particles of ferrites [7] and cobaltites [8] at the low temperatures. Suresh *et al* have reported the preparation and properties of fine particle nickel-zinc ferrites [9]. Metal hydrazine carboxylates has been used as solid solution precursors for the preparation of ultra fine cobaltite particles [10].

1-hydroxy-2-naphthoic acid is well known for its excellent co-ordination capability due to –OH group together with the carboxylic group on adjacent carbons. These molecules are used as chelating agents [11-13], as fluorescent indicators [14] and the manufacture of dyestuffs. Hydrazine, a versatile ligand acting in different fashions, monodentate, bidentate and monodentate cation leading to the formation of polymeric complexes [15, 16] can also act as a charge compensating species like $N_2H_5^+$ ammonium cation [17]. In this work, 1-hydroxy-2-naphthoic acid and hydrazine were used as ligands for the preparation of mixed ligand complexes and their thermal decomposition has been studied.

2. EXPERIMENTAL

2.1 Preparation of Hydrazinium 1-Hydroxy 2- Naphthoates

Hydrazine hydrate (0.05g;1m mol) was added to the solution of the 1-hydroxy-2 naphthoic acid (0.188g; 1m mol) in 1:1 aqueous mixture of ethanol (40 ml) and the mixture at pH 4, was reduced to its one half of its volume by heating over a hot water bath at 90°C. The pale amber coloured crystals of monohydrazinium salt obtained after 5 days were washed with ether and dried in a desiccator over $CaCl_2$.

2.2 Preparation of Metal 1- Hydroxy -2-Naphthoates Dihydrate

The metal complexes were prepared by adding 60 ml of the ligand solution containing monohydrazonium salt

to 20 ml of an aqueous solution of the respective metal nitrate (1mmol) at pH 6. The solution which appeared cloudy at first, turned out to be a micro crystalline solid on digestion by keeping it over a hot water bath at 90 ºC. Ior metal complexes Cd and Cu by mixing acid and base in the mmol ratio of 1:4, to 1mmol metal nitrate.It was cooled, filtered washed with distilled water, ethanol and then with ether and dried in a desiccator over anhydrous $CaCl_2$.

2.3 Physicochemical Technique

The compositions of the complexes were fixed by chemical analysis. Hydrazine content was determined by titrating against standard KIO_3 (0.025mol L^{-1}) under Andrew's conditions. Metal Contents were determined by titrating with EDTA (0.01mol L^{-1}) after decomposing the complexes with 1:1 nitric acid [18]. IR spectra of the complexes in the region 40-400 cm^{-1} were recorded as KBr pellets using a Perkin Elmer 597 spectrometer. Electronic spectra in the UV-Visible region were obtained using a Varian Cary 5000 recording spectrophotometer. The magnetic susceptibility of the complexes was measured using a vibrating sample magnetometer, VSM EG&G Model 155 at room temperature and the data were corrected for diamagnetism.

The X-ray powder diffractograms of the complexes were recorded using a Philips X-ray diffractometer (model PW 1050/70) employing Cu-Ká radiation with a nickel filter. The simultaneous TG-DTA experiments were carried out using SDT Q600 V8.3 instrument and Stanton 781 simultaneous thermal analyzer. Thermal analyses were carried out in air at the heating rate of 10°C min^{-1} using 5 to 10 mg of the samples. Platinum cups were employed as sample holders and alumina as reference. The temperature range was ambient to 800°C. The SEM images of the residual oxides were recorded using a Cambridge Scanning Electron Microscope with EDAX attachment (CF).

3. RESULTS AND DISCUSSION

All the complexes are microcrystalline solids, stable in air and insensitive to light. They are insoluble in water and in common organic solvents like ethanol, acetone and chloroform. The analytical data of the complexes are in very good agreement with the proposed formula for the complexes (Table 1).

3.1 IR Spectra

The IR spectra (Table 1) of hydrazinium salt show N-N stretching frequency at 954 cm^{-1} corresponding to N2H5+ ions [19]. The difference between symmetric and asymmetric õC=O is 143 cm^{-1} reveals the bidentate fashion of salt formation. In the IR spectrum of free acid, no band is found in the –OH stretching region. In the IR spectra of complexes a distinct band was located in OH region, 3334-3458 cm^{-1}, and a sharp, strong band around 823 cm-1.These may be owing to coordinated water molecules. The sharp bands at 3234 -3313 cm^{-1} which were not seen for free acids are due to õ NH of $N_2H_5^+$ ions. Further õN-N is also observed in the range 954-983 cm^{-1} due to uncoordinated $N_2H_5^+$. In all the complexes the asymmetric and symmetric stretching frequencies of the carboxylate ions are seen in the range 1577-1701 cm^{-1} and 1452-1465 cm^{-1}, respectively, with an average separation of in the range 229-241 cm^{-1}, indicating the monodentate coordination of carboxylate group [20]. The peak in the range 422-426 cm^{-1} is ascribed to the characteristic vibration of M-O bond.

3.2 Thermal Analysis

The hydrozonium salt undergoes complete decomposition from 148 to 206ºC showing a strong endotherm at 200ºC implying the elimination of water and hydrazine, and a broad exotherm centered at 481ºC due to oxidative decomposition of organic moiety . While comparing with the thermal behaviour of pure acid, it is understood that the decomposition of the hydrazinium salt occurs at much lower temperature than that of pure acid. This may be probably because of the fuel nature of hydrazine (Figure1 and Figure 2).

$(N_2H_5)_2[M\ \{C_{10}H_6\ (O)(COO)\}_2(H_2O)_2]$ (where M=Ni, Co, Cd, Cu and Zn)

The thermal analysis of metal complexes evinces the decomposition in three stages (Table 2). The hydrated metal complexes of 1-hydroxy-2-naphthoates are stable in air upto 120°C, and are then dehydrated by showing endothermic peaks in the temperature range of 100-286°C. The unstable compound immediately undergoes dehydrazination showing exothermic peaks at 276ºC (Ni), 297ºC (Co), 252ºC (Cd), and 270ºC (Zn) & 263ºC (Cu) forming the intermediate which ought to be respective metal hydroxy naphthoates. Final exothermic

decomposition occurs after 261-700ºC leading to the formation of the respective metal oxides (Figure3) XRD pattern of which were found to be conforming to those of metal oxides reported in Joint Committee Powder Diffraction Standards for analysis (Figure 4).

The metal oxides formed after the incineration of the complexes at their decomposition points found from DTA, followed by sintering at the same temperature for about 3-4 hrs were found to be pure and uniform in nano scale (17-25 nm) as noted from powder XRD using Scherer's formula [21]], D = Kë / B cosè .

The metal oxides obtained in this way are expected to be chemically more homogeneous, free of contamination by impurities and highly reactive. As a representative example, image of NIO from SEM is shown in Figure 5.

3.3 UV- Visible Spectra and Magnetic Susceptibility

The electronic spectra of the cobalt complexes show three d-d absorptions band at 9530-9570 cm^{-1}, 17705-17793 cm^{-1} and 20120-21090 cm^{-1} assignable to 4 T_{1g} (F) → 4 T_{2g} (F), 4 T_{1g} (F) → 4 A_{2g} (F), 4 T_{1g} (F) → 4 T_{1g} (P) transitions respectively, in conformity with octahedral stereochemistry around Co II ion [22]. The magnetic moment of Co (II) complex is 4.99 B.M. The two bands observed in nickel complexes at 17750-18000 cm^{-1} and 23950- 24000 cm^{-1} may be assigned to the transition arising from $1A_{1g}$ ground state to $1B_{2g}$ and $1B_{1g}$ excited state respectively. These values as well as magnetic moment value 3.80 B.M. support the octahedral geometry of Ni(II) complex.

The electronic spectra of the Cu complexes show two characteristic bands in range 13500-18600 cm^{-1}. These bands have been assigned to the following transitions to 2 B_{1g} → 2 A_{2g} , 2 B_{1g} → 2 B_{2g}. The magnetic moment of Cu(II) complex is 1.9 B.M. [23].

3.4 Powder X-ray Diffraction

X –ray powder diffraction of the complexes are given in Figure 6. The diffraction data of transition metal complexes infers that those with the formulation, $(N_2H_5)_2[\ M\{C_{10}\ H_6\ (O)(COO)_2\ \}(H_2O)_2]$ where M= Ni, Co, Cd, Cu and Zn have isomorphism.

4. CONCLUSION

Reaction of 1-hydroxy-2-naphthoic acid and hydrazine with transition metal ions form complexes $(N_2H_5)_2[M\{C_{10}H_6(O)(COO)\}_2(H_2O)_2]$ where M(II) = Ni, Co, Cd, Zn & Cu in which the acid behaves as dianion and the coordination of carboxylate group with metal ion is of monodental nature. The results of various physico chemical techniques used for characterization of the metal complexes imply that the coordination of the anions of acids and water around metal ion is distorted octahedral. Based on spectroscopic data, the structure of the metal complexes is as given below.

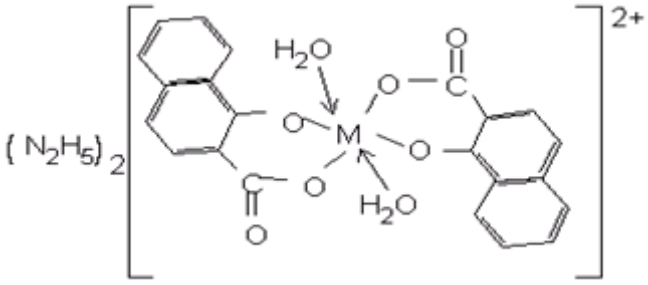

(where, M=Ni, Co, Cn, Zn and Cd)

The thermal behaviour of the complexes indicate that they undergo oxidative degradation in the temperature 310-509ºC to form metal oxides via the respective metal naphthoates. Because of the evolution various gases during decomposition N_2, H_2 and CO_2, the metal oxides formed are fine particles probably with nano size 17-25 nm. Hence it is suggested that the complexes may be used as precursors for fine particle nanometal oxides probably in nano size.

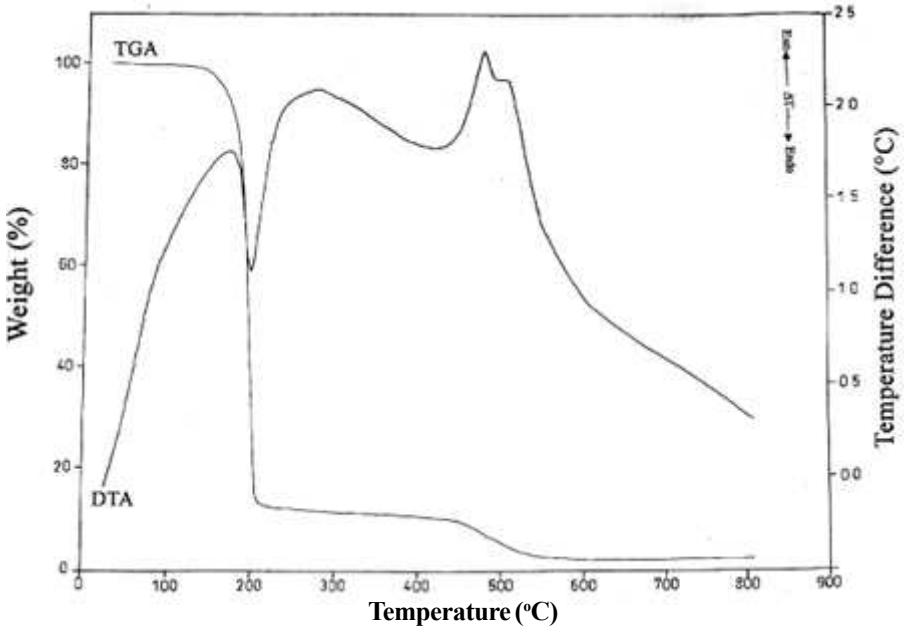

Fig. 1 Simultaneous TG-DTA of $(N_2H_5)(C_{10}H_6(O)(COO).3H_2O$

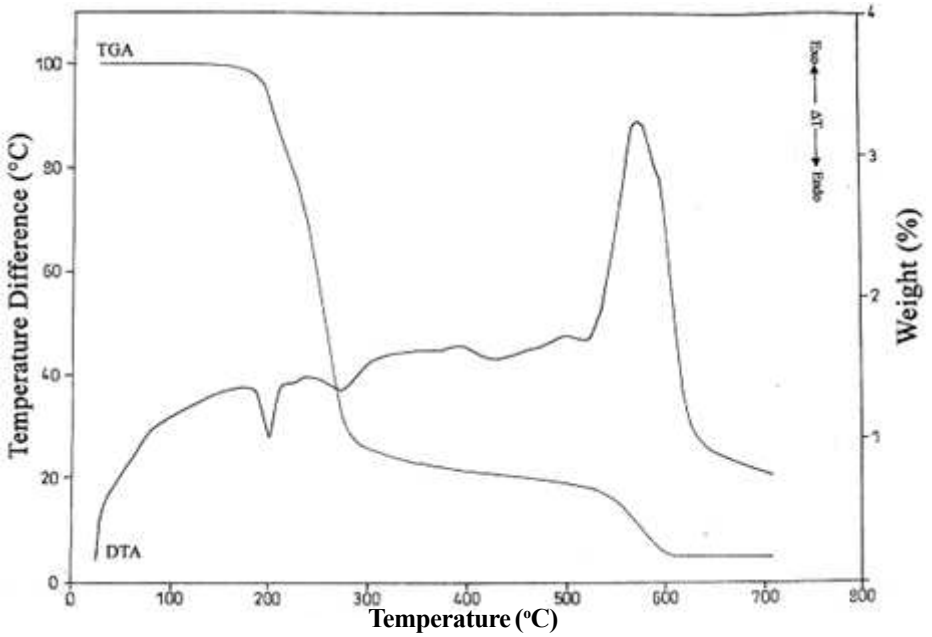

Fig. 2 Simultaneous TG-DTA of acid $(C_{10}H_6(OH)(COOH)$

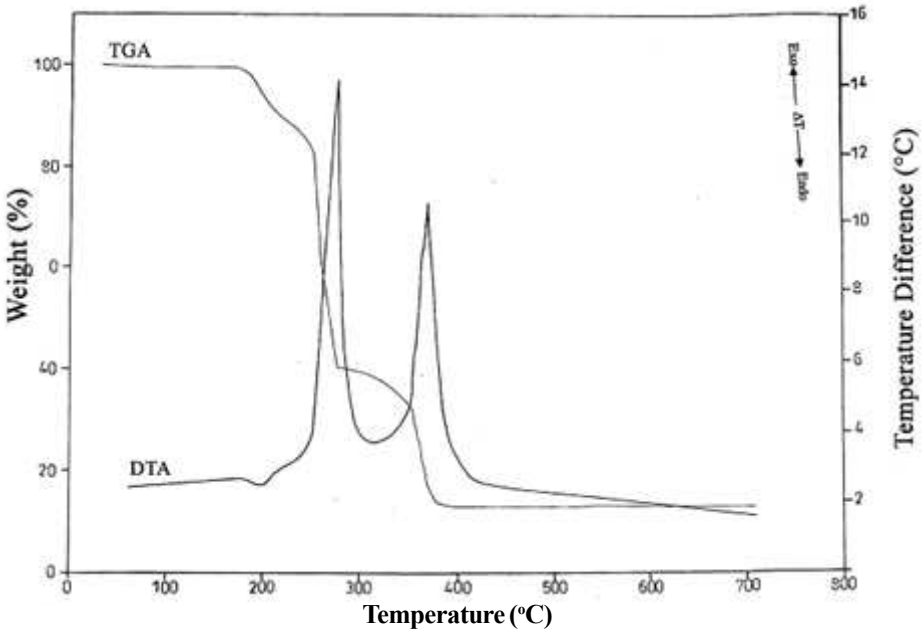

Fig.3 Simultaneous TG-DTA of $(N_2H_5)_2[Ni\{C_{10}H_6(O)(COO)\}2(H_2O)_2]$

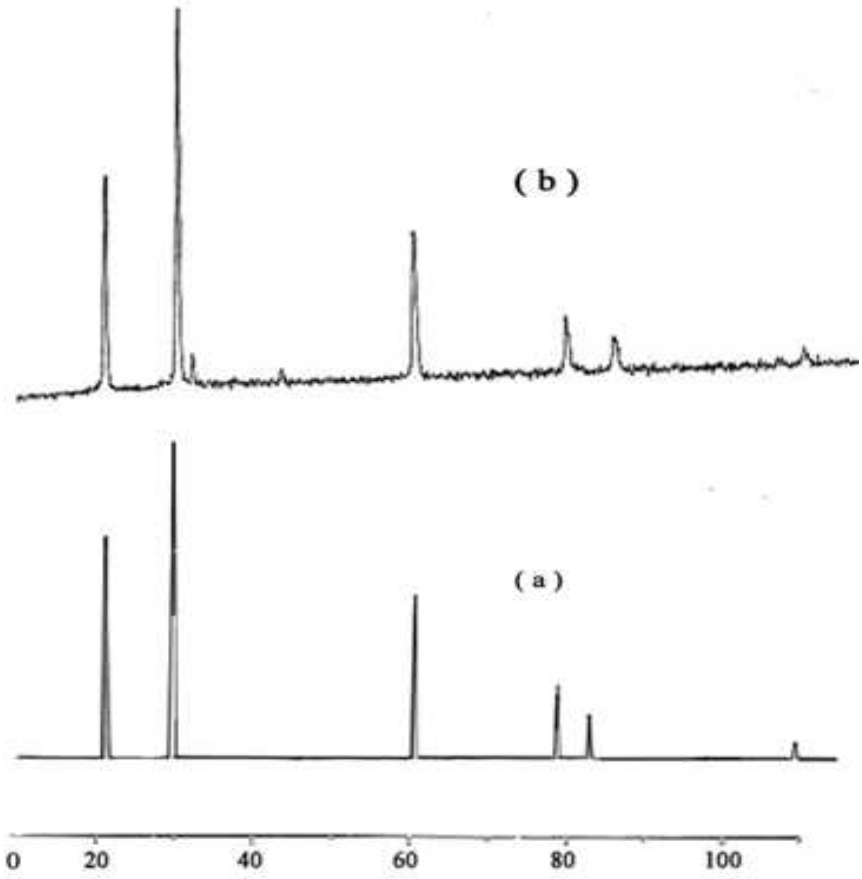

Fig. 4 Comparison of XRD of final product (a) Standard NiO (b) Sample NiO

Table 1 Analytical and IR Data of the Complexes

Molecular Formula of the Complexes	Colour	D.pt, /°C	Analytical data (%)					IR data					
			Carbon Fd. (calcd.)	Hydrogen Fd. (calcd.)	Nitrogen Fd. (calcd.)	Hydrazine Fd. (calcd.)	Metal Fd. (calcd.)	υ_{OH} cm^{-1}	$\upsilon_{C=O}$ asym cm^{-1}	$\upsilon_{C=O}$ asym cm^{-1}	υ_{M-O} cm^{-1}	υ_{M-N} cm^{-1}	υ_{NH} cm^{-1}
$(N_2H_5)_2[Ni\{C_{10}H_4(O)(COO)\}_2(H_2O)_2]$	Light Green	272	49.6 (49.6)	4.8 (4.9)	10.6 (10.5)	12.2 (12.0)	10.8 (11.0)	3440b	1695s	1454s	426b	956s	3313b
$(N_2H_5)_2[Co\{C_{10}H_4(O)(COO)\}_2(H_2O)_2]$	Pink	288	49.5 (49.5)	4.8 (4.9)	10.7 (10.5)	12.2 (12.0)	11.2 (11.1)	3458b	1683s	1454m	426m	975s	3311 m
$(N_2H_5)_2[Cd\{C_{10}H_4(O)(COO)\}_2(H_2O)_2]$	White	252	45.3 (45.0)	4.4 (4.4)	9.5 (9.5)	10.8 (10.9)	19.2 (19.2)	3334b	1701s	1465b	426b	962s	3305 m
$(N_2H_5)_2[Zn\{C_{10}H_4(O)(COO)\}_2(H_2O)_2]$	Light Brown	265	48.7 (48.9)	4.8 (4.8)	10.3 (10.4)	11.7 (11.9)	12.3 (12.1)	3446b	1685s	1452m	426b	977s	3311 m
$(N_2H_5)_2[Cu\{C_{10}H_4(O)(COO)_2\}(H_2O)_2]$	Black	255	50.1 (49.9)	4.7 (4.9)	10.3 (10.6)	12.1 (12.0)	10.3 (10.4)	3448b	1577s	1461b	422m	983s	3234b
$(N_2H_5)(C_{10}H_4(O)(COO).3H_2O$	Brown	350	43.0 (43.1)	5.2 (5.5)	8.9 (9.1)	11.7 (11.6)	-	3421b	1581s	1438s	-	954s	3328s

b = broad; s = sharp; m = medium

Fig.6 SEM Image of NiO

Fig.7 Comparison of XRD of complexes

(a) $(N_2H_5)_2[Ni\{C_{10}H_6(O)(COO)\}_2(H_2O)_2]$
(b) $(N_2H_5)_2[Co\{C_{10}H_6(O)(COO)\}_2(H_2O)_2]$
(c) $(N_2H_5)_2[Cd\{C_{10}H_6(O)(COO)\}_2(H_2O)_2]$
(d) $(N_2H_5)_2[Zn\{C_{10}H_6(O)(COO)\}_2(H_2O)_2]$ and
(e) $(N_2H_5)_2[Cu\{C_{10}H_6(O)(COO)\}_2(H_2O)_2]$

Table 2 Thermal Analysis

Molecular Formula of the Complexes	DTA Peak Temp(°C)	Thermogravimetry			Decomposition Products
		Temp. Range (°C)	Weight loss		
			Obsd.	Calcd.	
$(N_2H_5)_2[Ni\{C_{10}H_6(O)(COO)\}_2(H_2O)_2]$	200 (+) 276 (-) 370 (-)	180-231 231-279 279-700	6.8 54 85.4	6.8 54.0 85.9	$(N_2H_5)_2Ni\{C_{10}H_6(O)(COO)\}_2$ $Ni\{C_{10}H_6(O)(COO)\}$ NiO
$(N_2H_5)_2[Co\{C_{10}H_6(O)(COO)\}_2(H_2O)_2]$	120(+) 209(+) 297 (-) 436 (+)	116-262 262-317 317-700	6.7 54.3 85.6	6.8 54.0 85.9	$N_2H_5)_2Co\{C_{10}H_6(O)(COO)\}_2$ $Co\{C_{10}H_6(O)(COO)\}$ Co_3O_4
$(N_2H_5)_2[Cd\{C_{10}H_6(O)(COO)\}_2(H_2O)_2]$	137 (+) 252 (-)	100-286	50.3	50.6	$Cd\{C_{10}H_6(O)(COO)$
	364 (-) 440 (-) 493 (-)	286-700	78.3	78.1	CdO
$(N_2H_5)_2[Zn\{C_{10}H_6(O)(COO)\}_2(H_2O)_2]$	150 (+) 270 (-)	130-206 206-346	6.6 54.0	6.6 54.0	$(N_2H_5)_2Zn\{C_{10}H_6(O)(COO)\}_2$ $Zn\{C_{10}H_6(O)(COO)$
	420 (-) 465 (-)	346-700	84.7	84.9	ZnO
$(N_2H_5)_2[Cu\{C_{10}H_6(O)(COO)_2\}(H_2O)_2]$	174 (-) 201 (+)	150-261	21.7	21.8	$Cu\{C_{10}H_6(O)(COO)$
	263 (-) 315 (-)	261-700	75.4	75.1	CuO
$(N_2H_5)(C_{10}H_6(O)(COO).3H_2O$	200 (+) 481 (-) 509 (-)	148-700	97.9	-	Decomposition to Carbon Residue

(+),endotherm ; (-) ,exotherm.

REFERENCES

[1] P. Ravindranathan and K.C.Patil, "Thermal Reactivity of Metal Formate Hydrazinates", Thermochimica Acta, Vol.71, No.1-2, 1983, pp.53-57.

[2] G.V. Mahesh and K.C. Patil, "Thermal Reactivity of Meatl Acetate Hydrazinates", Thermochimica Acta, Vol.99, 1986, pp. 153-158.

[3] B.N. Sivasankar , "Studies on Metal Hydrazine Caboxylates", Ph.D., Thesis, Bharathiar University, Coimbatore, India, 1994.

[4] K.C. Patil, D. Gajapathy and K. Kishore, "Thermal Reactivity of Metal Oxalate Hydrazinates", Thermochim Acta, Vol.113, 1982, pp. 52-55.

[5] B.N. Sivasankar and S. Govindarajan, "Studies on Bis(hydrazine) Metal Malonates and Succinates", Synthesis and Reactivity in Inorganic, Metal- Organic and Nano-metal Chemistry, Vol. 24, No.9, 1994, pp.1573-1582.

[6] K.Kuppusamy, B.N.Sivashanker and S. Govindarajan, "Preparation, Characterisation and Thermal Properties of Some New Hydrazinium Carboxylates", Thermochim Acta, Vol. 259, No.2, pp. 251-262.

[7] D. Gajapathy and K.C. Patil, "Mixed Metal Oxalate Hydrazinates as Compound Precursors to Spinel Ferrites", Material Chemistry and Physics, Vol.9, No.4, 1983, pp. 423-438.

[8] B.N. Sivasankar and S. Govindarajan, "Hydrazine Mixed Metal Malonates – New Precursors for Metal Cobaltites", Materials Research Bulletin, Vol.31, No.1, 1996, pp. 47-54.

[9] K.Suresh, K.C.Patil, "Preparation And Properties of Fine Particle Nickel-zinc Ferrites: A Comparative Study of Combustion and Precursor Methods", Journal of Solid State Chemistry, Vol.99, No.1, 1992, pp.12-17.

[10] P.Ravidranathan, G.V. Mahesh and K.C.Patil, "Low-Temperature Preparation of Fine-particle Cobaltites", Journal of Solid State Chemistry, Vol.66, No.1, 1987, pp.20-25.

[11] A. Kula, "Preparation, Spectral and Thermal studies of Y(III) and Lanthanide (III)", Journal of Thermal Analysis and Calorimetry, Vol.68, 2002, pp. 957-964.

[12]Ye Bi and Cheng-Li Han, "Ammonium 1-hydroxy-2- naphthoate", Acta Crystallographica Section E, Vol.64, 2008, pp.813-817.

[13] Y.H. Deshpande, D.V. Jahagirdar and V. Ramachandra Rao, "Studies on Y(III), La(III), Ce(III), Pr(III), Nd(III) and Sm(III) Complexes of Some Hydroxy Naphthoic Acids", Journal of Inorganic Nuclear Chemistry,Vol.37, 1975, pp.1761-1765.

[14] A.N.Pant, R.N.Soni and S.L. Gupta, "Spectro-photometric Studies on Fe(III)-1-Hydroxy-2-Naphthoic Acid Chelate in 50% Ethanol", Journal of Inorganic Nuclear Chemistry, Vol.34, 1972, pp. 763-766.

[15] T. Premkumar and S. Govindarajan, "Synthesis and Spectroscopic, Thermal and Xrd Studies on Trivalent Lighter Rare-earth Complexes of 2,3-pyrazine Di Carboxylate with Hydrazinium Cation", Inorganic Chemistry Communications, Vol.6, 2003, pp.1385-1389.

[16] S.Yasodhai and S.Govindarajan, "Hydrazinium Oxydiacetates and Oxydiacetate Dianion Complexes of Some Divalent Metals with Hydrazine", Journal of Thermal Analysis and Calorimetry, Vol.62, 2000, pp. 737-745.

[17] S. Vairam, S. Govindarajan, "Hydrazinium Complexes of Lanthanide and Transition Metal Squarates", Polish Journal of Chemistry, Vol.80, 2000, pp. 1601-1614.

[18] A.I. Vogel, "A Text Book of Quantitative Inorganic Analysis", Longmans Green, London , 1975.

[19] A. Braibanti, F. Dallavalle, M.A. Pellinghelli and E. Leporati, "The Nitrogen-Nitrogen Stretching Band in Hydrazine Derivatives and Complexes," Inorganic Chemistry, Vol.7, No.7, 1968, pp.1430-1433.

[20] K. Nakamoto, "Co-ordination Compounds, Infrared and Raman Spectra of Inorganic and Co-ordination Compounds", IV Ed., Wiley, New York, 1986.

[21] Guozhong Cao, "Nano Structures and Nano materials, Synthesis, Properties and Applications", Imperial College Press, London, 2004.

[22] A.P. Lever, "Inorganic Electronic Spectroscopy", Elsevier, Amsterdam 1968.

[23] F.A. Cotton and G. Wilkinson, "Advanced Inorganic Chemistry", 2nd Ed., Wiley, New York ,1966.

STUDIES ON TECHNO-ECONOMIC VIABILITY OF CASCADE COMPRESSION - ABSORPTION HYBRID REFRIGERATION SYSTEM FOR DAIRY INDUSTRIES

S. Tharves Mohideen[1], G. Rajendiran[2], P. Kumar Babu[3] and S. R. Devadasan[4]

[1]Department of Mechanical Engineering, Institute of Road and Transport Technology, Erode District - 638 316, Tamil Nadu

[2]Department of Automobile Engineering, Tamilnadu College of Engineering, Coimbatore- 641 659, Tamil Nadu

[3]Department of Mechanical Engineering, Bannari Amman Institute of Technology, Sathyamangalam - 638 401, Erode District, Tamil Nadu

[4]Department of Mechanical Engineering, PSG College of Technology, Coimbatore - 641 004, Tamil Nadu

E-mail : dharvish_stm@yahoo.com, rajendirang@sify.com , pkbbit@rediffmail.com

(Received on 27 October 2008 and accepted on 10 December 2008)

Abstract

There are many industries which require simultaneous heating and cooling for their processes. Dairy industry is one among them, which requires heat for milk pasteurization, powder production and cooling for pasteurization, milk storage and butter storage. The temperature required for the process of butter storage is -30 °C and the multi pressure system is employed for this process. The high power consumption and the use of Ozone depleting Chloroflorocarbon(CFC) refrigerants in vapour compression refrigeration are the main limitations. In this work a noble idea of combining vapour compression refrigeration vapour absorption refrigeration to produce low temperature of the order of - 30°C is proposed and named as Hybrid refrigeration system.

Heat operated cooling systems are attractive when thermal energy is available freely or at low cost, and high-grade electrical energy is expensive. In the present work the thermodynamic analysis of the Hybrid refrigeration system driven by high temperature waste heat source available at the dairy processing industries was performed by computer simulation. The variation of Power per ton of refrigeration and COP of the system with respect to operating parameters such as condensers temperatures and evaporator temperatures are studied. The power per ton for the existing and proposed system were found to be 1.323 kW/TR and 0.605 kW/TR respectively. Further the COP the existing and proposed system were found to be 3.45 and 0.63 respectively. The savings obtained from the lower value of power per TR for the proposed system, the payback period have been estimated to be 2 years.

It has been observed that the proposed Hybrid System requires only half of the power needed to drive the compressor for lower cycle and can be commercially viable. As water-LiBr working pair has 0% ODP and 0% GWP, it has the edge over the conventional refrigerants. The complete Thermodynamic analysis and techno economic feasibility studies of Hybrid cascade refrigeration system suitable for dairy industries have been discussed. Simulations have been dealt with C programme by varying the operating parameters.

Keywords : *Butter Storage, COP, Dairy Industry, Hybrid Refrigeration System, Milk Pasteurization, Multi Pressure System,Payback Period, Power Per TR*

NOMENCLATURE

h	Enthalpy, kJ/Kg
TR	Ton of Refrigeration
COP	Co-efficient of Performance
VCR	Vapor Compression Refrigeration
R-134a	Tetra flouro ethane
CR	Compression Ratio
W	Power input, kW
Qe	Cooling capacity, kW
Te	Evaporator Temperature, ^{0}C
Tcond	Condenser temperature, ^{0}C
m_1,m_2	Mass flow rate, Kg/sec

SUBSCRIPTS

LP	Low pressure side
HP	High pressure side
P	Total Power
h_1,h_2.....	Enthalpies at different points
r	Refrigerant
a	Absorber
g	Generator
ss	Strong solution
e	Evaporator
c	Condenser
COP_1, COP_2	Co-efficient of Performances on higher and lower cycle

1. INTRODUCTION

The chloro-floro carbon(CFC) family of refrigerants used in compression chillers is primarily responsible for the ozone layer depletion and this has called for 100% phasing out of CFC refrigerants by Montreal Protocol where India is also a signatory country [1-7]. The future Heating Ventilating and Air conditioning Industry (HVAC) is rapidly switching over to absorption technology from compression chillers [10].

Paul E.Hufford states that the recoverable heat is two variable to wate in inefficient process [11]. The high efficiency of absorption chillers using direct exhaust gas steam from the heat recovery boiler or extraction steam from turbine offers new opportunities to enhance the efficiency of the gas turbines that power the cogeneration system. Radermarcher *et al* concluded that the enlarged investigations of absorption systems in recent years are seems to be fruitful [3]. In heating mode operating of heat actuated heat pumps at efficiency levels above those of other heating systems can give absorption a performance advantage it has never had. In cooling mode, the higher efficiencies of the coming absorption cycles indicate that refrigeration efficiency can be increased to competitiveness on an energy input as with those of vapour compressing system.

Saravanan R and Maiya [13] performed computer simulation of VARS using water as refrigerant and 16 different solution combination as absorbent. This study revealed that H_2O-LiBr, H_2O-LiCl and H_2O-$ZnCl_2$ combination are better from the combinations in terms of COP and efficiency ratio point of view. The H_2O-LiCl combination is better from the view point of cut-off temperature and circulation ratio. The properties of H_2O-Libr system is established by Rosenfeld and Karnauk [12] and Mc Neely L A [8].

Radermarcher *et al* worked with a cascaded system in which the vapor-compression equipment cooled the building space, and the absorption equipment "pumped" the heat rejected from the vapor compression system up to the temperature needed to reject it to the ambient air [3]. In this case, the vapor-compression condenser and the absorption system evaporator are in thermal communication. The temperature raise for both refrigeration systems was reduced. Milind V. Rane concluded that heat operated refrigeration system could be used to lower energy cost [9]. Waste heat operated refrigeration system can be used to reduce the life cycle cost and also co-generation of electricity and refrigeration can lead to maximum savings.

1.1 The Existing System

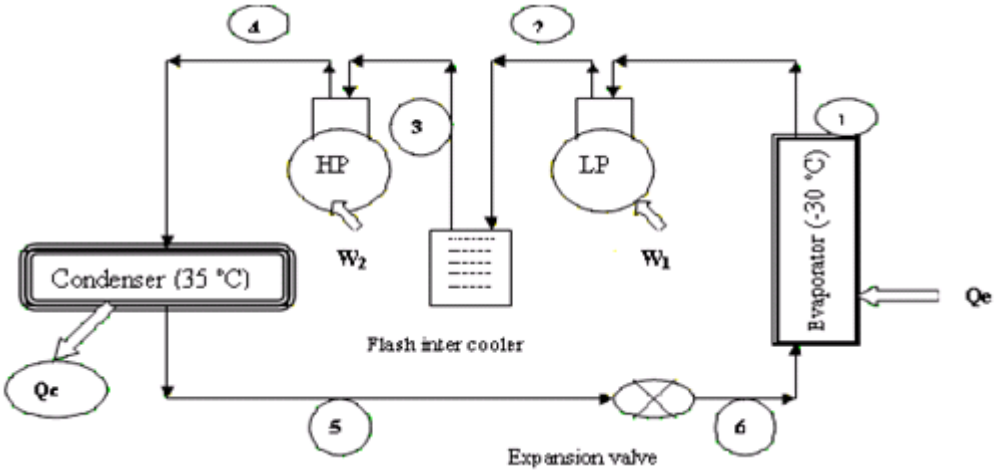

Fig. 1 Flow diagram for conventional multi pressure VCR system

2. PROPOSED SYSTEM

2.1 Hybrid Cascade Refrigeration System .

The Hybrid Cascade Refrigeration System is divided in to two cycles. One is Higher Cycle and another is lower cycle as shown in Figure 2. The higher cycle consists of absorber, solution pump, generator and condenser and the lower cycle comprises compressor, expansion vale and evaporator. The Cascade condenser interconnects these two cycles.

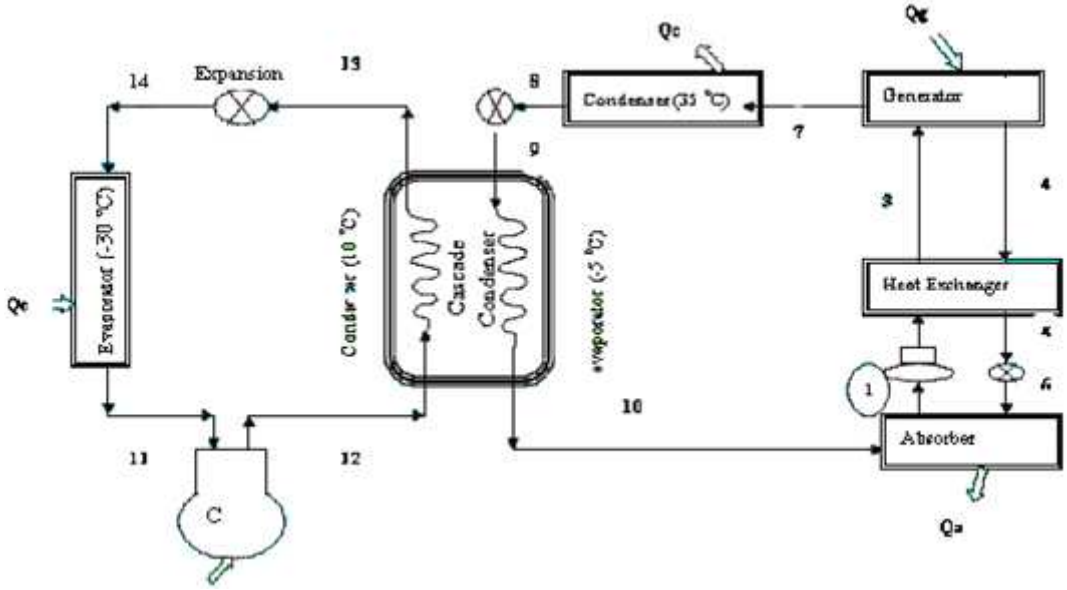

Fig. 2 Layout of proposed system

3. THERMODYNAMIC ANALYSIS OF EXISTING MULTI PRESSURE VAPOUR COMPRESSION SYSTEM INPUT DATA

Capacity of the plant	: 1 TR
Working fluid	: R-134a
Condensing Temperature	: 35^0C
Evaporator Temperature	: - 30^0C

Governing equations

The thermodynamic analysis of the existing system based on the following governing equations from the literature [6].

.

Power Required for compressors

$$W_{LP} = m_1 (h_2 – h_1) \quad (1)$$
$$W_{HP} = m_3 (h_4 – h_3) \quad (2)$$

Total Power required for the plant

$$W_p = W_{LP} + W_{HP} \quad _k W \quad (3)$$
COP of the system = TR/ Total Power (4)

3.1 Thermodynamic Analysis for Proposed Compression-Absorption Hybrid Refrigeration System Higher Cycle

The following steps are referred from Radermatcher [3].

i. Select the operating pressures corresponding to the temperatures for the cycles

ii. Find out the concentration for weak and strong solutions

iii. Circulation ratio is given by

$$CR = \frac{(1 - X_4)}{(X_1 - X_4)}$$

iv. find out the enthalpies at various state points ($h_1$to, h_{10}) using chat and steam table

v. Mass of the refrigerant is given by

$$m_r = \frac{1.5 \text{ TR X } 3.54}{(h_{10} - h_9)} \text{ kg /sec}$$

vi. Calculate the mass of the weak and strong solutions using

$$CR = \frac{m_{ss}}{m_r}$$
$$m_{ss} = m_r + m_{ws}$$

3.2 Lower Compression Cycle

i. Calculate Enthalpies at various state points (h_{11}, h_{12}, h_{13}, h_{14})

ii. Mass of the refrigerant

$$m_r = \frac{1.5 \text{ TR X } 3.54}{(h_{11} - h_{14})} \text{ kg /sec}$$

iii. Power required for compressor $W = m_r (h_{12} - h_{11})$

4. RESULTS AND DISCUSSION

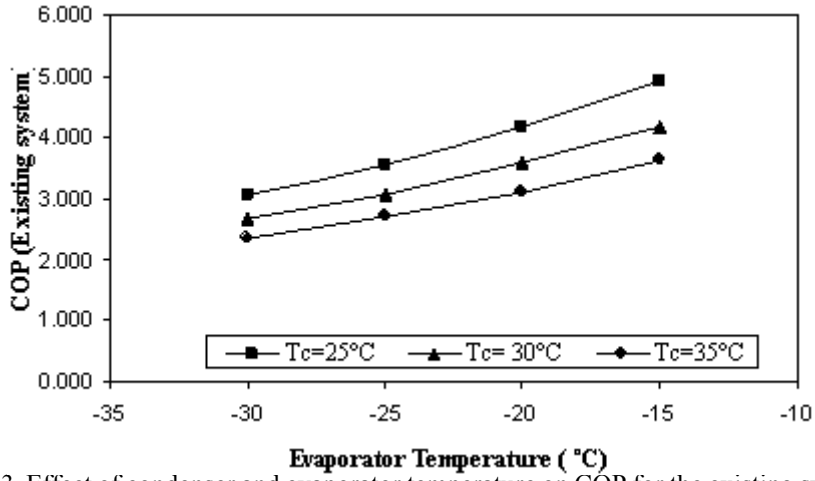

Fig.3 Effect of condenser and evaporator temperature on COP for the existing system

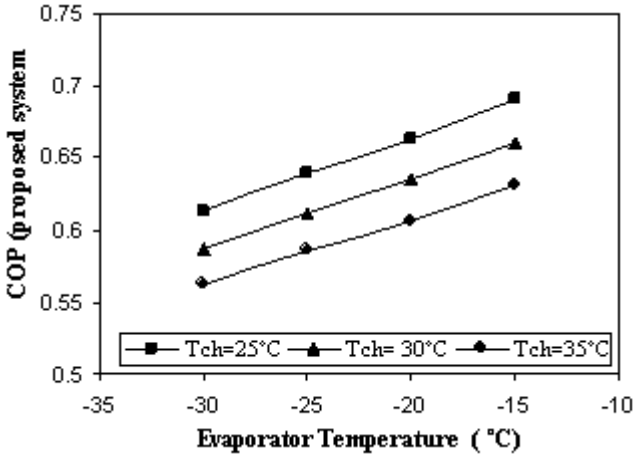

Fig. 4 Effect of condenser and evaporator temperature on COP for the proposed system.

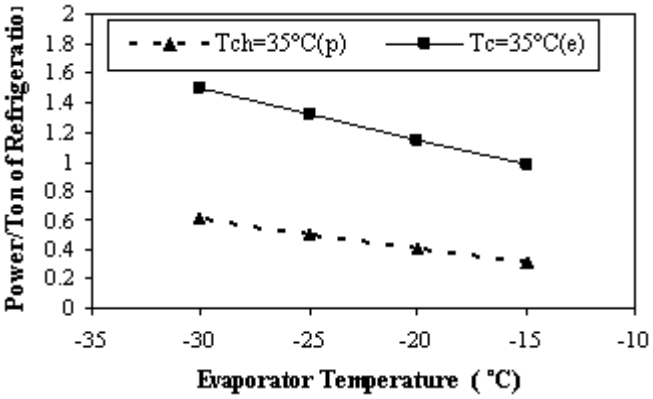

Fig. 5 Effect of condenser and evaporator temperature on power per tonne of refrigeration for the existing and proposed systems.

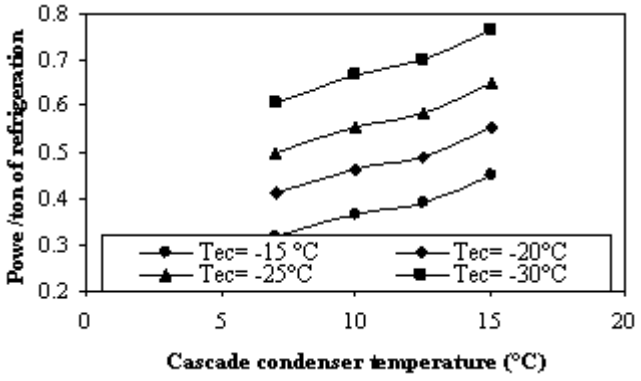

Fig. 6 Effect of cascade condenser and evaporator temperature on power per tonne of refrigeration for the proposed systems Tg= 90°C, Ta= 30°C and Tch = 25°C.

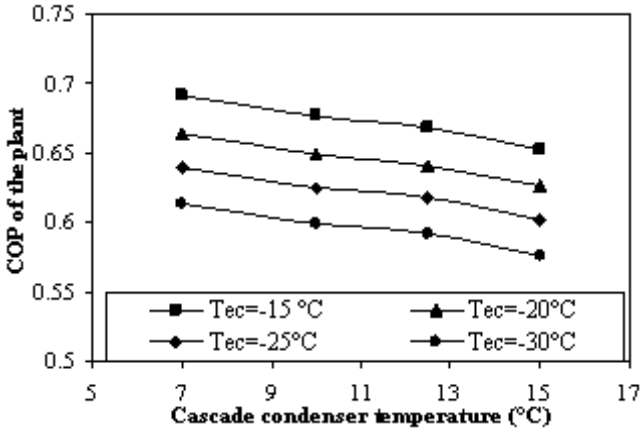

Fig. 7 Effect of cascade condenser and evaporator temperature on COP for the proposed systems Tg= 90°C, Ta= 30°C and Tch = 25°C

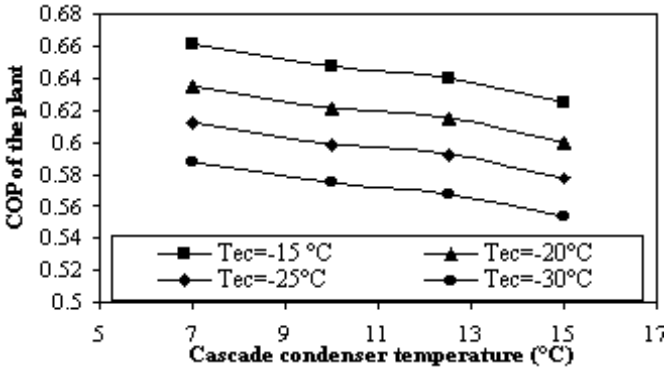

Fig. 8 Effect of cascade condenser and evaporator temperature on COP for the proposed systems Tg= 90°C, Ta= 35°C,, Tch = 30°C.

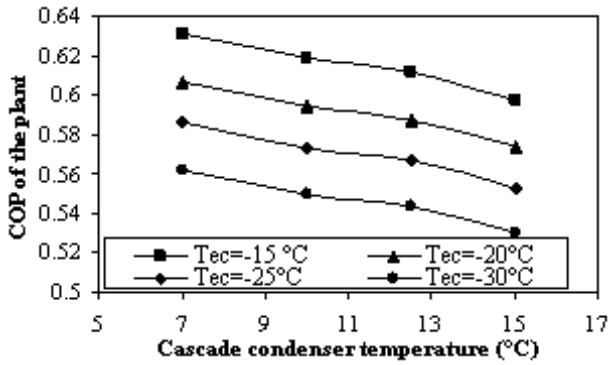

Fig. 9 Effect of cascade condenser and evaporator temperature on COP for the proposed systems Tg= 90°C, Ta= 35°C, Tch = 35°C.

A 'C' programme has been developed to predict the performance of hybrid cascade refrigeration system at various condensing temperatures (Tc) for higher and lower cycles. The evaporator temperature (Te) and their performance were compared with the conventional multipressure system.

4.1 Effect of Condenser and Evaporator Temperature on COP & Power Per Tonne of Refrigeration for the Proposed Systems

It can be observed that from Figure 3 that at constant condensing temperature if the evaporator temperature is increased from -30°C to -15°C the COP is found to increase from 0.58 to 0.66. This is because at lower evaporator temperature the vapour pressure in the evaporator is very low, which necessitates the higher energy for compressor and also the COP is very low.

It can be observed that from Figure 4 that at constant condensing temperature if the evaporator temperature is increased from -30°C to -15°C the power per tonne of refrigeration is found to declined from 0.605 to 0.36. This is because at higher evaporator temperature the evaporator pressure is maintained as high as the design value, which reduces the power consumption in the compressor and also from the Figure 5, the decrease in power per tonne of refrigeration is due to the fact that the enthalpy drop across the compressor is also declining when evaporator temperature is increased.

It is obvious from the Figure 6 that at constant sink temperature of 30°C and cascade sink temperature of 10°C. If the evaporator temperature is increased from -30°C to -15°C, the enthalpy drop across the evaporator increases and hence improving COP.

It is clear from the Figure 7, 8 and 9 at a constant evaporator temperature of -30°C and at a constant cascade condenser temperature of 10°C, if the sink temperature is increased from 25 to 35°C the COP of the plant is declining. This because when condensing temperature is increased from 25 to 35°C, the refrigeration effect is reduced, which reduces the COP.

5. PAYBACK PERIOD

Pay Back Period is the period during which the initial investment of "Hybrid Cascade Refrigeration System" can be recovered. Firms expect to receive a pay back of their capital expenditure in a minimum period of time.

$$\text{Pay back period} = \frac{\text{Initial Investment}}{\text{Annual Savings}}$$

$$= 29{,}720{,}25 \,/\, 14{,}\,55{,}620$$
$$= 1.8 \text{ years}$$

6. CONCLUSION

The variation of Power per tonne of refrigeration and COP of the system with respect to operating parameters such as condensers temperatures and evaporator temperatures are studied. The power per ton for the existing and proposed system were found to be 1.323 kW/TR and 0.605 kW/TR respectively. Further the COP the existing and proposed system were found to be 3.45 and 0.63 respectively.

For a 100 TR refrigeration plant, the annual saving of Rs. 14.5 lakhs is estimated due to the lower power/TR of the proposed system.

REFERENCES

[1] "Dairy Science Facts", Department of Food Science, Stocking Hall, Ithaca, NY 14853.

[2] K. Herold, L. Howe and R. Radermacher, "Analysis of a Hybrid Compression Absorption Cycle Using Lithium Bromide and Water as the Working Fluid", International Journal of Refrigeration Vol.14, No.2, 1991, pp 356-378.

[3] K. Herold and R. Radermacher, "Absorption Chillers and Heat Pumps", CRC press, London, 1996.

[4] Joyce and Burgi, "A Survey of Australian Dairy Processors in 1981-82", Vol. 1,1993, pp 278-326.

[5] R.S. Khurmi, "Refrigeration and Air Conditioning Tables", S Chand and Co.Ltd., 1990.

[6] C.P. Arora , 'Refrigeration and Air Conditioning', Tata McGraw Hill,New Delhi, 1997.

[7] Manohar Prasad, "Refrigeration and Air Conditioning", Wisley Eastern Ltd., 1993.

[8] L.A. Mc Neely L. A., "Thermodynamic Properties of Aquous Solution of Lithium-Bromide", ASHRAE Transactions, Vol.85, No,1, 1979, pp.413-434.

[9] V. Rane Milind, "Oportunities for Energy Conservation in RAC", Indian Refrigeration and Air-Conditioning Journal, Vol .2, 1998, pp 204-213.

[10] W. Neibergall, "Absorption Refrigerating Machines", Hand book, Vol .7, 1959.
[11] E. Paul Hufford, "Absorption Chillers Maximizes the Co-generation Efficiency", Journal of Combined Heat and Power Cycles, Vol.6, 1992, pp.256-264.
[12] LM. Rosenfeld and Mc Karunaukh, "Kholodilaaya Tekhnika", Vol.1, No 1, 1958, pp.37-42.
[13] R. Saravanan and Maiya, "Computer Simulation of Vars Using Water as Refrigerant" International Conference on Natural Fluid Refrigerants, New York USA, 1998.

ENHANCEMENT OF NOISY SPEECH USING FREQUENCY DEPENDENT SPECTRAL SUBTRACTION METHOD

M. G. Sumithra[1], D. Deepa[1] and K. Thanushkodi[2]

[1]Department of Electronics and Communication Engineering, Bannari Amman Institute of Technology, Sathyamangalam - 638 401, Erode District, Tamil Nadu

[2]Akshaya College of Engineering and Technology, Coimbatore - 641 109, Tamil Nadu

E-mail: mgsumithra@rediffmail.com, deepa_dhanaskodi@yahoo.co.in, Thanush_dr@rediffmail.com

(Received on 28 October 2008 and accepted on 12 December 2008)

Abstract

The speech processing systems used to communicate or store speech are usually designed for a noise free environment. But in a real-world environment, the presence of background interference in the form of additive background and channel noise drastically degrades the performance of these systems. To obtain a more intelligible speech signal noise reduction is needed. Most implementations and variations of the basic spectral subtraction technique advocate subtraction of the noise spectrum estimate over the entire speech spectrum. However the spectrum of actual or physical noise does not affect the speech signal uniformly over the entire spectrum. This paper proposes a frequency dependent spectral subtraction method, which takes into account of the fact that the background noise affects the speech spectrum differently at various frequencies. This proposed approach outperforms the standard power spectral subtraction method resulting in superior speech quality for various noise types and its performance is evaluated by objective and subjective measure like signal to noise ratio (SNR) and Itakuro-Saito (IS) distance measure.

Keywords: *Noisy Spectrum, Noise Estimate, Spectral Subtraction,Signal to Noise Ratio (SNR), Itakuro-Saito (IS)*

1. INTRODUCTION

Speech enhancement aims at improving the performance of acoustic systems in noisy environments. Various speech processing systems have found their way in our everyday life through their drastic use in voice communication, speech and speaker recognition, aid for the hearing impaired and numerous other applications. In many situations of practical interests, the speech signal gets corrupted by one or more of the following: additive background noise, reverberation and speech from other speakers. These degradations will lower the quality and intelligibility of speech message. The speech enhancement methods aim to improve the quality and intelligibility of degraded speech. The processed speech signals should be more comfort for listening and also should give better performance in tasks like automatic speech and speaker recognition. The additive background noise is random in nature and also uncorrelated with speech. Speech from other speakers may also get mixed with desired speaker's speech in an additive fashion. Since the characteristics of degradation are different in each case, degraded speech may need to be processed in different ways.

In the present work, we focus on speech degraded predominantly by additive background noise, in this work such speech signal is termed as noisy speech. Additive background noise is uncorrelated with the speech signal and present in various environment scenarios like offices, cars, city streets, fans, factory environments, helicopters etc. In case of additive background noise, the assumptions made for developing enhancement methods are,(i) speech and noise signals are uncorrelated atleast over a short-time basis, (ii) noise is either stationary or slowly varying over several frames of speech, and (iii) noise can be represented as zero mean random process. The degradation level of additive background noise is normally specified by Signal to Noise Ratio (SNR) and is defined as the ratio of signal energy to noise energy.

Speech enhancement schemes currently available to enhance noisy speech can be divided into single channel and multi-channel methods, depending on whether the

noisy speech from the environment is collected over single or multiple channels. In most common scenario like mobile communication, hearing aids etc., usually a second channel may not be available. Therefore, single channel systems mostly make use of different statistics of speech and unwanted noise. The performance of these methods are limited in the presence of non stationary noise as most of the methods make an assumption that noise is stationary. Multiple channel speech enhancement technique take advantage of availability of multiple signal input to the system, making possible, the use of noise references for enhancement.

The conventional power spectral subtraction method for single channel speech enhancement [2] substantially reduces the noise levels in the noisy speech, it also introduces an annoying distortion in the speech signal called musical noise or residual noise. This distortion is caused due to the inaccuracies in the short-time noise spectrum estimate resulting in large.

The proposed approach is a frequency dependent speech enhancement based on the proven spectral subtraction method. However, the spectrum of real world noise does not affect the speech signal uniformly over the entire spectrum. In this work, the fact that is taken into account that the background noise affects the speech spectrum differently at various frequencies, considering this factor the spectral subtraction is performed independently on each band by estimating noise.

The noise estimation in this work is updated by averaging the noise speech spectrum using a time and frequency dependent smoothing factor, which is adjusted based on signal presence probability in subbands. Signal presence is determined by computing the ratio of the noisy speech power spectrum to its local minimum, which is computed by averaging past values of the noisy speech power spectra with a look-ahead factor. This local minimum estimation algorithm adapts very quickly to highly non stationary noise environments. By using this noise estimation algorithm, this method outperforms the standard power spectral subtraction method resulting in superior speech quality and largely reduced musical noise in single microphone system.

2. ENHANCEMENT OF NOISY SPEECH

Spectral subtraction method is a well known noise reduction method based on the STSA (Short Time Spectral Amplitude) estimation technique. The basic power spectral subtraction technique, as proposed by Boll [2], is popular due to its simple underlying concept and its effectiveness in enhancing speech, degraded by additive noise. The basic principle involved in this method is to subtract the magnitude spectrum of noise d(n) from the noisy speech y(n).

$$y(n) = s(n) + d(n) \qquad \text{.....} \qquad (1)$$

Where, s(n) is the clean speech. The noise is assumed to be uncorrelated and additive to the speech signal. The estimate of the noise is measured during silence or non-speech activity in the signal. The power spectrum of the noisy signal can be written as:

$$|Y(k)|^2 = |S(k)|^2 + |D(k)|^2 \qquad \text{.....} \quad (2)$$

Since the noise power spectrum D(k) cannot be directly obtained, a time-average of the noise power spectrum is calculated during a period of silence, an estimate of the modified speech spectrum can be given as:

$$\left|\hat{S}(k)\right|^2 = \left|Y(k)\right|^2 - \alpha\left|\hat{D}(k)\right|^2 \qquad \text{.....} \quad (3)$$

Drawbacks in spectral subtraction method are residual noise(musical noise) and distortions due to half wave rectification. The effectiveness of noise removal is dependent on accurate spectral estimate of noise signal. The better noise estimate gives lesser residual noise content in the resultant spectrum. The modified spectrum may contain some negative values due to the errors in the estimated noise spectrum. These values are rectified using half-wave rectification (set to zero) or full wave rectification (set to its absolute value). This can lead to further distortions in the resulting time signal. The accurate estimate of noise will overcome those drawbacks.

3. PROPOSED METHOD

The proposed frequency dependent spectral subtraction method offers better quality of the resulting

enhanced speech with reduced residual noise. Research in spectral subtraction methods [8,10] has focused on a non-linear approach to the spectral subtraction procedure. This approach has been justified due to variation in signal to noise ratio across the speech spectrum. White Gaussian noise has a flat spectrum, whereas the actual or physical real world noise is not flat. Colored noise affects the speech spectrum differently at various frequencies, we use a multi-band approach to spectral subtraction.

The speech spectrum is divided into N non-overlapping bands, and spectral subtraction is performed independently in each band. The estimate of the clean speech spectrum in the i^{th} band is obtained by:

$$\left|\hat{S}_i(k)\right|^2 = \left|\overline{Y}(k)\right|^2 - \alpha_i \delta_i \left|\hat{D}_i(k)\right|^2$$
$$b_i \le k \le e_i \qquad \ldots\ldots \quad (4)$$

Where, b_i and e_i are the beginning and ending frequency bins of the i^{th} frequency band, $á_i$ is the over subtraction factor and $ä_i$ is the band subtraction factor. Over subtraction factor provides a degree of control over the noise subtraction level in each band, the use of multiple frequency bands and the use of the $ä_i$ weights provide an additional degree of control within each band.

4. NOISE ESTIMATION

Noise estimation plays an important role in speech enhancement. For an efficient noise estimation algorithm, the resultant signal estimation will have great accuracy. Several noise estimation algorithms have been proposed for speech enhancement applications [3-5, 7,8, 10-13]. Most of the noise estimation algorithms can be classified into two classes. The first class is based on updating the noise estimate by tracking the silence regions of speech and other class is based on updating noise estimate using the histogram of the noisy speech power spectrum.The noise estimator used in this paper is under the first class. The smoothened power spectrum of noisy speech is computed using the following first-order recursive equation:

$$P(\alpha,k) = gP(\alpha-1,k) + (1-g)\left|Y(\alpha,k)\right|^2 \ldots\ldots \quad (5)$$

Where, P(á,k) is the smoothed power spectrum, á is the frame index, k is the frequency index, |Y(á,k)| 2 is the short-time power spectrum of noisy speech and g is a smoothing constant [8].

In any speech sentence, there are pauses between words which do not contain any speech, those frames will contain only background noise. The noise estimate can be updated by tracking only those noise frames [13]. To identify those frames, a simple procedure is used which calculates the ratio of noisy speech power spectrum to the noise power spectrum at 3 different frequency bands, each band correspond to the frequency bins of 1 KHz, 3KHz and the sampling frequency respectively. If all the three ratios are smaller than the threshold, that frame is identified as a noise only frame. Otherwise, if any one or all the ratios are greater than the threshold, that frame is considered as speech present frame.

The noise estimate is updated in noise only frames with a constant smoothing factor. In speech with noise frames the noise is updated by tracking the local minimum of noisy speech and the deciding speech presence in each frequency bin separately using the ratio of noisy speech power to its local minimum.

4.1 Tracking the Minimum of Noisy Speech

Various methods [9,10,13] were proposed for tracking the minimum of the noisy speech power spectrum over a fixed search window length. These methods were sensitive to outliers and also the noise update was dependent on the length of the minimum-search window. A different non-linear rule is used in our method for tracking the minimum of the noisy speech by continuously averaging past spectral values [3]. In this algorithm, if the value of the noisy speech spectrum in the present frequency bin is greater than the minimum value of previous frequency bin, then the minimum value is updated, else the previous value is maintained as it is.

4.2 Speech-Presence Detection

The approach taken to determine speech presence in each frequency bin is similar to the method used by Cohen [5]. Let the ratio of noisy speech power spectrum and its local minimum be defined as,

$$S_r(á,k) = \frac{P(á,k)}{P_{min}(á.k)} \quad \text{..... (6)}$$

This ratio is compared with a frequency dependent threshold. If the ratio is found to be greater than the threshold, it is taken as a speech-present frequency bin else it is taken as a speech-absent frequency bin. This is based on the principle that the power spectrum of noisy speech will be nearly equal to its local minimum when speech is absent. Hence the smaller the ratio, the higher the probability that it would be a noise-only region and vice versa. It can be noted from equation(5) that, a fixed threshold was used. From the above rule, the speech-presence probability, P(á,k), is updated using the following first-order recursion:

$$p(á,k) = (ä)\ p(á\ -1,k) + (1-\ ä\ )\ I\ (á,k) \text{ ..... (7)}$$

Where, ä is a smoothing constant. Note that the above recursion in equation (7) implicitly exploits the correlation for speech presence in adjacent frames. This may result in slight overestimate of the noise spectrum but will not likely have much effect on the enhanced speech. Using the above speech-presence probability estimate in equation (7), we compute the time-frequency dependent smoothing factor as follows:

$$a_s(á,k) = a_d + (1-a_d)\ p(á,k) \quad \text{.....} \quad (8)$$

Where, a_d is a constant.

4.3 Update of Noise Spectrum Estimate

Finally, after computing the frequency dependent smoothing factor a(á,k), the noise spectrum estimate is updated as

$$D(á\ ,k) = a_s(á\ ,k)D(á\text{-}1,k)+(1-a_s(á\ ,k))|Y(á\ ,K)|^2 \text{ ...(9)}$$

Where, D(á,k) is the estimate of the noise power spectrum. Hence, the overall algorithm can be summarized as follows: after classifying the frequency bins into speech present/absent, we update the speech-presence probability and then use this probability to update the time-frequency dependent smoothing factor. Finally the noise spectrum estimate is updated using the time–frequency dependent smoothing factor.

The estimated noise is then subtracted from the input noisy speech signal in each frequency band, finally the output of each band is combined by using overlap and add method (OLA) to get an estimate of clean speech (Enhanced speech).

5. PERFORMANCE EVALUATION

Objective measures are based on a mathematical comparison of the original and processed speech signals. The majority of objective quality measures quantify speech quality in terms of a numerical distance measure or a model of the perception of speech quality by the human auditory system. It is desired that the objective measures be consistent with the judgment of the human perception of speech [14]. However, it has been seen that the results obtained by objective measures are not highly correlated with those obtained by subjective measures. The signal-to-noise ratio (SNR) and the Itakura-Saito (IS) measure are two of the most widely used objective measures.

5.1 Signal-to-Noise Ratio (SNR)

The SNR is a popular method to measure speech quality. As the name suggests, it is a calculated as the ratio of the signal to noise power in decibels.

$$SNR_{dB} = 10\log_{10}\left(\frac{\sum_n S^2(n)}{\sum_n \left[S(n)-\hat{S}(n)\right]^2}\right) \quad \text{.....} \quad (10)$$

If the summation is performed over the whole signal length, the operation is called global SNR.

5.2 Itakura - Saito Distance (IS)

Itakura - Saito measure is one of the distance measures. It is based on the dissimilarity between the original and the enhanced speech and is computed between sets of LP (Linear Prediction) parameters estimated over synchronous frames. This measure is heavily influenced by spectral dissimilarity due to mismatch in formant locations, with little contribution from errors in matching spectral valleys. Lower the IS distance, better will be the quality of speech.

The average Itakura-Saito measure (as defined by the following formula) across all speech frames of the given sentence will be computed to evaluate the spectral noise subtraction algorithm.

$$d(a,b) = \frac{(a-b)^r R(a-b)}{a^r Ra} \qquad \text{.....} \quad (11)$$

Where, a is the vector for the prediction coefficients of the clean speech signal,vector R is the autocorrelation matrix of the clean speech signal and vector b is the prediction coefficients of the enhanced signal. A typical range of results for the IS measure is 1 to 10, with lower values indicating lesser distance and better speech quality.

6. EXPERIMENTAL RESULTS

Test samples are taken from SpEAR (Speech Enhancement Assessment Resource) database of CSLU (Center for Spoken Language Understanding) with different noises like white, pink, burst, cellular and car noise. The time domain results, global SNR and SNR improvements for the proposed method and comparison with other methods are shown below: (Figure 1a to c)

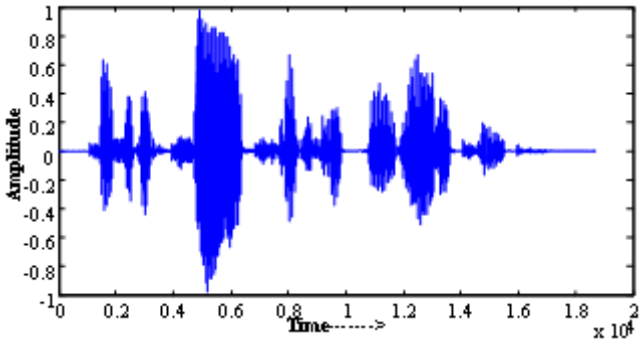

(a)

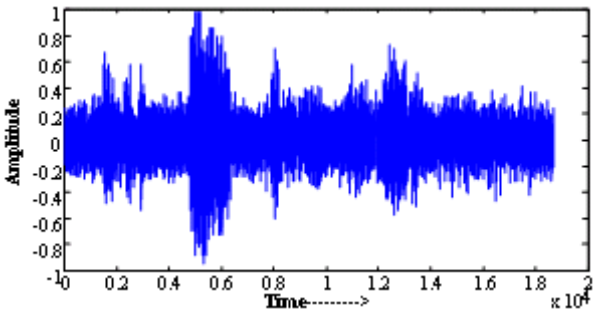

(b)

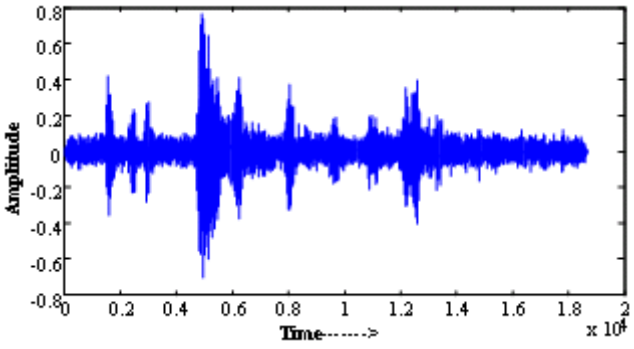

(c)

Fig.1 a) Clean speech (Female), b) Clean speech with car noise, c) Estimated (enhanced)clean speech

Signal recorded in room environment while uttering “hello hello hello hello hello hello”(male) was considered for test.The corresponding time domain results are shown in Figure 2.

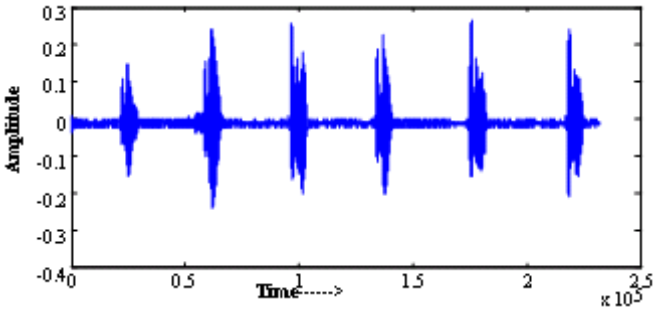

(a)

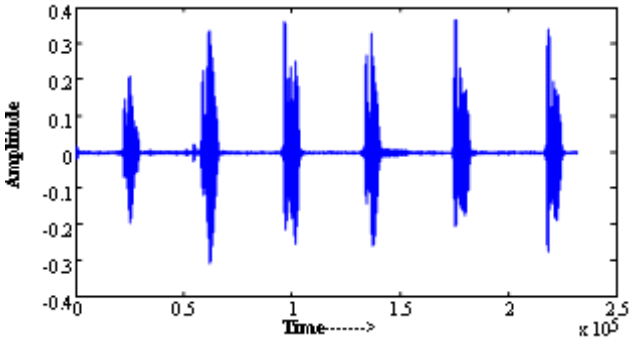

(b)

Fig.2 a) Noisy speech, b) Enhanced speech

Table 1 Obtained Global SNR and SNR Improvement for Different Noisy Inputs

Input Signal	Global SNR For Estimated Signal in dB	SNR Improvement in dB
White Stationary 0dB Noisy Signal	9.54	9.54
White Stationary 7 dB Noisy Signal	11.82	4.82
White Bursting 0 dB Noisy Signal	5.67	5.67
White Bursting 3 dB Noisy Signal	9.48	6.48
Pink Stationary 0 dB Noisy Signal	3.83	3.83
Pink Stationary 3 dB Noisy Signal	7.90	4.90
Cellular Noise 0 dB Signal	4.41	4.41
Car Noise With Global SNR of 0 dB	11.42	11.42

It can be observed from Figure 3, that the result obtained for proposed method is better than the conventional spectral subtraction method and SNR value is getting improved while increasing the number of bands. Table1shows the obtained Global SNR, SNR improvement for different noisy inputs and Table 2 shows the comparison of obtained global SNR with the output of other methods from which we conclude that the proposed method gives better results than other approaches.

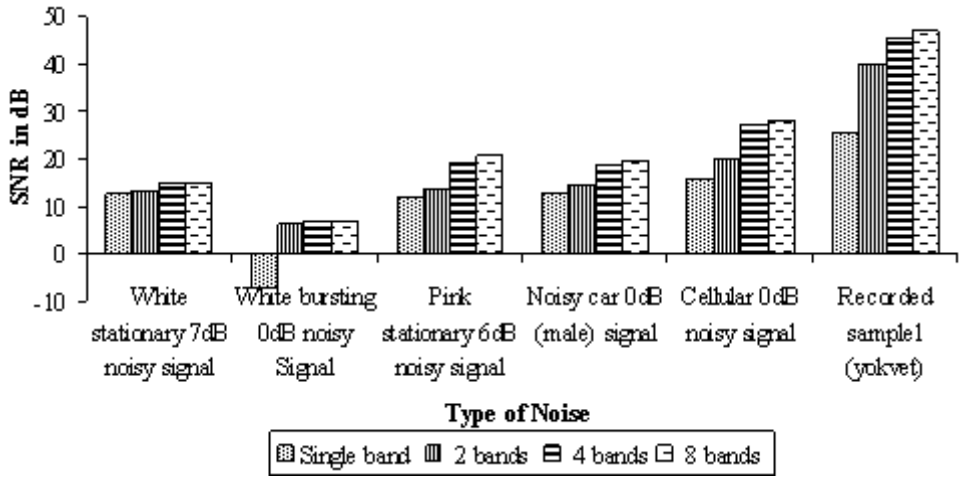

Fig.3 SNR with increasing number of bands

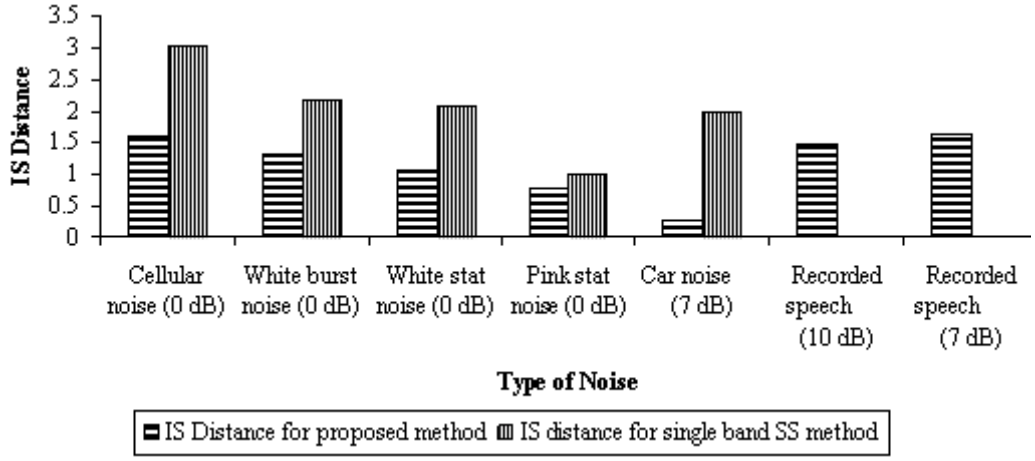

Fig. 4 Comparison of IS distance measure for different noisy inputs with conventional approach

Figure 4 shows that the IS distance measure for proposed method lower than conventional one and indicating better speech quality for the proposed method.

Table 2 Comparison of Global SNR of Proposed Method with Other Approaches

Signal	For Single Band Enhancement	For Multi Band Enhancement (4bands) (PROPOSED METHOD)	Spectral Subtraction Method	SNR Improvement in DEKF Algorithm
White Stationary 0 dB Noisy Signal	7.3520	11.9943	6.48	7.60
White Stationary 7 dB Noisy Signal	12.5618	14.7002	5.67	11.76
White Bursting 0 dB Noisy Signal	-7.1698	6.9705	6.94	9.95
White Bursting 3 dB Noisy Signal	-5.4098	4.1600	4.82	10.07
Pink Stationary 0 dB Noisy Signal	16.0103	23.0739	5.42	5.50
Pink Stationary 6 dB Noisy Signal	11.9217	19.3779	--	9.99
Noisy Car 0dB (male) Signal	12.4940	18.4940	--	--
Car Noisy (female) Signal	10.2432	16.8196	--	--
Cellular 0 dB Noisy Signal	15.9386	26.9860	--	5.39

7. CONCLUSION

The frequency dependent multi band spectral subtraction method provides a definite improvement over the conventional power spectral subtraction method and does not suffer from musical noise. The improvement can be attributed to the fact that the multi-band approach takes into account the non-uniform effect of non stationary noise on the spectrum of speech. The added computational complexity of the algorithm is minimal and it adapts with non stationary noise environments.

This algorithm can be implemented in real-time on a fixed point Digital Signal Processor (DSP) platform for evaluation in real-world conditions. Methods can be developed to preserve the transitional regions and unvoiced regions, which contain low speech levels.

REFERENCES

[1] J. Lim and A. Oppenheim, "Enhancement and Bandwidth Compression of Noisy Speech", Proceedings IEEE, Vol.67, December 1979, pp.1586-1604.

[2] S. Boll, "Suppression of Acoustic Noise in Speech Using Spectral Subtraction," IEEE Transactions Acoustics Speech, Signal Processing, Vol.27, April 1979, pp.113-120.

[3] G. Doblinger, "Computationally Efficient Speech Enhancement by Spectral Minima Tracking in Subbands", Proceedings Euospeech Vol.2, 1995, pp.1513-1516.

[4] Y. Ephraim and D. Malah, "Speech Enhancement Using a Minimum Mean-square Error Short-term Spectral Amplitude Estimator", IEEE Transactions on Acoustics Speech, Signal Processing, Vol.32, No.6, December 1984, pp.1109-1121.

[5] I. Cohen, "Noise Estimation by Minima Controlled Recursive Averaging for Robust Speech Enhancement", IEEE Signal Processing, Letter, Vol.9, No.1, 2002, pp.12-15.

[6] I. Cohen, "Noise Spectrum Estimation in Adverse Environments: Improved Minima Controlled Recursive Averaging", IEEE Transaction Speech Audio Processing, Vol.11, No.5, 2003, pp.466-475.

[7] H. Hirsch and C. Ehrlicher, "Noise Estimation Techniques for Robust Speech Recognition", Proceedings, IEEE International Conference on Acoustics, Speech Signal Processing, 1995, pp.153-156.

[8] L. Lin, W. Holmes and E. Ambikairajah, "Subband Noise Estimation for Speech Enhancement Using a Perceptual Wiener Filter", Proceedings, IEEE International Conference on Acoustics, Speech Signal Processing, I, 2003, pp.80-83.

[9] D. Malah, R. Cox and A. Accardi, "Tracking Speech-presence Uncertainty to Improve Speech Enhancement in Non-stationary Environments", Proceedings, IEEE International Conference on Acoustics, Speech Signal Processing, 1999, pp.789-792.

[10] R. Martin, "Spectral Subtraction Based on Minimum Statistics", Proceedings on Eurosip Signal Processing, 1994, pp.1182-1185.

[11] R. Martin, "Noise Power Spectral Density Estimation Based on Optimal Smoothing and Minimum Statistics", IEEE Transcations Speech Audio Processing, Vol.9, No.5, 2001, pp.504-512.

[12] M. Nilsson, S. Soli and J. Sullivan, "Development of Hearing in Noise Test for the Measurement of Speech Reception Thresholds in Quiet and in Noise", J. Acoust. Soc. Amer. Vol.95, No.2, 1994, pp.1085-1099.

[13] S. Rangachari, P. Loizou and Y. Hu, "A Noise Estimation Algorithm with Rapid Adaptation for Highly Nonstationary Environments", Proceedings IEEE International Conference on Acoustics Speech Signal Processing I, 2004, pp.305-308.

[14] S. Quackenbush, T. Barnwell and M. Clements, "Objective Measures for Speech Quality Testing," Prentice-Hall, 1988.

IMPLEMENTATION OF INFORMATION PROCESSING FOR ENTERPRISE APPLICATION INTEGRATION

R.S. Kumar[1] and K. Prakasan[2]

[1]Department of Computer Science and Engineering, Dr. N.G.P. College of Engineering, Coimbatore - 641 035, Tamil Nadu

[2]Department of Production Engineering, PSG College of Technology, Coimbatore - 641 004, Tamil Nadu

E-mail: rs_kmr@yahoo.com

(Received on 29 October 2008 and accepted on 05 January 2009)

Abstract

Industries world wide have long envisioned the need for a universal methodology to help alleviate the roadblocks presented by localized business practices and platforms. Standardization can alleviate trade barriers and enhance Collaborative Product Commerce when companies unite in developing methods that foster consistency, reliability, and efficiency. Current standards have not fully met these criteria. More emphasis is on Collaborative Design, Build and Maintenance. All the stakeholders in the Product life cycle need to contribute seamlessly. Necessary Information Technology (IT) tools are to be available to implement this extended enterprise integration. Various aspects of IT tools are undergoing vast changes. Standards are continuously evolving. Electronic Data Interchange (EDI) , Standard for Exchange of Product (STEP) model data are few of the evolving and complimentary standards. The evolution is towards incorporating XML – a universally accepted data integration tool. Product LifeCycle Management (PLM) is growing area where Enterprise Application Integration is very much required. An implementation towards the objective of Information processing is achieved through InfoEngine of Windchill software.

Keywords: *Collaborative Product Commerce, Information Technology, INFOENGINE, XML*

1. INTRODUCTION

The manufacturing enterprises face new challenges. New products hit marketplace keenly competing with the existing ones. There is no chance of error in product design. Product life cycles which used to be measured in years are now drastically cut into few months. A web-centric collaborative technology has helped business acquire increased globalization.

The internet has fostered the growth of Collaborative Product Commerce (CPC). CPC allows the users, sellers, buyers and business partners to form a virtual enterprise by way of collaboration. The result - successfully complete in the market place.

Research shows 70% of the costs of production are locked during the development phases of a product – CPC is well positioned to address this large potential in cost savings. CPC allows more people to contribute in the early stages of product lifecycle, so that costly prototype and mass production changes can be avoided

2. LITERATURE REVIEW OF COLLABORATIVE PRODUCT COMMERCE

The vision of collaborative business is a seamless flow of information with everyone sharing the information as shown in Figure 1. The Aberdeen Group [1] defines CPC as: "A class of software and services that uses Internet Technologies to permit individuals- no matter what role they have in the commercialization of a product, no matter what computer-based tools they use, no matter where they are located geographically or within the supply net - to collaboratively develop, build and manage products through out their entire life cycle. Collaborative Product Commerce (CPC) uses Web Technologies during all phases of product development".

The CPC is based on the Principles of services [14, 15, 16] on demand. A CPC environment is comprised of a combination of best practices and technologies such as Product Data Management (PDM), collaboration, and visualization, Enterprise Application Integration (EAI). Product Lifecycle Management (PLM) and synthesize

product information from existing Supply Chain Management (SCM), Enterprise Resource Planning (ERP), and Customer Relationship Management (CRM).

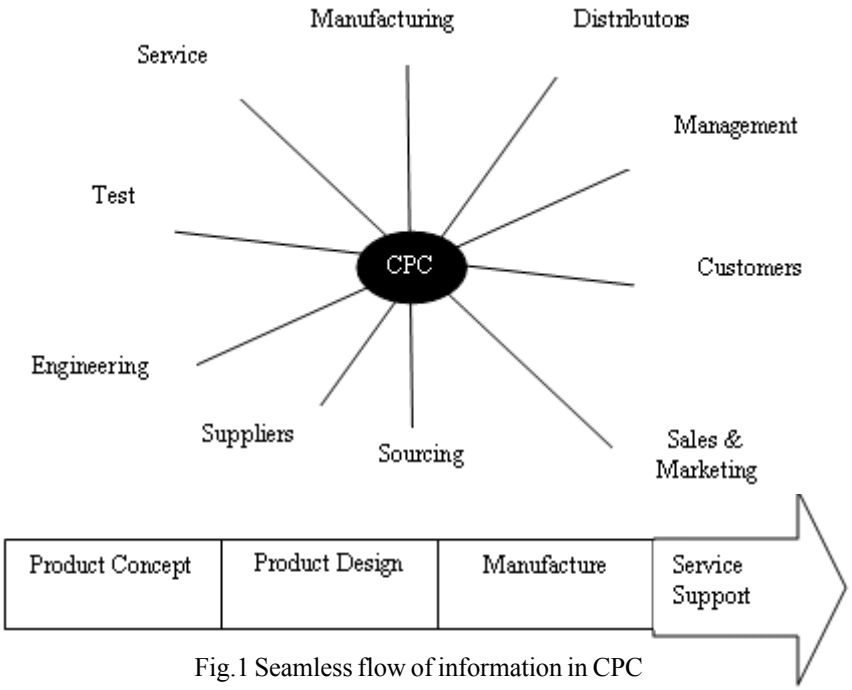

Fig.1 Seamless flow of information in CPC

3. COLLABORATION TECHNIQUES

Collaboration involves a number of different technologies [7] that include

- Web browser, email to correspond messages between members.
- Audio conferencing to provide verbal communication.
- Real –time Teleconferencing.
- Collaborative visualization tools for synchronous 2D, 3D view and markup.
- Data Translation to enable CAD data to be imported into the collaboration Tools.
- System Administration tools to control access and manage collaborative data and relationships.

4. REQUIREMENTS OF IT ENABLED CPC ENVIRONMENT

The CPC solutions should offer high levels of service to a large number of web-based users. The requirements [5, 12] are like any other large web-services application. Figure 2 depicts a generic framework of CPC [14]. Some of the common requirements are

- Accessibility from both intranet and extranet. The external supplier and business partners are now part of the expanded design team but geographically separated from the enterprise.
- Access to legacy enterprise data. The existing solutions like ERP, PDM is needed to be integrated with the CPC solution.
- Security Information is made available on need-to-know basis. Users see only up-to-date information.
- Applications are available on a continuous basis to the extended design team.
- Performance and scalability users can be added easily over time. New business requirements can also drive the development of additional application services.
- Open Standard Software. The software standards software enables creation of reusable software components that can be assembled for the end-user.
- Simplify systems management. The software environment based on open management environment used in the CPC implementation provides a means to simplify management of the hardware supplied by multiple Vendors and located at multiple geographic locations.

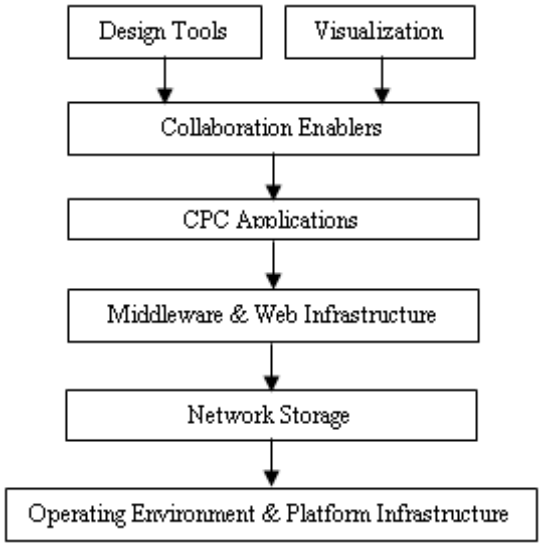

Fig. 2 The CPC Framework

5. STANDARDS

Industries worldwide spend billions of dollars as a result of poor interoperability between computer – aided engineering software tools [10]. The networked organizations today are only partially integrated islands of information. They tend to have a static view of the use of information rather than viewing CPC as a holistic control system, to continuously adapt to the business and operational success [4].

Currently e-commerce is mainly supported by Electronic Data interchange (EDI) and Web- based electronic catalogs. Obvious problem of Web-based electronic catalog is the lack of interoperability [8]. In 2001, more than 2 trillion US dollars were transacted via traditional EDI architecture. Many of these enterprises have been reluctant to extend this EDI solution into XML based implementations. We need to move from product data exchange to product information exchange and eventually to product knowledge exchange [6]. This exchange will take place over the web (Figure 3). For this, we require both syntactic and semantic interoperability of various systems.

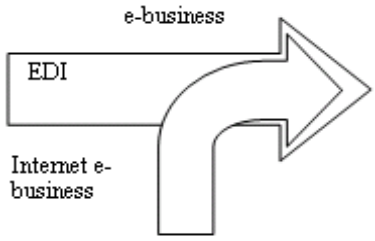

Fig. 3 EDI and e-business coexists

Standards are required for architecture frameworks [13] such as Zachman Framework and Department of Defense Framework (DODAF). Standards such as ISO 10303, informally known as Standard for Exchange of Product model data (STEP), National Institute of Standards and Technology (NIST) model MOKA (Methodology and tools Oriented to knowledge based engineering Application) address the content issues. Prime examples of Information modeling standards are Express, Resource Description Format (RDF), Unified Modeling Language (UML), Ontology Web Language (OWL). Industry Consortia, standard organizations and software vendors have come out with Electronic Business using Extensible Markup Language (ebXML). Information exchange standards are EDI, Electronic Data Interchange for Administrators, Commerce and Transport (EDIFACT), Extensible Markup Language, simple Object Access Protocol (SOAP). Extensions to Extensible Markup Language have been in the area of electronic exchange to replace traditional EDI standards with ebXML standards.

Through the 3D Industry Forum (3DIF) Intel is working with other companies to develop standards for 3D data. The Universal 3D (U3D), X3D an open standard XML enabled 3D file format are intended to simplify the transformation of complex 3D data into a standard format that can be streamed, compressed and viewed.

Traditional description and implementation methods for STEP are not as popular or well known as Web-Oriented technologies, such as XML and UML. STEP provides significant standardized content models and XML, UML provide enhanced implementation methods [2]. Combined they are as powerful force for lowering the barriers to the wide spread digital exchange and sharing of technical information [11]. Emerging XML, UML based STEP implementations (Figure 4) promise greater interoperability [3].

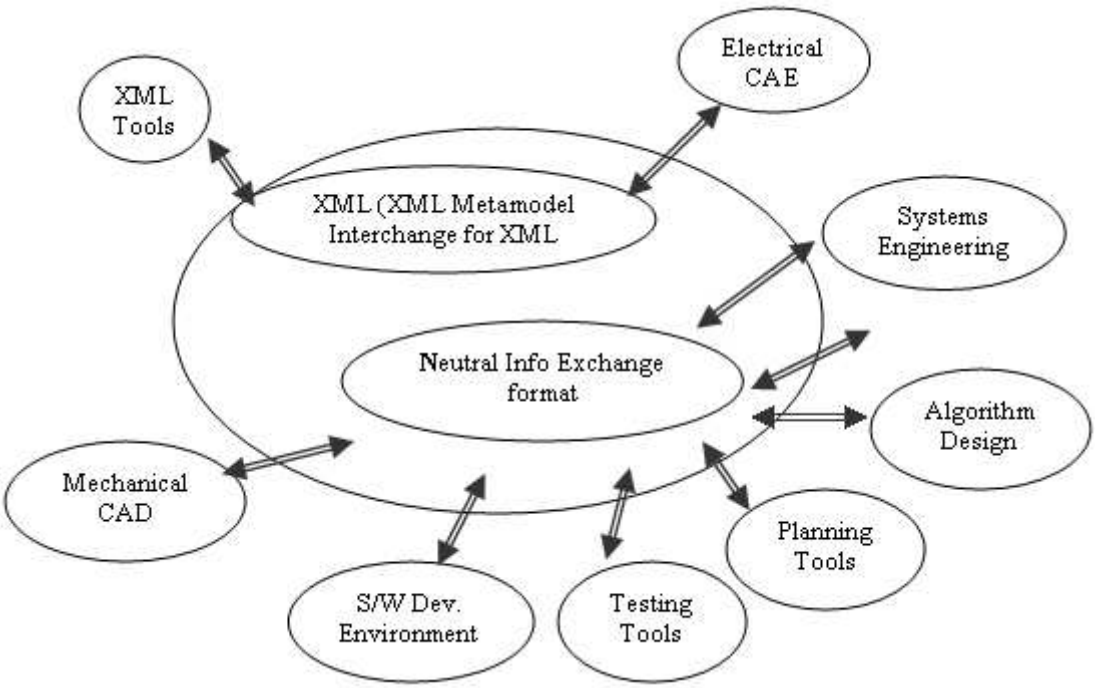

Fig. 4 Complementary use of STEP, UML, and XML

6. IMPLEMENTATION OF INFORMATION PROCESSING BY INFO*ENGINE

INFO * Engine available in windchill is a web-based [20] request broker. The method of EAI in Windchill is by the use of Webjects, which represent the breaking down of a major business task into subtasks. These are Hypertext Markup Language, like tags and are inserted in the task definitions written in Extensible Markup Language and can be called in workflow expressions used in the Product Lifecycle Management. When invoked, they will execute the expressions and return the expected results to the browser. An example can be a query for a part with its effectivity, revision, associated documents, CAD documents, quantity available in the stores, supplier details and price. These are a few attributes that may be expected at a higher level in the organization. This task can be broken down as

- Retrieve information from a PDM system like Windchill pertaining to effectivity, references, revision level, etc.,
- Retrieve information from an ERP system for other attributes like supplier, quantity available and price and
- Group these two sets of information into a single group for display in an appropriate format. The information at the end of each activity (subtask) is stored in a virtual database (VDB), which is also called a group (Figure 5).

Virtual data base of Info*engine (VDB)

(Webject 2)
Group 2

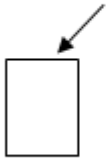

Part Number	Part Name	Supplier	Qty
6545645	Special part	LMW	10
5454654	HUB	PSG	22
8787877	BRAKE ASSY	ABC	15
4544658	CAP	ELGI	7
5456454	PIN	PTC	15
5458787	SCREW	NTC	2
7878789	CABLE	XYZ	11

Fig. 5 Information Retrieval from ERP System and its storage in VDB

The structure of the webject used may look like:

```
<html>
<body>
<webject name = query-objects type = obj>
<param name  = instance data = pdmadapter/>
<param name = class data = parttable/>
<param name = attribute data = revision level/>
<param name = attribute data = partname/>
<param name = attribute data = partnumber/>
<param name = where data = type = special part/>
<param name = group-out data = pdminfo/>
------------------------------webject1-------------------------
<webject name = query-objects  type = obj>
<param name = instance data = erpadapter/>
<param name = class data = parttable/>
<param name = attribute data = price/>
<param name = attribute data=supplier/>
<param name = attribute data = quantity/>
<param name = attribute data = partname/>
<param name = attribute data=partnumber/>
<param name = where data = type = special part/>
<param name = group-out data = erpinfo/>
------------------------------webject2-------------------------
<webject name= join-groups type = grp>
<param name = group-in data = pdminfo/>
<param name = group-in data = erpinfo/>
<param name = group-out data = combinfo/>
</webject>
------------------------------webject3-------------------------
</body>
</html>
```

The corresponding task may look like this. In this task, the above webjects are inserted.

```
<?xml version  =  "1.0" standalone = "yes"?>
<!doctype process>
<process  name = " get combined info">
<description>

This is to retrieve a combined info using ERP system and PDM system

</description>
<webject>---------</webject>
<webject>---------</webject>
<webject>---------</webject>
</process>
```

When this task is saved in the task directory of Info*Engine and the Uniform Resource Locator (URL) representing this XML file is invoked from the browser, the output in XML is produced. Further this data can be formatted with the help of display webjects and XSL for a suitable presentation.

7. CONCLUSION

Too many standards are in the market place. Still the fruits of CPC are only partially available for the product development industry. The shift from proprietary solutions to Web - enabled infrastructures is inevitable. Solutions like EDI will not disappear. They will coexist with existing standards. New architectures have to complement earlier standards and enhance them. So it will be more of evolution rather than technical revolution. XML is all over the interoperability solutions. An implementation of Enterprise Application Integration using XML is achieved through INFO*ENGINE.

REFERENCES

[1] Aberdeen Group Inc, PLM – It's for Any Manufacturer Striving for Product Excellence, An Executive White Paper, July, 2002.

[2] C. Burkett William, "Product Data Markup Language: A New Paradigm for Product Data Exchange and Integration", Computer Aided Design, Vol.33, 2001, pp.489-500.

[3] Chaudhari Avinash and Patil Venkatesh, "Future Trends in Collaborative Product Data Management Systems", Paper Presented at Product Data Technology, Turin, Europe, 2002, May 7-9.

[4] Chen David and Doumeingts Guy, "European Initiatives to Develop Interoperability of Enterprise Applications-Basic Concepts", Framework and Roadmap, Annual Reviews in Control, Vol.27, 2003, pp.153-162.

[5] CIMdata, Program review of SAP's my SAP Product Life Cycle Management cPDM Program, 2001, October.

[6] Dr. Hale Jacques, "From EDI to Web Services- The Evolution of E- Commerce", Butler Group, White Paper, June 2002,

[7] IBM Business Consulting Services, Now or Never, The Automotive Collaboration Imperative, Future Series, 2002.

[8] Jinsoo Park and Sudha Ram, "Information Systems Interoperability: What Lies Beneath?", ACM Transactions on Information Systems, Vol.22, No.4, 2004, pp.595-632.

[9] S. Linthicum David, "Remember ebXML, XML Journal", 2004, Feb, 30-31.

[10] Mackrell John, "Exchanging Product Design Data", Business Benefits of the Collaboration Gateway, 2004, April, http//www. CIMdata.Com

[11] S. Peak Russell, Lubell Joshua, Srinivasan Vijay and C. Waterbury Stephen, "STEP, XML and UML Complementary Technologies", Journal of Computing and Information Science in Engineering, ASME, Vol. 4, Dec, 2004, pp.379-390.

[12] Seger Arie and Bichler Martin, "Component Based Electronic Commerce", Hand Book on Electronic Commerce, Springer 2000.

[13] Subramanian Eswaran, Rachuri Sudarsan, J. Fenves Steven, Foufou Sebti and D. Sriram Ram, "Product Lifecycle Management Support: A Challenge in Supporting Product Design and Manufacturing in A Networked Economy", International Journal of Product Life Cycle Management, Vol.1, No.1, 2005.

[14] Sun Microsystems, Collaborative Product Commerce (CPC) Solutions from Sun, White paper, November, 2001.

[15] Sun Microsystems, Dot-com your Manufacturing Enterprise with Collaborative Product Commerce, White paper.

[16] Sun Microsystems, Collaborative Product Commerce (CPC) Solution with PTC Windchill, A Solution Set White Paper, April., 2001.

[17] Szykman Simon, J. Fenves Steven, Keirouz Walid and B. Shooter Steven, "A Foundation for Interoperability in Next – Generation Product Development Systems", Computer Aided Design, Vol.33, 2001, pp.545-559.

[18] http://www.ibm.com/xml.

[19] http://www.ebXML.org.

[20] Windchill R5 INFO*ENGINE users Guide

EXPERIMENTAL INVESTIGATION ON JATROPHA BIODIESEL IN A DI DIESEL ENGINE WITH EGR

E. Rajasekar[1], R. Venkatachalam[2], R. Subramanian[3], K. Mayilsamy[4] and N. Nedunchezhian[5]
[1,2,3&5]Department of Automobile Engineering, [4]Department of Mechanical Engineering
Institute of Road and Transport Technology, Erode District - 638 316, Tamil Nadu
E-mail: rajasekarirtt@yahoo.co.in
(Received on 02 November 2008 and accepted on 07 January 2009)

Abstract

Biodiesel has the potential to provide a reliable and a cost effective alternative to India's increasing future energy demands. Due to rapid industrialization and increased number of vehicles on the road, the energy needs of India are increasing rapidly. The present study aims to study the prospects and opportunities of using indigenous biodiesel produced from Jatropha curcas plant (jatropha methyl ester - JME) as fuel in diesel engines. To meet the stringent emission norms in biodiesel fueled diesel engines, a low cost technique of exhaust gas recirculation (EGR) was effectively used in this study. NOx emissions were reduced when the engine was operated with B20 (20% JME blend) under hot EGR levels of 0-20%. The EGR level was optimized as 15% based on adequate reduction in NOx emissions, minimum possible smoke, HC emission and reasonable brake thermal efficiency.

Keywords: *Alternative Fuel, Bio-Diesel, EGR, Jatropha Methyl Ester, NOx Reduction*

1. INTRODUCTION

The higher efficiency of compression ignition, direct injection diesel engines compared to spark ignited gasoline engines makes them desirable for automotive and truck vehicles, especially now with ever increasing crude oil prices, driven mainly by significant increases in demand. The doubling times of vehicles worldwide would be reduced from 26 years to 6-10 years due to the emergence of active consumer economies from nations such as China, India, Mexico and former USSR [1]. Biodiesel is an environmental friendly alternative fuel to the fossil diesel and holds promise to mitigate the future energy needs and also to usher economic prosperity in the poor and backward areas of India [2]. There is an immense potential for jatropha biodiesel plant cultivation in the country. Jatropha biodiesel is now successfully used by Indian Railways, Mahindra & Mahindra tractors, Haryana roadways, Daimler-Chrysler cars etc.

2. PROPERTIES OF JATROPHA CURCAS OIL

The fatty acid composition of jatropha curcas classifies it as a linoleic or oleic acid type, which are unsaturated fatty acids, as shown in Figure 1. Palmitic (16:0) and stearic (18:0) are the two most common saturated fatty acids, with every vegetable oil containing at least a small amount of each. Studies involving the use of raw vegetable oils as a replacement fuel for diesel fuel indicate that a diesel engine can be successfully fueled with 100% vegetable on a short term basis [3]. However, long term engine durability studies showed that fueling diesel engines with 100% vegetable oil causes engine failure due to engine oil contamination, stuck piston rings and excessive carbon build-up on internal engine components, injector coking, poor fuel injector spray patterns and flow problems due to the very high viscosity [4,5]. A short term 50 hours endurance experiment with neat jatropha curcas oil on a single cylinder water cooled direct injection CI engine was conducted and the observed engine coking are presented in Figure 2 and Figure3. All these problems can be reduced by converting the raw oil into its methyl or ethyl esters which are formed by transesterification process.

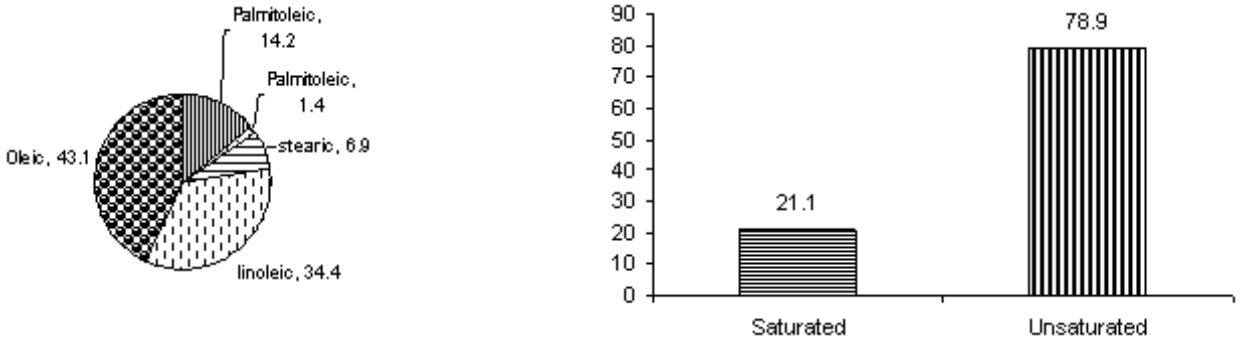

Fig.1 Fatty acid composition of jatropha curcas oil

Fig. 2 Coking on piston

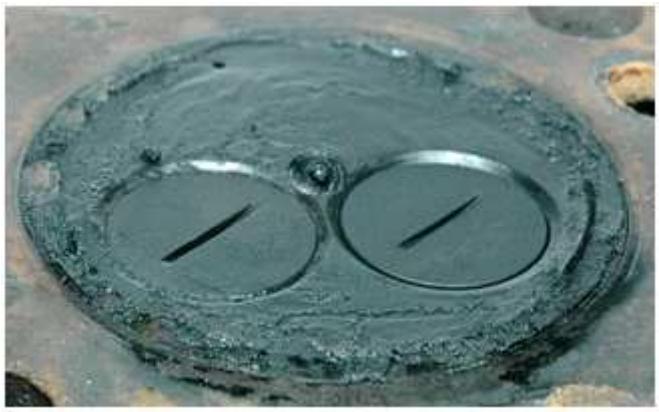

Fig. 3 Coking on cylinder head

2.1 Production Process of JME

Considering the availability of jatropha, pungamia, neem and other vegetable oils in the local areas, biodiesel processor based on the transesterification process was designed and fabricated at IRTT, Erode, India. The process employed is the base-catalyzed process.

Raw jatropha curcas oil was pre-heated to remove water contents at about 100°C in an appropriate vessel. Methanol and sodium hydroxide were then mixed in a separate vessel to prepare sodium methoxide. Sodium methoxide was added to the pre-heated oil of jatropha curcas. The Oil-methoxide mixture was then agitated for one hour at 60°C and allowed to settle under gravity in a separating funnel. The separated ester was purified by washing it gently with warm water and allowed to settle under gravity for 8 hours.

2.2 Properties of JME

Biodiesel is characterized by determining its density, viscosity, higher heating value, cetane number, cloud and pour points, characteristics of distillation, flash point and combustion points according to ISO norms. The higher heating values of biodiesel fuels, on a mass basis, are 10% lower than petroleum diesel fuel.

Jatropha methyl ester synthesised from jatropha curcas oil by the use of alkaline catalyst conforms to ASTM, European and proposed BIS specifications as shown in Table 1. The kinematic viscosity of jatropha curcas oil is 10 times more than that of diesel at 40°C and after esterification, it was reduced to 4.4 cSt, which is comparable with petroleum diesel of 3.5 cSt at 40°C. The calorific value of JME is 38.45 mJ/kg, which is less than that of diesel (42 mJ/kg), but its higher density tends to counteract the effects of the lower energy content. Unlike petroleum diesel, biodiesel is biodegradable and non-toxic, and it significantly reduces toxic product and after emissions when burned as a fuel [6,7].

Table 1 Physico-Chemical Properties of JME

Sl. No.	Property (Units)	ASTM 6751 Test Methods	ASTM 6751 Limits	IS15607 Test Methods	IS15607 Limits	JME
1	Flash Point (°C)	D-93	Min.130	IS 1448 P:21	Min.120	1.63
2	Viscosity @ 40°C (cSt)	D-445	1.9-6.0	IS 1448 P:25	2.5-6.0	4.40
3	Sulphated Ash (% mass)	D-874	Max.0.02	IS 1448 P:4	Max.0.02	0.002
4	Sulphur (% mass)	D-5453	Max.0.05	ASTM D 5453	Max.0.005	0.004
5	Cloud Point (°C)	D- 2500	N.A	IS 1448 P:10	N.A	4
6	Cu Corrosion	D-130	Max. 3	IS 1448 P: 15	Max. 1	1
7	Cetane Number	D-630	Min. 47	IS 1448 P:9	Min. 51	57.1
8	Water and Sediment (Vol. %)	D-2709	Max. 0.05	D-2709	Max. 0.05	0.05
9	CCR 100% (% Mass)	D-4530	Max. 0.05	D-4530	Max. 0.05	<0.01
10	Neutralization Value (mg, KOH/gm)	D-664	Max. 0.80	IS 1448 P:1	Max. 0.50	0.48
11	Free Glycerin (% Mass)	D-6584	Max. 0.02	D-6584	Max. 0.02	0.01
12	Total Glycerin (% Mass)	D-6584	Max. 0.24	D-6584	Max. 0.25	0.02
13	Phosphorus (%Mass)	D-4951	Max. 0.001	D-4951	Max. 0.001	<0.001
14	Distillation Temperature	D-1160	90% at 360°C	Not under spec.	---	90%
15	Oxidation Stability, Hrs	N.A	N.A	EN 14112	Min. 6h	3.23

3. PERFORMANCE CHARACTERISTICS OF JME-DIESEL BLENDS

Experiments were conducted in a four-stroke single cylinder direct-injection water-cooled CI engine. Transient exhaust smoke was measured using the AVL smoke meter. Oxygen and NOx concentration in exhaust were measured by electrochemical method using the AVL Digas 4000 analyzer. Exhaust HC, CO and CO2 concentrations were measured by NDIR method with the same analyzer.

3.1 Brake Thermal Efficiency (BTE)

The variation of BTE of the engine with various diesel-JME blends with engine load is shown in Fig. 4.

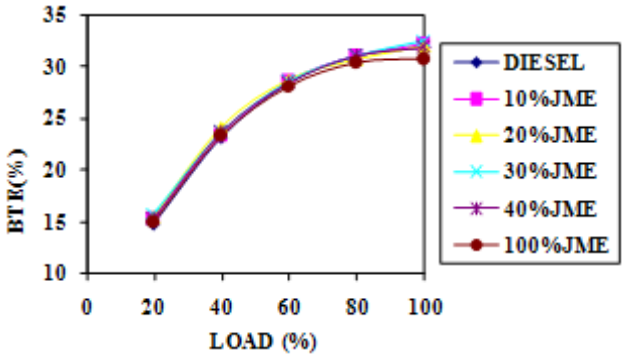

Fig. 4 Effect of engine load on BTE

The effect of load on BTE shows a steady increase in efficiency as the load increases. The maximum BTE of 31.1% was observed with 100% JME operation compared to 31.9% for diesel. The BTE was slightly lower than diesel fuel for different diesel-JME blends which was due to poor mixture formation as a result of low volatility, higher viscosity and density of JME.

3.2 Brake Specific Energy Consumption (BSEC)

The variations of BSEC with load for different fuels are presented in Figure 5.

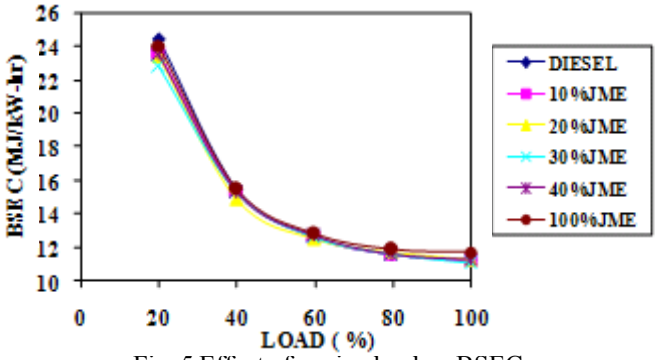

Fig. 5 Effect of engine load on BSEC

BSEC decreased with increase in load for all tested fuels and this could be due to the higher percentages of increase in brake power with load as compared to energy consumption. For various diesel-JME blends the observed BSEC was on par with diesel fuel.

4. EMISSION CHARACTERISTICS OF JME-DIESEL BLENDS

4.1 CO and HC Emissions

The effects of engine load on CO and HC emissions for all fuels tested are shown in Figure 6 and 7 respectively. When 100% JME is used, the dissolved oxygen in the fuel may promote a more complete combustion and effectively reduce the formation of unburned HC and CO emissions.

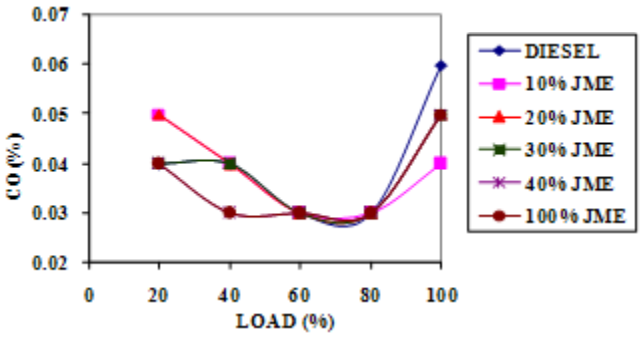

Fig.6 Effect of engine load on CO emission

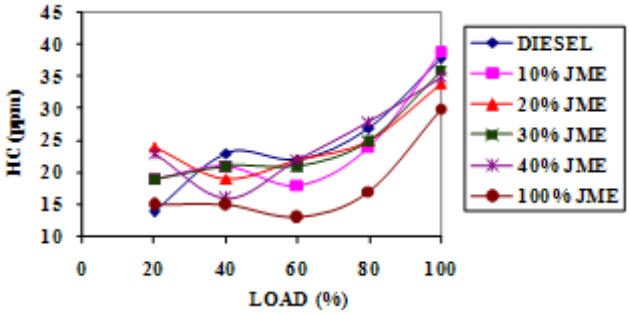

Fig. 7 Effect of engine load on HC emission

4.2 NOx Emission

The effect of engine load on NOx emission for all tested fuels is shown in Figure 8. Higher oxygen content in biodiesel tends to react with nitrogen component in the surrounding air, which results in larger amount of NOx formation [8]. Considerable reduction in NOx emission for diesel-JME fuel blends and 75-100 ppm reduction for 100% JME operation in all loads was observed.

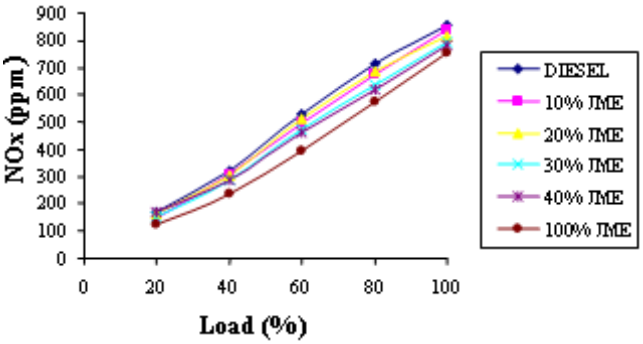

Fig. 8 Effect of engine load on NOx emission

4.3 Smoke Emission

Figure 9 depicts the effect of engine load on smoke opacity. In part load conditions as the JME content in the blend increased, smoke opacity increased by about 4-6% than petroleum diesel. This was due to the higher viscosity of JME at low temperatures which reduced the rate of spray atomization and at low starting temperatures fuel evaporation was more difficult. These lead to worse fuel/air mixing and thus to more intense soot formation. At medium and high loads, a significant smoke reduction was observed when diesel-JME fuel blend was used and this reduction was even higher (6-8%) as the JME concentration in the blend increased.

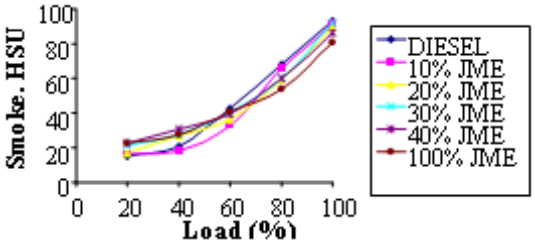

Fig. 9 Effect of engine load on smoke emission

5. NO_x REDUCTION STRATEGIES

Even though some cetane improving additives are capable of reducing NOx level, the amount of reduction is reported to be inadequate. Moreover, most of the additives are expensive and can promote auto-oxidation in biodiesel [9]. Retarded injection is an effective method employed in diesel engines for NOx control. However, this method leads to increased fuel consumption, reduced power, increased HC and excess smoke. Water injection on the other hand is leads to corrosion. Hot EGR, a low cost technique of exhaust gas recirculation, is effectively used in this program to meet the stringent emission norms. Cooled EGR method even though effective, is expensive and difficult to implement [10].

6. EGR IN BIODIESEL FUELED ENGINE

Recently EGR has emerged as a necessary means to meet the United States Environmental Protection Agency (EPA) NOx regulations for heavy-duty diesel engines with the implementation of the 2004 regulations where NOx release is restricted to 2.5 g/bhp-h [11]. Experiments were conducted at a speed of 1800 rpm. Static injection timing of 23 degree bTDC was used for diesel and 20% JME-diesel blend (B20). The EGR flow was controlled manually by a valve and the EGR level was determined volumetrically as the percentage reduction in volume flow rate of air at a fixed engine operating point.

6.1 Effects of EGR

EGR reduces oxygen concentration and peak combustion temperature, which results in reduced NOx level. On the other hand EGR significantly increases smoke emission, fuel consumption and reduces thermal efficiency unless suitably optimized [12,13]. The use of EGR was more effective (higher NOx reduction with lower increase in smoke) in the case of B20 combustion compared to diesel.

6.2 Brake Thermal Efficiency

Figure 10 shows the comparison of BTE for B20 and diesel with EGR at 50% and 100% loads. Comparable efficiency values were obtained for both fuels. BTE is reduced from 32% to 28.5% for B20 at 100% load and from 28.8% to 25.9% at 50% load at 20% EGR. But irrespective of EGR rate, BTE of B20 is higher than that of diesel fuel.

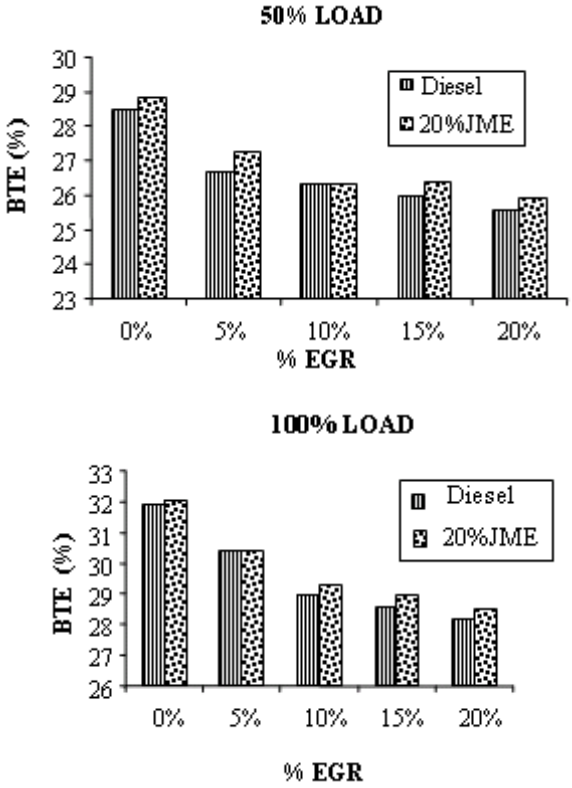

Fig. 10 Effect of EGR on thermal efficiency

6.3 Brake Specific Energy Consumption

To compare fuels of different calorific value, BSEC is more effective than BSFC. Figure 11 indicates the variation of full load BSEC with EGR rate at 50% and 100% loads. BSEC of B20 was slightly lower for all levels of EGR than that of diesel fuel. This is presumably due to higher calorific value and lower boiling point of B20.

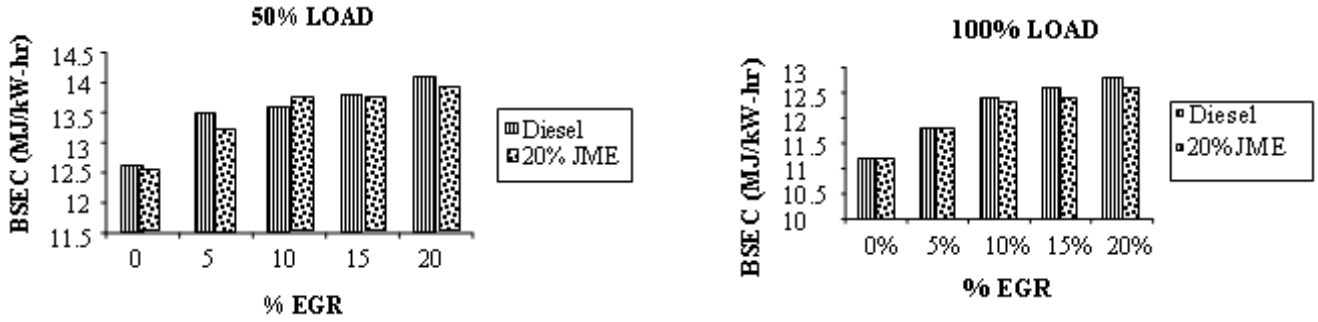

Fig. 11 Effect of EGR on brake specific fuel consumption

6.4 HC Emission

Figure 12 shows the variation of HC emission with EGR rate at 50% and 100% loads. HC emission increases from 24 to 35 ppm at 50% load and from 34 to 45 ppm at 100% load for B20 with 20% EGR. The increase in HC was not significant as the EGR rate was increased for biodiesel, due to the oxygen content in biodiesel compensating for oxygen deficiency and promoting complete combustion. However, 15% and 45% reduction in HC emission at 50% and 100% load respectively was observed for B20 than in diesel fuel with 15% EGR.

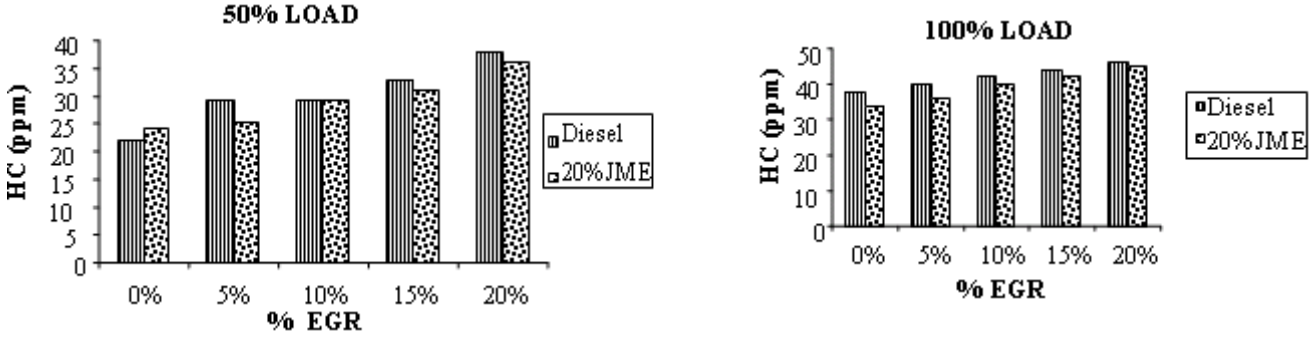

Fig. 12 Effect of engine load on hydrocarbon emission

6.5 NOx Emission

Figure 13 shows the variation of NOx emission with EGR rate at 50% and 100% loads. NOx emission from B20 at both loads, for EGR rates of 5 to 20%, was lower compared to that of diesel fuel for the same EGR rates. NOx emission decreases from 510 to 240 ppm (53% reduction) at 50% load and from 800 to 450 ppm (44% reduction) at 100% load for B20 with 15% EGR. One reason for the higher NOx reduction is probably the different composition of the engine exhaust gas obtained from the combustion of JME. Even though 15% and 20% EGR were able to reduce NOx by a large amount, considerable increase in smoke emission and BSEC were observed.

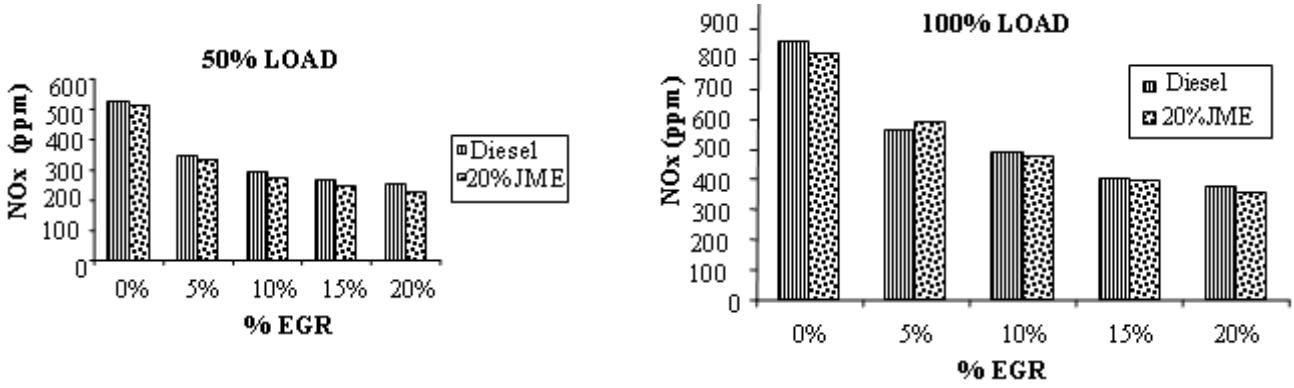

Fig. 13 Effect of engine load on oxides of nitrogen

6.6 Smoke Emission

Figure 14 depicts the variation of smoke capacity with EGR rate at 50% and 100% loads. With 15% EGR, only 5.5% increase in smoke was observed for B20 at full load. By using higher EGR rate, there was considerable increase in smoke opacity level due to reduction in oxygen available for combustion. EGR level was optimized as 15% based on adequate reduction in NOx emission, minimum possible smoke, HC emission and reasonable brake thermal efficiency.

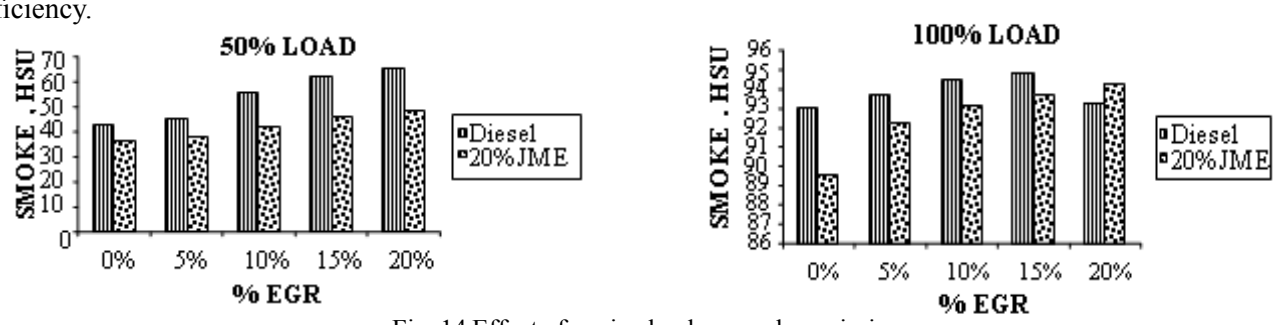

Fig. 14 Effect of engine load on smoke emission

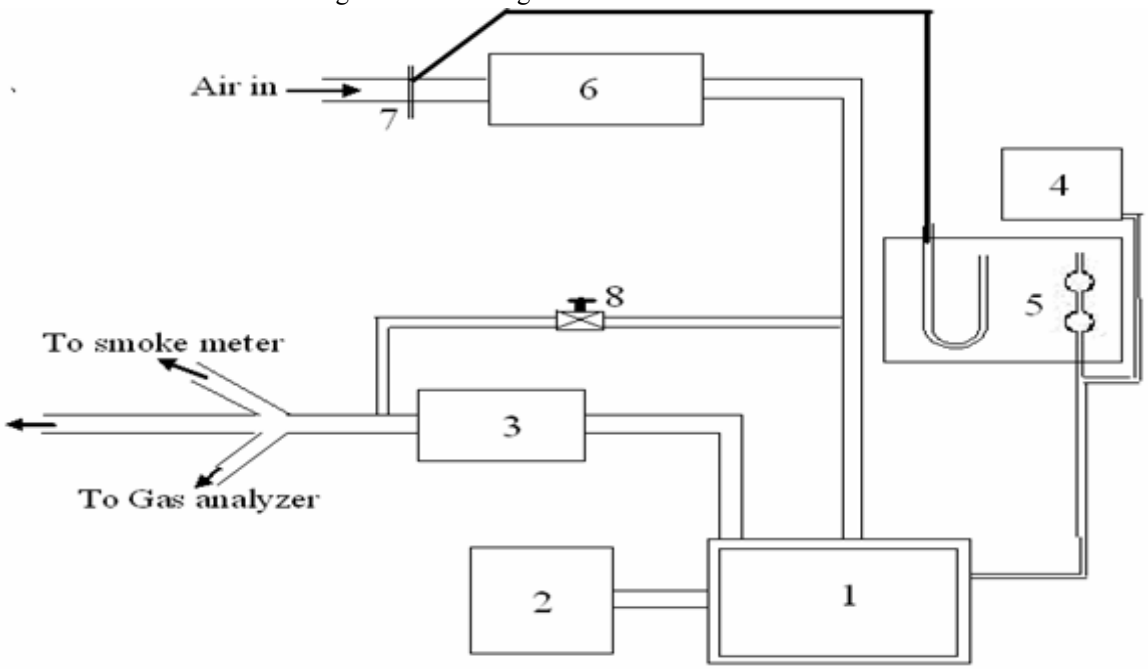

Appendix-1. Experimental setup

1. Engine 2. Dyanamometer 3. Muffler 4. Fuel tank 5. Fuel metering unit 6. Inlet air tank 7. Orifice 8. EGR valve

Appendix-2 Test engine with EGR pipe lines

7. CONCLUSIONS

The following are the main conclusions based on the present experimental investigation:

- Raw vegetable oils can be used as 100% replacement fuel for diesel fuel on a short-term basis. However, long term engine durability studies show that 100% vegetable oil operation causes engine failures.
- Experimental work carried out shows that the performance of JME fuel is on par with petroleum diesel fuel and emission characteristics of JME are much better than petroleum diesel fuel.
- With experimental investigations it was found that 15% EGR gives optimum results for B20. Drastic reduction of NOx emission by 53% and 44% was obtained with 15% EGR rate for B20 at 50% and 100% load respectively.
- Biodiesel and in particular jatropha biodiesel, can be a valuable and interesting alternative diesel fuel due to its similar performance like diesel fuel and its better emission characteristics than diesel fuel.

REFERENCES

[1] Ayhan Dermirbas, "Progress and Recent Trends in Biodiesel", Prog. Energy Combust. Sci.Vol.33, 2007, pp.1-18.

[2] S. Biswas, N. Kaushik and G. Srikanth, "Biodiesel: Technology & Business Opportunities - An Insight, Report Submitted to Technology Information, Forecasting and Assessment Council (TIFAC)", Department of Science and Technology, New Delhi. 2005.

[3] Deepak Agarwal and Avinash Kumar Agarwal, "Performance and Emissions Characteristics of Jatropha Oil (Preheated And Blends) in a Direct Injection Compression Ignition Engine", Applied Thermal Engineering. Vol.27, 2007, pp.2314-3.

[4] Sudesh Bekal and T.P. Ashok Babu, "Bio-fuel Variants for Use in Ci Engine at Design and Off-Design Regimes: An Experimental Analysis", Fuel Vol.87, 2008, pp.3550-61.

[5] R.J. Crookes, "Comparative Biofuel Performance in Internal Combustion Engines", Biomass & Bioenergy Vol.30, 2006, pp.461-8.

[6] ToshioShudo, Atsushi Fujibe, Motoharu Kazahaya, Yuzo Aoyagi, Hajime Ishii and Yuichi Goto, "The Cold Flow Performance and the Combustion Characteristics with Ethanol Blended Biodiesel Fuels", SAE 2005; 2005-01-3707:1-7.

[7] Rakesh Sarin, Meeta Sharma, S. Sinharay and R.K. Malhotray, "Jatropha-palm Biodiesel Blends: An Optimum Mix for Asia", Fuel 2007; 86:1365-1.

[8] Morino Takayuki and Morimune Takaaki, "Diesel Engine Operation and Exhaust Emissions When Fueled with Animal Fats", SAE 2005; 2005-01-3673:1-7.

[9] J. Syzbrst, et al. Potential Methods for NOx Reduction from Biodiesel, SAE 2003; 2003-01-3205.

[10] V. Pradeep and R.P. Sharma, "Use of Hot EGR for NOx Control in a Compression Ignition Engine Fuelled with Biodiesel from Jatropha Oil", Renewable Energy Vol.32, 2007, pp.1136-54.

[12] Timothy Jacobs, Dennis Assanis and Zoran Filipi, "The Impact of Exhaust Gas Recirculation on Performance and Emission of a Heavy-duty Diesel Engine", SAE 2003; 2003-01-1068.

[13] A. Tsolakis, A. Megaritis, M.L. Wyszynski and K. Theinnoi, "Engine Performance and Emission of a Diesel Engine Operating on Diesel-rme (Rapeseed Methyl Ester) Blends With Exhaust Gas Recirculation (Egr)", Energy Vol. 32, 2007, pp.2072-0.

[14] C.D. Rakopoulos, D.C. Rakopoulos, D.T. Hountalas, E.G. Giakoumis and E.C.Andritsakis "Performance and Emissions of Bus Engine Using Blends of Diesel Fuel With Biodiesel of Sunflower or Cottonseed Oils Derived from Greek Feedstock. Fuel", Vol.87, 2008, pp.147-7.

AN ALGORITHM FOR SELECTION OF MIMO/ADAPTIVE ANTENNA SYSTEMS FOR WIDE AREA NETWORKS AND THEIR PERFORMANCE ANALYSIS

C. Poongodi
Department of Electronics and Communication Engineering, Bannari Amman Institute of Technology, Sathyamangalam - 638 401, Erode District, Tamil Nadu
E-mail: poongi_cj@yahoo.co.in
(Received on 05 November 2008 and accepted on 10 January 2009)

Abstract

In mobile communication environment, the wireless channel is time varying due to the mobility of the wireless terminal and multi-path propagation. It has been shown that MIMO will give multiplexing gain and/ or better quality of service. It has also been proved that Adaptive Antenna Systems (AAS) can provide improved spectral efficiency because AAS uses spatial multiplexing technique. This paper proposes an algorithm for reconfigurable communication system based on both Multiple Input and Multiple Output (MIMO) and AAS. MIMO performs well in scattering rich environment. AAS performs well, when there are one or two propagation paths, by properly forming the beam of radiation in the direction of user. As the user is moving, the number of paths would change time to time. In this system, either MIMO or AAS will used at a time according to the environment. Channel capacity and bit error rate are used as performance metrics. Theoretic capacity of an MIMO system increases linearly with the number of elements, but the capacity offered by the MIMO system is reduced if the various signals at the receiver are correlated. Correlation at the receiver is mainly due to mutual coupling between the transmit and/or receive antenna elements. We use different array configuration to improve the channel capacity with mutual coupling. To validate the performance of the system, necessary simulations are performed.

Keywords: *AAS, Beam Forming, Channel Capacity and Bit Error Rate, MIMO*

1. INTRODUCTION

In the last few years wireless services have become more and more important. Likewise the demand for higher network capacity and performance has been increased. MIMO systems are increasingly being adopted in communication systems for the potential gains in capacity they realize when using multiple antennas. Multiple antennas use the spatial dimension in addition to the time and frequency ones, without changing the bandwidth requirements of the system. Smart antenna systems consist of multiple antenna elements at the transmitting and receiving side of the communication link. Depending on whether the processing is performed at the transmitter, receiver or both ends of the communication link, the smart antenna technique is defined as multiple input single output (MISO), single input multiple output (SIMO) or multiple input multiple output (MIMO) [1]. In most wireless channels, no direct LOS propagation exists between the transmitter antennas and receive antenna because of natural and constructed obstacles. The transmitter signal may arrive at the receiver over many paths. This causes multi-path fading at a specific location and strength of the wave changes randomly. This multipath is often detrimental in case of single transmit and receive antennas. This unwanted is instead exploited in MIMO case to increase the channel capacity and quality [2]. In MIMO, both transmitter and receiver are provided with more than one antenna.

MIMO performs well in scattering rich environment [3,4]. For rich scattering environment channel it is possible to increase the data rate by transmitting separate information streams on each antenna. For example, using four transmit and four receive antennas, four times the capacity of a single antenna system can be achieved. Quality of service is improved through space diversity by transmitting same signal over multiple antennas [1].

The wide area network is sometimes limited with only one or two dominant paths. In that case adaptive antenna system is used. The primary goal of adaptive antennas is the automatic generation of beams (beam forming) that track a desired signal and possibly reject interfering sources through linear combining of the signals captured by the different antennas [5]. The algorithm used in this system is MVDR (Minimum Variance Distortion less Response). The power gain of the receiving signal for only one path (LOS) between transmitter and receiver is given by square root of Nt (number of transmit antennas) and Nr(number of receive antennas). For two dominant paths the power gain is reduced by half, so when the number of paths increases bit error rate also increases. Besides beam forming another application of antenna arrays is Direction Of Arrival (DOA) estimation for source or target localization purposes [5].

The Challenges for wide area networks are

i. Interference

The wide area environment experiences significant levels of interference due to dense deployments and large cells. In such environments, rejection of interference and high throughput are both necessary.

ii. Limited Scattering

The wide area scattering environment can in some cases be limited with only one or two dominant paths which limit the use of spatial multiplexing techniques.
Successful implementations of MIMO in wide area networks share two key attributes

iii. Interference Suppression

In wide area case the additional degrees of freedom available through the antenna array at both ends of the link should be used at least in part to reduce interference. Interference mitigation both at the transmitter and receiver can dramatically reduce network interference compared to systems with only interference rejection at one end.

iv. Robust Solutions

Solutions can be developed that account for a limited number of dominant propagation paths. Significant performance gains can still be achieved through coherent combining at both the transmitter and receiver even in channels with limited scattering. The performance improvement can be achieved with adaptive array processing techniques at the base station combined with similar processing at the mobile terminal [6].

The key challenge faced by future wireless communication systems is to provide high-data-rate wireless access at high quality of service (QoS).A significant portion of the ultimate MIMO gains can be achieved now in existing wide-area networks without changes to existing protocols and without waiting for completion of new protocols. Substantial performance improvements can be achieved with adaptive array processing techniques at the base station combined with similar processing at the mobile terminal. In fact, theory indicates that this is the optimal approach under many of the channel conditions common in wide-area networks. These gains both in terms of signal strength and also in interference suppression are critical for the evolution of wide-area networks. As Robert Syputa, Senior Analyst at Maravedis Telecommunications Research, recently noted, "To live up to the promise of providing metro/wide area network coverage at true broadband data rates, both WiMAX and future versions of 3GPP must adopt MIMO and AAS technologies."

2. PROPOSED METHOD

This paper proposes an algorithm for reconfigurable communication system based on both MIMO and AAS. In MIMO system, capacity depends mainly on the channel and the antenna characteristics. The capacity can be improved by proper design of antenna elements and choosing appropriate array configuration [7]. The mutual coupling [8] also changes the capacity considerably. When the spacing between the elements is less than 0.5λ, the effect of mutual coupling is more. The aim of this paper is to evaluate the capacity for side by side, echelon and collinear dipole array configurations and compare the performance. The effect of mutual coupling is also incorporated in the simulation for all the configurations.

2.1 Algorithm for Proposed Method

MIMO performs well in scattering rich environment. But AAS performs well, when there are only one or two

dominant paths between transmitter and receiver. The transmitter has no knowledge of the channel state. Knowledge of the channel state however can be made available to the transmitter by first estimating the channel matrix H at the receiver and then sending this estimate to the transmitter via a feedback channel. The received signal contains both direct path and multi-path signals which are from various direction of arrivals (θ). So the selection of any one system out of MIMO/AAS will be based on number of scattering paths. Flow chart for selection of MIMO/AAS system is shown in Figure1. Steps in this algorithm are:

Step 1: Channel matrix estimation.
Step 2: Rank calculation.

Rank of the matrix depends upon the number of scattering paths, for distinguish path the rank is of full.

- For one or two dominant path, rank will be less than or equal to 2, In that case adaptive antenna system is used. The main function of AAS is beam forming.

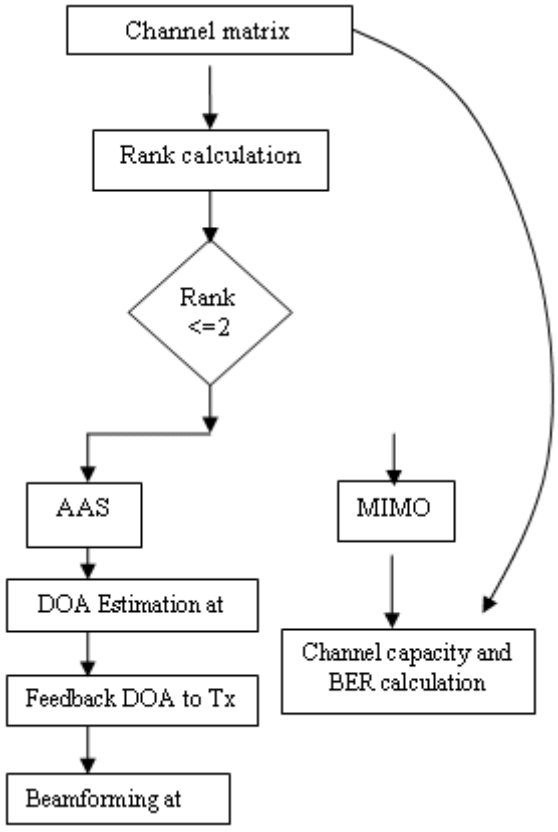

Fig.1 Flow chart for selection of MIMO/AAS system

- For beam forming, first direction of arrival (DOA) is estimated at the receiver, and then this information is sent to the transmitter via a feedback signal.
- Finally, beam forming is performed at the transmitter which tracks the desired signal and rejects the interference signal.

Step 3: For MIMO system, channel capacity and bit error rates are used to analyze the performance of the system.

2.1.1 DOA Estimation

The estimation of the direction of arrival of a signal is of great importance. There are many DOA estimation algorithms, among them MUSIC is the best. This algorithm is based on eigen value decomposition of the correlation matrix of noise corrupted signal [9]. MUSIC algorithm estimates the DOA in noise subspace, which is defined by the eigen vectors of covariance matrix of the sampled signal. The eigen values and their corresponding eigen vectors for a typical input signal x(n) is given in Table1. First two low eigen values are corresponds to noise subspace and remaining to the signal subspace. So the numbers of signal components are two and their corresponding eigen vectors determine the direction of arrival. The direction of arrival for the input signal x(n) is shown in Figure 2.

Table 1 Eigen Values and DOA Using MUSIC Algorithm

Eigen Values	0.0303,0.04901,1.0054, 7.3057
Direction of arrival	29.96 & 44.77 in deg.
Number of signal components	2

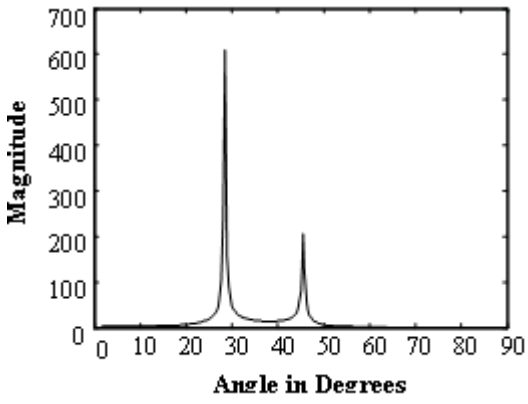

Fig.2 Direction of arrival estimation based on MUSIC algorithm.

3. CHANNEL CAPACITY AND BER

3.1 MIMO Multipath Channel

The Nt transmit antenna and Nr receive antenna are placed in uniform linear arrays of normalized length Lt and Lr respectively. The normalized separation between the antenna is Δ=L/n [10]. There is an arbitrary number of physical path between the transmitter and receiver, the ith path has an attenuation of ai, makes an angle of ϕi (Ωi=cosϕi). The channel matrix is given by

$$H = \sum a_i^b e_r(\Omega_{ri}) e_t(\Omega_{ti})^* \quad \text{.....} \quad (1)$$

where $a_i^b = a_i \sqrt{n_t n_r}\, \exp(-j2\pi d/\lambda)$ ..... (2)

and $$e(\Omega) = 1/\sqrt{n_t} \begin{bmatrix} 1 \\ \exp(-j2\pi r) \\ \text{M} \\ \exp(-j2\pi(n_t-1)r) \end{bmatrix} \quad \text{.....} \quad (3)$$

3.2 Channel Capacity

The ergodic capacity of a MIMO flat-fading channel, involves the determinant of an Nt by Nr sum matrix followed by the logarithm to the base2 [11]. This formula is the log-det capacity formula for a Gaussian MIMO channel, capacity of MIMO system is given by

$$C = E\left[\log_2(\det(I_{Nr} + \rho HH^+ / N))\right] \quad \text{....} \quad (4)$$

H is the Nt * Nr channel matrix and ρ is the average signal to noise ratio at each receiver, the capacity of a MIMO system is the sum of capacities of single input single output channels.

3.3 Capacity Including Mutual Coupling

When antenna elements are placed close to each other, the electromagnetic field generated by the current flowing in one antenna causes a voltage to be induced in neighboring antennas. This is called mutual coupling. If the spacing between antenna elements is less than 0.5λ, then there will be coupling between antenna elements. The effect of coupling between antenna elements is included in the channel matrix as given below.

$$H_{mc} = C_b H C_m \quad \text{.....} \quad (5)$$

where C_b is the coupling matrix at the base station and C_m is coupling matrix at the mobile. The expression for coupling matrix is defined as[12]

$$C = (Z_A + Z_T)(Z + Z_T I_N)^{-1} \quad \text{.....} \quad (6)$$

ZA is antenna impedance in isolation, IN is identity matrix .ZT is the impedance of the receiver at each antenna element, chosen as the complex conjugate of ZA to obtain an impedance match for maximum power transfer and Z is the Nt*Nr mutual impedance matrix. For two element array of dipoles, there are three classic configurations [13]. There are shown in figure 3 and there are referred to as the side by side, collinear and echelon

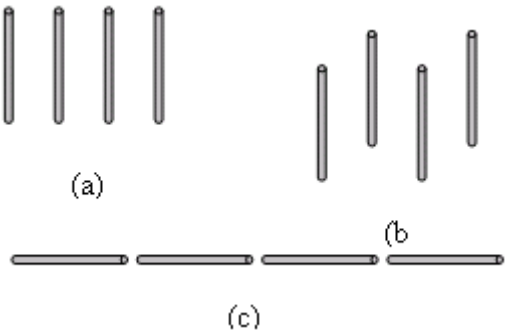

Fig. 3.Basic antenna configurations (a) Side by side (b) Echelon (c) Collinear

3.3.1 Mutual Coupling Expressions

Mutual coupling for three classical arrangements are given by [14]. The self impedance of the dipole is

$$Z_{mm} = 30[0.5772 + \ln(2kl) - C_i(2kl)] + j[30(S_i(2kl))] \quad \text{.....} \quad (7)$$

The mutual impedance for side by side configuration is

$$R_{21m} = \frac{\eta}{4\pi}[2C_i(u_o) - C_i(u_1) - C_i(u_2)] \quad \text{....} \quad (8)$$

$$X_{21m} = \frac{\eta}{4\pi}[2S_i(u_o) - S_i(u_1) - S_i(u_2)]$$

The mutual impedance for collinear configuration is

$$R_{21} = -15\cos(v_0)[-2C_i(2v_0) + C_i(v_2) + C_i(v_1) - 1n(v_3)] + 15\sin(v_0)[2S_i(2v_0) - S_i(v_2) - S_i(v_1)]$$

$$X_{21} = -15\cos(v_0)[2S_i(2v_0) - S_i(v_2) - S_i(v_1)] + 15\sin(v_0)[2C_i(2v_0) - C_2(v_2) - C_2(v_1) - 1n(v_3)] \quad \text{.....} (9)$$

where and

$$v_3 = (d^2 - l^2)/d^2 \quad \text{..... (10)}$$

l is the length of the antenna and s is the spacing between adjacent antennas. and.
k is the wave number and d=l + s.

$$C_i(x) = \int_{-\infty}^{\infty} \frac{\cos x}{x} dx \text{ and } S_i(x) = \int_{-\infty}^{\infty} \frac{\sin x}{x} dx$$

The mutual impedance for Echelon configuration is

$$\begin{aligned} R_{21} &= -15\cos(w_0)[-2C_i(w_1) - 2C_i(w_1') + C_i(w_2) \\ &+ C_i(w_2') + C_i(w_3) + C_i(w_3')] \\ &+ 15\sin(w_0)[2S_i(w_1) - 2S_i(w_1') + S_i(w_2) \\ &+ S_i(w_2') - S_i(w_3) + S_i(w_3')] \quad \text{..... (11)} \end{aligned}$$

$$\begin{aligned} X_{21} &= -15\cos(w_0)[2S_i(w_1) + 2S_i(w_1') - S_i(w_2) \\ &- S_i(w_2') - S_i(w_3) - S_i(w_3')] \\ &+ 15\sin(w_0)[2C_i(w_1) - 2C_i(w_1') + C_i(w_2) \\ &+ C_i(w_2') - C_i(w_3) + C_i(w_3')] \quad \text{..... (12)} \end{aligned}$$

where,

$$w_0 = kh, w_1 = k\left(\sqrt{d^2+h^2}+h\right), w_1' = k\left(\sqrt{d^2+h^2}-h\right)$$

$$w_2 = k\left(\sqrt{d^2+(h-l)^2}+(h-l)\right), w_2' = k\left(\sqrt{d^2+(h-l)^2}-(h-l)\right)$$

$$w_3 = k\left(\sqrt{d^2+(h+l)^2}+(h+l)\right), w_3' = k\left(\sqrt{d^2+(h+l)^2}-(h+l)\right)$$

Here h is the level of misalignment of the second antenna. k is the wave number and d is the spacing between adjacent antennas. Here Side by side arrangement exhibits larger mutual effects since the antennas are placed in the direction of maximum radiation.

3.4 Bit Error Rate

We use sphere decoding algorithm for detection in the case of MIMO.

3.4.1 Sphere Decoding

The signal received by the antenna is given by

$$y = Hx + V \quad \text{..... (13)}$$

The main idea in SD is to reduce the number of candidate vector symbols to be considered in the search. This goal is achieved by constraining the search to only those points that lie inside a hypersphere with radius R around the received point [15,16]. The corresponding in equality is referred to as the sphere constraint (SC)

where $\hat{y} = QH$ ..... (14)

Channel matrix is triangularized using QR decomposition according to H=QR, where R is upper triangular matrix. We start at level i=MT and set

. The partial (squared) Euclidean distances (PEDs) are given by

$$T_i(s^{(i)}) = T_{i+1}(s^{(i+1)}) + \left|e_i(s^{(i)})\right|^2 \quad \text{..... (15)}$$

where i=MT,MT-1,…1 where the distance increments

$\left|e_i(s^{(i)})\right|^2$ can be obtained as

$$\left|e_i(s^{(i)})\right|^2 = \hat{y} - \sum_{j=i+1}^{M_T} R_{ij} S_j \quad \text{..... (16)}$$

Finally, d(s) is the PED of the corresponding leaf: d(s)=T1(s). Since the distance increments are nonnegative, it follows immediately that whenever the PED of a node violates the (partial) SC given by

$$T_i(s^{(i)}) < R^2 \quad \text{..... (17)}$$

then the PEDs of all of its children will also violate the SC. Consequently, the tree can be pruned above this node. This approach effectively reduces the number of transmit vector symbols (i.e., leaves of the tree) to be checked. The decoding complexity critically depends on the choice of radius. The complexity and dependence of the throughput on the initial radius can be reduced by shrinking the radius whenever a leaf is reached.

4. RESULTS AND DISCUSSION

The capacity and BER depends upon the number of paths. When the number of paths increases the capacity also increases.

Figure 3 shows the average capacity versus number of paths for MIMO systems with NxN transmit and receive antennas, holding total transmit power constant. From equation (5) when the number of element increases channel capacity also increases. The SNR is varied from

2 to 20db and the corresponding capacities over this SNR range with N transmit and receive antennas, holding total transmit power constant is plotted in figure 4. The inter element spacing at the transmitting and receiving end is fixed at 1.25 λ so that mutual coupling can be ignored at the transmitting and receiving end. But the capacity can increase when either the spatial correlation drops or when the received SNR increases.

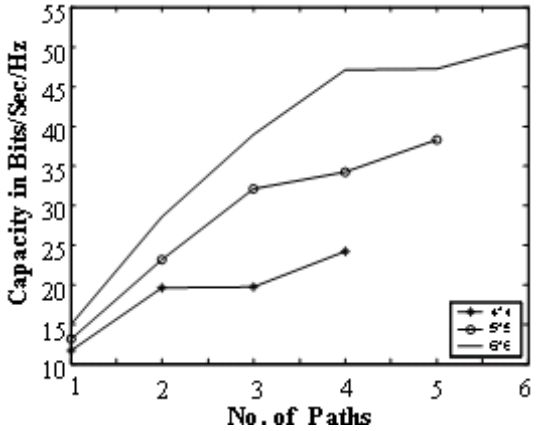

Fig.3 Effect of number of path on the channel capacity for MIMO system.

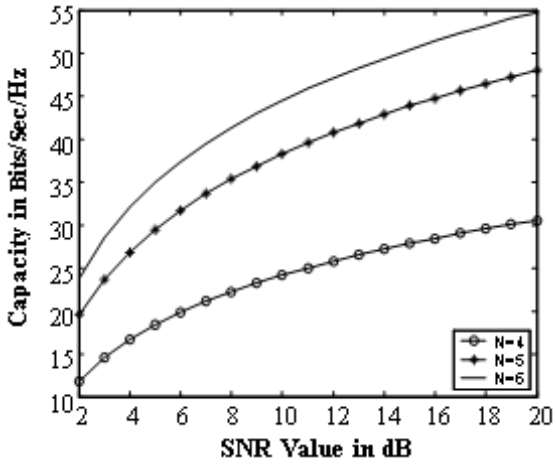

Fig. 4 Mean capacity as a function of SNR.

Figure 5 shows the mean capacity versus number of transmit antennas for nr=5, SNR=10db,dr=2 ë and Lt =5 ë . The number of transmit antennas are varied from 1 to 35 and the corresponding capacity for different antenna configuration are plotted. From equation (7) ZA is the antenna's impedance in isolation (for l = λ/2 dipole, ZA = 73+j42.5Ω), IN is the identity matrix and Z is the Nt*Nr mutual impedance matrix. The mutual impedance for three classical configurations are shown in section 3, in that side by side arrangement exhibits larger mutual effects since the antennas are placed in the direction of maximum radiation. So it has been observed that the collinear and echelon arrangement both at base and mobile station offer better capacity results than side by side arrangement.

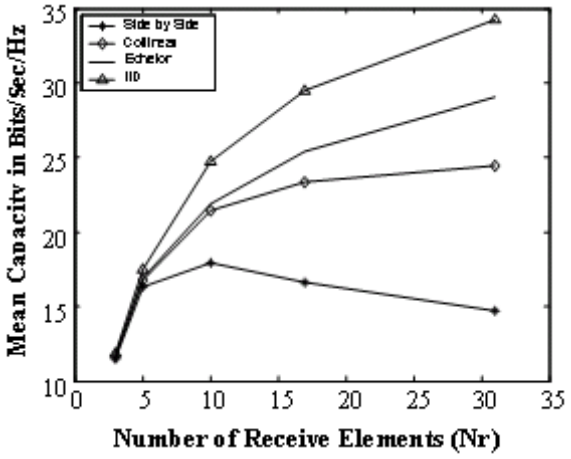

Fig. 5 Mean capacity as a function of number of receive elements

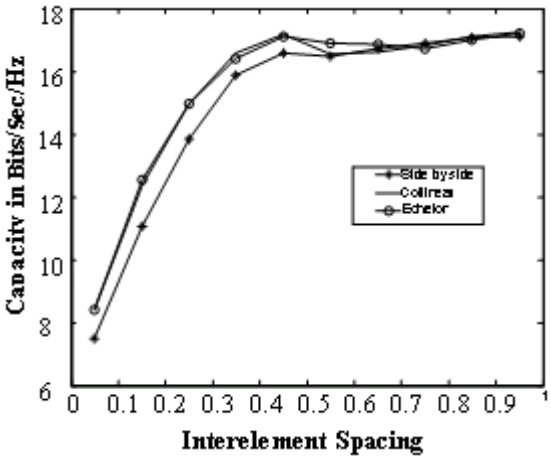

Fig. 6 Mean capacity versus Interelement spacing for different antenna configurations.

The mean capacity versus interelement spacing for different antenna configuration is shown in figure 6. The separation between base-elements is held at db = 3λ and mobile element is varied from 0.05 to 1λ . When the spacing between the antenna element increases, mutual coupling decreases and the channel capacity increases.

It has been observed that the mean capacity is maximum for the collinear and echelon arrangement both at base and mobile station because side by side arrangement exhibits larger mutual effects.

Figure 7 shows the BER versus numbers of paths for MIMO systems with NrxNt antennas and AAS system, holding total transmit power constant. In MIMO systems when the number of path increases, size of the channel matrix increases. So the points of Hs that lie inside a hypersphere with radius 'r' around the received point y increases. T1(s) and PED are calculated from equation (15) and (16) respectively. Figure 7 shows that when the number of paths increases bit error decreases. But in AAS system for two dominant paths the power gain is reduced by half, so when the number of paths increases bit error rate also increases.

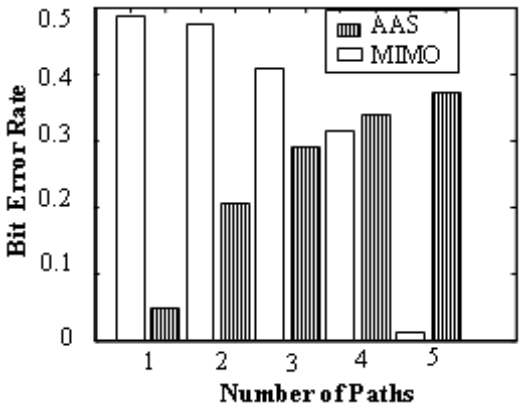

Fig. 7 BER Versus number of paths for MIMO and AAS system.

5. CONCLUSION AND FUTURE SCOPE

This paper proposed a system which works based on both MIMO and AAS. The proposed system gives better performance than mere MIMO and AAS. This work also paves the way to try out a possibility of simultaneous coexistence of both systems. In addition, the effect of number paths on channel capacity and BER has been clearly brought out. Channel capacity including effect of mutual coupling has been evaluated. Mean Capacity as a function of Number of elements and interelement has been evaluated for different antenna configurations which shows that collinear and arrangement both at base and mobile station, offer better capacity result than side by side arrangements.

There are several interesting open problems in MIMO channel estimation some of them are pointed out here.

A realistic channel models can be used to perform simulations. One ring channel model is widely used model for microcell and picocell environment. We can analyse the capacity of MIMO systems for the 3GPP-3GPP2 Spatial Channel Model (SCM) also.

REFERENCES

[1] Angeliki alexiou and Martin Haardt, "Smart Antenna Technologies for Future Wireless Systems: Trends and Challenges" IEEE Communication Magazine, Vol.42. No.9, September 2004, pp.90- 97.

[2] A.Paulraj, R.Nabar and D.Gore, "Introduction to Space-Time Wireless Communications" Cambridge University Press, 2003.

[3] David Gesbert et al, "An overview of MIMO Space-Time Coded Wireless Systems" IEEE Journal on Selected Areas in Communication, Vol.21. No.3, April 2003, pp.281- 302.

[4] G.J.Foschini and M.J.Gans, "On Limits of Wireless Communications in a Fading Environment when Using Multiple Antennas" Wireless Pers. Communication, Vol.6, March 1998, pp.311-335.

[5] A.J.Paulraj et al, "Smart Antennas for Mobile Communications" Encyclopedia for Electrical Engineering, John Wiley Publishing Co.,2000.

[6] "Leveraging MIMO in Wide-Area Networks" November 18, 2005, ArrayComm. LLC.

[7] T. Svantesson, "A Physical MIMO Radio Channel Model for Multi-element Multi-polarized Antenna Systems," in Proc. IEEE 54th Veh. Technol.Conf., Atlantic City, Vol. 2, NJ, Oct. 7–11, 2001, pp.1083-1087.

[8] Ramakrishna Janaswamy, "Effect of Element Mutual Coupling on the Capacity of Fixed Length Linear Arrays", IEEE Antennas and Wireless Propagation Letters, Vol. 1, 2002, pp.157-160.

[9] Ralph O.Schmidt, "Multiple Emitter Location and Signal Parameter Estimation", IEEE Transaction on Antenna and Propagation, Vol. AP- 34, No.3, March 1986, pp.276- 280.

[10] David Tse, "Fundamentals of Wireless Communication", Cambridge University Press, 2005.

[11] Simon Haykin "Modern Wireless Communication", Pearson Education, 2005.

[12] T. Svantesson and A. Ranheim, "Mutual Coupling Effects on the Capacity of Multielement Antenna Systems," in Proceedings IEEE Int. Conf. Acoustics,Speach, and Signal Processing, Salt Lake City, UT, Vol. 4, May 7-11, 2001, pp.2485–2488.

[13] P. S. Carter, "Circuit Relations in Radiating Systems and Applications to Antenna Problems", Proceedings of the Institute of Radio Engineers, Vol.20, No.6, June 1932, pp.1004- 1041.

[14] A.Balanis, " Antenna Theory Analysis and Design," John Wiley & Sons, April 2005.

[15] Andreas Burg et al,"VLSI Implementation of MIMO Detection Using the Sphere Decoding Algorithm", IEEE Journal of Solid State Circuits, Vol.40, No.7, July 2005, pp.1566-1577.

[16] Zhan Guo "A VLSI Implementation of MIMO Detection for Future Wireless Communications" The 14th IEEE International Symposium on Personal, Indoor and Mobile Radio Communication Proceedings 2003, Vol 3, September 2003, pp.2852-2856.

INHIBITION OF MILD STEEL CORROSION USING SOLANUM XANTHOCARPUM IN HYDROCHLORIC ACID MEDIUM

M. Shyamala and A. Arulanantham
Government College of Technology, Coimbatore -641 013, Tamil Nadu
E-mail: shymalam@rediffmail.com
(Received on 12 November 2008 and accepted on 18 January 2009)

Abstract

Corrosion inhibition of mild steel in 1N Hydrochloric acid by aqueous extracts of Solanum xanthocarpum was studied using the weight loss method, Gasometric method, Potentiodynamic polarization and Impedance method. The maximum inhibition efficiency was found to be 99.6 % in the optimum concentration of the Extract 8% in v/v for a period of 3 hours. Similarly, in Gasometric method, maximum efficiency was found to be 98.6% in the same optimum concentration. It was confirmed by Potentiodynamic Polarization and Impedance method which showed a maximum efficiency of 99.7% and 99.6 % efficiency respectively in 8% in v/v. Potentiodynamic polarization curves indicated that the plant extract behaves as mixed type inhibitor. The adsorption of Solanum xanthocarpum follows Langmuir adsorption isotherm. The results obtained shows that the aqueous extract of the leaves of Solanum xanthocarpum could serve as an effective inhibitor on the corrosion of mild steel in 1N Hydrochloric acid media. The inhibition action is due to the presence of the alkaloid Solasodine present in Solanum xanthocarpum

Keywords: *Adsorption,Gasometry, Hydrochloric Acid, Impedance, Mildsteel, Polarization, Solanum Xanthocarpum, Solasodine, Weightloss.*

1. INTRODUCTION

Solanum xanthocarpum, belonging to Solanaceae family is widely found throughout India. The whole plant contains high concentration of Solasodine. In an attempt to find Corrosion inhibitors which are environmentally safe and readily available, there has been a growing trend in the use of natural products such as leaves of plant extracts as Corrosion inhibitors for metals in acid cleaning process [1-10]. In this present study, the inhibitory action of aqueous extract of Solanum xanthocarpum on the acid dissolution of mild steel in hydrochloric acid solution has been investigated using Weight loss method, Gasometric method, Potentiodynamic polarization method and Impedance method.

2. MATERIALS AND METHODS

2.1 Material Preparation

Mild steel strips of size 4.5cm × 2cm × 0.2cm containing 0.14% C, 0.35% Mn, 0.17% Si, 0.025% S , 0.03% P and the remainder Fe were used for weight loss and gasometric method. For electrochemical studies, mild steel strips of the same composition coated with lacquer with an exposed area of 1 cm2 were used. Mild steel strips were polished mechanically with emery papers of 1/0 to 4/0 grades and subsequently degreased with trichloroethylene before use. Analytical reagent grade HCl and double distilled water were used for preparing test solutions for all experiments.

2.2 Solution Preparation

The leaves of Solanum xanthocarpum were taken and cut into small pieces and they were dried in an air oven at 80ºC for 2 hrs and ground into powder. From this, 10g of the sample was refluxed in 100mL distilled water for 1h, filtered carefully and made up to 100 mL using double distilled water. The concentration of the stock solution is expressed in term of % (v/v). From the stock solution 2% to 10% v/v concentration were prepared.

2.3 Weight Loss Method

The experimental solution, 1N HCl with concentrations 2% to 10% extract was used. The pretreated specimens were immersed in the experimental solution with the help of glass hooks. The initial weight of the specimens was noted and it was immersed completely into the experimental solution at 30°C for three hours. After three hours, the specimens were taken out, washed thoroughly with distilled water, dried completely and their final weights were noted. From the initial and final weights of the specimen, the loss in weight was calculated and tabulated. The corrosion rate (mmpy) and the efficiency of inhibitors can be calculated using the formula,

Corrosion rate (mmpy) = KW / ATD

where K = 8.76 X 104 (constant), W= weight loss in g, A=area in sq.cm, T= Time in hours and D=density in gm/ cu.cm (7.86).

Inhibition efficiency (%) =(WB–WI)/WB × 100

where WB and WI are weight loss per unit time in the absence and presence of inhibitors.

The degree of surface coverage (θ) was calculated from the weight loss measurement results using the formula,

Surface coverage (è) = WB – WI / WB

where, WB is the weight loss in the absence of inhibitor, WI is the weight loss in the presence of inhibitor.

2.3 Gasometric Method

This technique gives accurate results compared to that of conventional weight loss method provided, the inhibitor does not react with hydrogen and the hydrogen penetration into the metal is small compared to the total volume of hydrogen gas. The gasometric studies were carried out as described [11]. The inhibition efficiency was calculated using the formula,

Inhibition efficiency (%) = V0-V1 / V0 x 100

Where, V0 is the volume of hydrogen evolved in the absence of inhibitor, V1 is the volume of hydrogen evolved in the presence of inhibitor.

2.4 Potentiodynamic Polarization Studies

Potentiodynamic polarization measurements were carried out using Solartron Electrochemical analyzer. The polarization measurements were made to evaluate the corrosion current, corrosion potential and Tafel slopes. Experiments were carried out in a conventional three-electrode cell assembly. The working electrode was mild steel specimen of 1sq.cm.area which was exposed and the rest being covered with red lacquer. A rectangular Pt foil was used as the counter electrode. To exert uniform potential on the working electrode, it is designed in such a way that the counter electrode is much larger in area compared to the working electrode. The reference electrode used was SCE. Instead of salt bridge a luggin capillary arrangement was used to keep SCE close to the working electrode to avoid the ohmic contribution. A time interval of 10 – 15 minutes was given for each experiment to attain the steady state open circuit potential.

The polarization was carried from a cathodic potential of – 800mV (vs SCE) to an anodic potential of – 200mV (Vs SCE) at a sweep rate of 1mV per second. From the polarization curves, Tafel slopes, corrosion potential and corrosion current were calculated. The inhibitor efficiency was calculated using the formula,

$$IE\ (\%) = \frac{Corr - I^{*}Corr}{ICorr} \times 100$$

Where Icorr and I*corr are corrosion current in the absence and presence of inhibitors.

2.5 Impedance Measurements

The electrochemical AC-impedance measurements were performed using Solatron Electrochemical analyzer. Experiments were carried out in a conventional three electrode cell assembly as that used for Potentiodynamic polarization studies. The working electrode was mild steel specimen of 1 sq.cm. area which is exposed and the rest being covered with red lacquer. A rectangular Pt foil is used as the counter electrode. A sine wave with amplitude of 10mV was superimposed on the steady open circuit potential. The real part (Z') and the imaginary part (Z") were measured at various frequencies in the range of 100 KHz to 10 MHz.

A plot of Z' vs Z" was made. From the plot, the charge transfer resistance (Rt) were calculated and the double layer capacitance was then calculated using the equation,

$$Cdl = 1 / 2\pi \, fmax \; Rt$$

Where Rt is charge transfer resistance and Cdl is double layer capacitance. The experiments were carried out in the absence and presence of different concentrations of inhibitors. The percentage of inhibition efficiency was calculated using the equation,

$$IE\ (\%) = \frac{Rt^* - Rt}{Rt^*} \times 100$$

Where Rt* and Rt are the charge transfer resistance in the presence and absence of inhibitors.

3. RESULTS AND DISCUSSION

3.1 Weight Loss Method

The weight loss method was done with concentrations ranging from 2% to 10% v/v. The weight loss data are listed in Table-1. It was found that with the rise in concentration of the Solanum xanthocarpum extract from 2.0 to 10% in v/v, the weight loss of mild steel decreased, the corrosion rate also decreased while the inhibition efficiency increased. The optimum concentration was found to be 8 % v/v. At the optimum concentration of 8% in v/v, Solanum xanthocarpum has shown a maximum inhibition efficiency of about 99.6 % for a period of 3 hours. This result indicated that Solanum xanthocarpum could act as an efficient corrosion inhibitor.

Table 1 Corrosion Parameters Obtained from Weight Loss Measurements for Mild Steel in HCL Containing Different Concentrations of Solanum Xanthocarpum Extract

Sl.No.	Concentration of Extract (% in v/v)	Corrosion Rate (mmpy)	Inhibition Efficiency (%)	Surface Coverage (θ)
1	Blank	30.67	--	--
2	2.0	4.18	86.4	0.86
3	4.0	3.00	90.2	0.90
4	6.0	1.35	95.6	0.96
5	8.0	0.12	99.6	1.00
6	10.0	0.74	97.6	0.98

3.2 Gasometric Method

This technique gives accurate results compared to that of conventional weight loss method provided, the inhibitor does not react with hydrogen and the hydrogen penetration into the metal is small compared to the total volume of hydrogen gas. Table-2 shows the Inhibition efficiency obtained from Gasometric method for mild steel in 1N HCl for different concentrations of Solanum xanthocarpum extract.

It was observed that with increase in concentration of Solanum xanthocarpum extract from 2 % to 10 % in v/v, the volume of hydrogen gas evolved at 30Ú± 1Ú C was found to decrease and with optimum concentration of 8% in v/v, the volume of hydrogen gas evolved was only 0.1 mL showing 98.6 % inhibition efficiency.

Table 2 Inhibition Efficiency Obtained from Gasometric Method for Mild Steel in 1N HCL for Different Concentrations of Solanum Xanthocarpum Extract

Sl.No	Concentration of Extract (% in v/v)	Volume of Hydrogen Gas Evolved at 30°± 1° C (mL)	Inhibition Efficiency (%)
1	Blank	7.0	--
2	2.0	1.0	85.7
3	4.0	0.7	90.0
4	6.0	0.3	95.7
5	8.0	0.1	98.6
6	10.0	0.2	97.1

3.3 Potentiodynamic Polarization Method

The Potentiodynamic polarization measurements were studied to evaluate the corrosion current, corrosion potential and Tafel slopes. Fig 1 shows the polarization curves for mild steel in 1N HCl with different additions of Solanum xanthocarpum extract. Inspection of the figure reveals that the polarization curves shift towards less negative potential and lower current density values upon the addition of the extract. This behaviour reflects the inhibitive action of Solanum xanthocarpum extract. The Potentiodynamic polarization parameters for mild steel in 1N HCl containing different concentrations of Solanum xanthocarpum extract were obtained from the curves of Figure 1 and given in Table 3.

The data in Table-3 shows that the corrosion potential shifts to less negative values as the concentration of added extract is increased. On the other hand, the corrosion current density is markedly decreased upon addition of the extract. The extent of its decrease increases with increased extract concentration. Moreover, the numerical values of both anodic and cathodic Tafel constants decreased as the concentration of extract was increased. It was observed that with increase in concentration of Solanum xanthocarpum extract from 2 % to 10 %, the maximum inhibition efficiency was observed in the optimum concentration 8% in v/v of 99.7 % efficiency.

Table 3 Potentiondynamic Polarization Parameters for Mild Steel in HCL Containing Different Concentrations of Solanum Xanthocarpum Extract

Concentration of Extract (% in v/v)	E_{corr} (V)	I_{corr} (mA/cm^2)	Tafel Slope mV/decade		Inhibition Efficiency (%)
			b_a	b_c	
Blank	-0.4826	3.57	78	122	-
Solanum xanthocarpum					
2.0	-0.4811	0.46	76	122	87.1
4.0	-0.4795	0.30	78	126	91.6
6.0	-0.4799	0.13	74	124	96.4
8.0	-0.4808	0.01	76	122	99.7
10.0	-0.4738	0.07	72	118	98.0

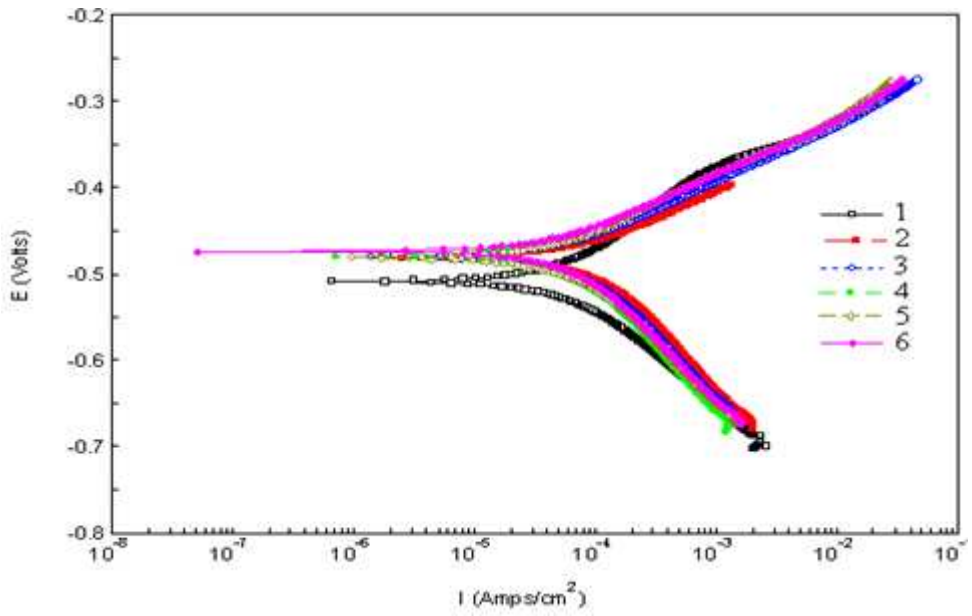

Fig.1 Potentiodynamic polarization curves for mild steel in 1N HCl solution in theabsence and presence of different concentrations of solanum xanthocarpum extract (1) Blank, (2) 2.0 (%v/v) , (3) 4.0 (% v/v) , (4) 6.0 (% v/v) ,(5) 8.0 (% v/v), (6) 10.0 (%v/v)

3.4 Impedance Method

The corrosion behaviour of mildsteel in 1N HCl in the absence and presence of Solanum xanthocarpum extract was also investigated by Impedance method. to evaluate the charge transfer resistance (Rt) and double layer capacitance (Cdl) and through these parameters the inhibition efficiency was calculated. Fig 2 shows the impedance diagrams for mild steel in 1N HCl with different concentrations of Solanum xanthocarpum extract and the impedance parameters derived from these investigations are mentioned in Table 4.

As noticed from Figure 2, the obtained impedance diagrams are almost a semi-circular appearance, indicating a charge - transfer process mainly controls the corrosion of mild steel. Deviations of perfect circular shape are often referred to the frequency dispersion of interfacial impedance. This anomalous phenomenon may be attributed to the inhomogeneity of the electrode surface arising from surface roughness or interfacial phenomena.

In fact, the presence of Solanum xanthocarpum extract enhances the value of Rt in acidic solution. Values of double layer capacitance are also brought down to the maximum extent in the presence of inhibitor and the decrease in the values of Cdl follows the order similar to that obtained for Icorr in this study. The decrease in Cdl shows that the adsorption of this inhibitor takes place on the metal surface in acidic solution.

Moreover, the increase in the value of Rt with the inhibitor concentration leading to the increase in the corrosion inhibition efficiency. The maximum Rt value of 1685.46 Ù cm2 and minimum Cdl value of 1.22 µF/cm2 is obtained for the optimum concentration 8% in v/v with a maximum inhibition efficiency of 99.6%. A good agreement is observed between the results obtained in non-electrochemical methods (weight loss method and gasometric method) and electrochemical methods (Potentiodynamic polarization method and Impedance method).

Table 4 Impedance Parameters for the Corrosion of Mild Steel in HCL in the Absence and Presence of Different Concentrations of Solanum Xanthocarpum Extract at 300c

Concentration of Extract (% in v/v)	R_t (Ω cm^2)	C_{dl} (µF/cm^2)	Inhibition Efficiency (%)
Blank	7.58	285.34	-
Solanum xanthocarpum			
2.0	60.26	36.02	87.4
4.0	85.92	25.01	91.2
6.0	235.46	4.02	96.8
8.0	1685.46	1.22	99.6
10.0	485.45	4.51	98.4

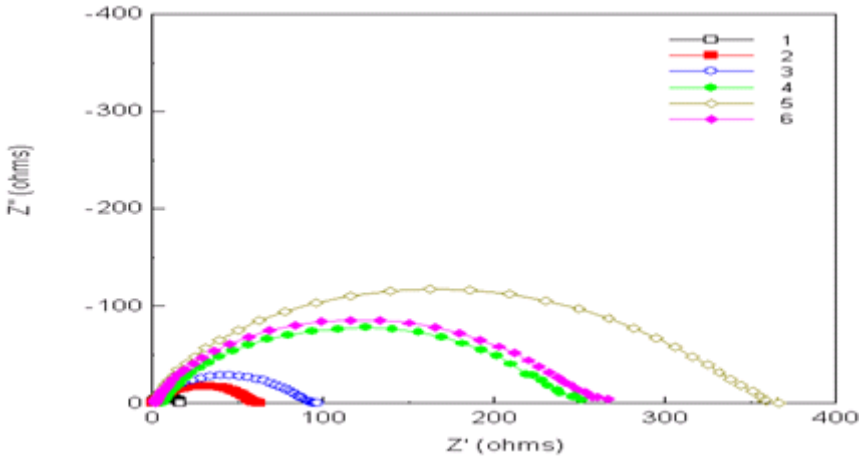

Fig. 2 Impedance diagrams for mild steel in 1N HCl solution in the absence and presence of different concentrations of solanum xanthocarpum extract (1) Blank, (2) 2.0 (% v/v), (3) 4.0 (% v/v), (4) 6.0 (% v/v), (5) 8.0 (% v/v), (6) 10.0 (% v/v)

3.5 Kinetics and Reason for the Corrosion Inhibition

From literature survey[12] it was found that the Steroidal alkaloid Solasodine is the principal alkaloid present in Solanum xanthocarpum. The inhibition of Solanum xanthocarpum may be due to the presence of the major alkaloid Solasodine containing nitrogenous compounds and hydroxyl groups.

Solasodine

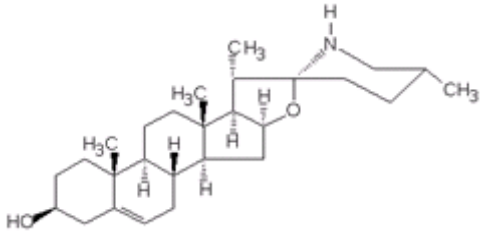

The inhibition mechanism involved is, the inhibitor gets adsorbed on the surface of the metal and provokes the small corrosion on the surface of the metal and also it is adsorbed forming a compact protective thin layer forming a precipitate on the surface of the metal.

The corrosion of mild steel in HCl solution is a heterogonous one, composed of anodic and cathodic reactions. Based on this, the kinetic analyses of the data were considered The Arrehenius plot for mild steel immersed in 1N HCl solution in the absence and presence of optimum concentration (8 %v/v) of Solanum xanthocarpum extract is given in Figure3 revealing the effect of temperature.

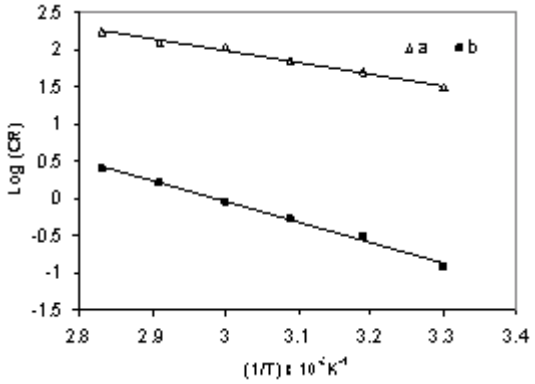

Fig. 3 Arrhenius plots for mild steel immersed in 1N HCl solution in the absence and presence of optimum concentration (6.0 %v/v) of solanum xanthocarpum (a) Blank (b) of Solanum xanthocarpum

The use of adsorption isotherms provides useful insight into the corrosion inhibition mechanism. The adsorption of different concentrations of Solanum xanthocarpum extract on the surface of mild steel in 1N hydrochloric acid follows Langmuir adsorption isotherm (Figure 4).

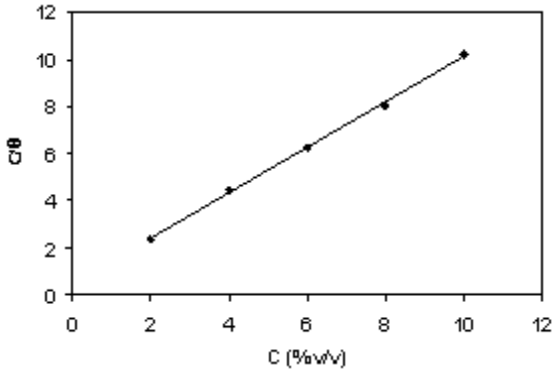

Fig. 4 Langmuir adsorption isotherm plot for the adsorption of different concentrations of solanum xanthocarpum extract on the surface of mild steel in 1N HCl solution

3.6 Surface Analysis

Surface examination of the mild steel specimens were made using JEOL –Scanning electron microscope (SEM) with the magnification of 1000X. The mild steel specimens after immersion in 1N HCl solution for three hours at 30°C in the absence and presence of optimum concentration 8 % v/v of the Solanum xanthocarpum extract, the specimens were taken out, dried and kept in a dessicator. The protective film formed on the surface of the mild steel was confirmed by SEM studies (Figure 5 and 6).

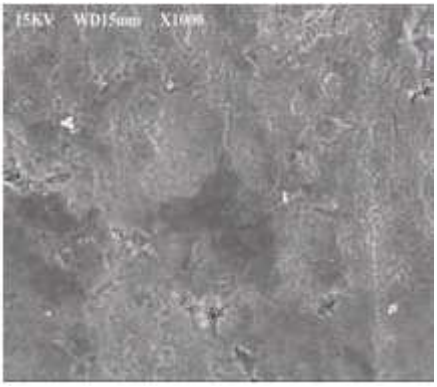

Fig 5 SEM Photograph of mild steel immersed in 1N HCl solution (blank)

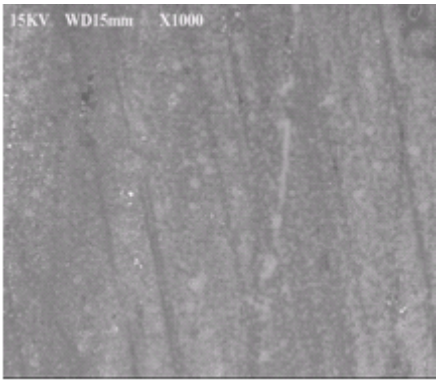

Fig. 6 SEM Photograph of mild steel immersed in 1N HCl solution containing an optimum concentration (8% v/v) of solanum xanthocarpum

4. CONCLUSION

- Solanum xanthocarpum can act as good and efficient inhibitor for corrosion of mild steel in 1N Hydrochloric acid.
- The maximum inhibition efficiency was found to be 99.6% in the optimum concentration of the extract 8% in v/v in Weight loss method.
- In Gasometric method, maximum inhibition efficiency was found to be 98.6% in the same optimum concentration 8% in v/v.
- Potentiodynamic Polarization and Impedance method showed maximum inhibition efficiency of 99.7% and 99.6 % efficiency respectively in 8% v/v.
- Results obtained in non electrochemical methods (Weight loss method and Gasometric method) where very much in good agreement with the electrochemical methods (Potentiodynamic polarization method and Impedance method).
- The use of Solanum xanthocarpum as corrosion inhibitor is environmentally safe, less toxic, ecofriendly, cost effective, easily & readily available.
- The corrosion inhibition action is due to the presence of the alkaloid Solasodine in Solanum xanthocarpum.

REFERENCES

[1] A.M Abdel-Gaber, B.A Abd - El -Nabey, I.M Sidahmed, A.M El -Zayady and M. Saadawy, "Inhibitive Action of Some Plant Extracts on the Corrosion of Steel in Acidic Media", Corrosion Science, Vol.47, 2005.

[2] P. Bommersbach, C.Alemany - Dumont, J.P. Millet and B. Normand, "Formation and Behaviour Study of an Environment - Friendly Corrosion Inhibitor by Electrochemical Methods", Electochemica Acta, Vol.51, 2005, pp. 1076-1084.

[3] A.Bouyanzer, B. Hammouti and L.Majidi, "Pennyroyal Oil from Mentha Pulegium as Corrosion Inhibitor for Steel in 1m HCL", Materials Letter, Vol 60, 2006.

[4] A.Y El - Etre, M. Abdullah and Z.E. El - Tantawy, "Corrosion Inhibition of Some Metals Using Lawsonia Extract", Corrosion Science Vol.47, 2005, pp.385-395.

[5] A.Y El - Etre, "Inhibition of Aluminium Corrosion Using Opuntia Extract", Corrosion Science, Vol.45, 2003, pp. 2485-2495.

[6] Emeta E. Oguzie, "Studies on the Inhibitive Effect of Occimum Viridis Extract on the Acid Corrosion of Mild Steel", Materials Chemistry and Physics, 2005.

[7] G. Gunasekaran and L.R.Chauhan, "Ecofriendly Inhibitor for Corrosion Inhibition of Mild Steel in Phosphoric Acid Medium", Electrochemica Acta, Vol.49, 2004, pp. 4387-4395.

[8] K.O.Orubite and N.C.Oforka, "Inhibition of the Corrosion of Mild Steel in Hydrochloric Acid Solutions by the Extracts of Nypa Fruticans Wurmb", Materials letters, Vol.58, 2004, pp.1768-1772.

[9] M.A. Quraishi and Dileep Kr.Yadav, "Proceedings of Corrosion and its Control by Some Green Inhibitors", Fourteenth National Congress on Corrosion Control, Vol.42, 2008.

[10] Yan li, Peng Zhao, Qiang Liang and Baorong Hou, "Berberine as a Natural Source Inhibitor for Mild Steel in 1M H2SO4", Applied Surface Science, Vol.252, 2005, pp.1245-1253.

[11] M. Shyamala and A. Arulanantham, "Ocimum Sanctum (Tulasi) as Corrosion Inhibitor on Mild Steel in Hydrochloric Acid", Nature Environment and Pollution Technology ,Vol.7, No.3, 2008, pp.415-422.

[12] http://www.himalayahealthcare.com/herbfinder/h_xantho.htm.

SOME STUDIES ON NOVEL WRAP YARNS

C. Rameshkumar[1] and N. Anbumani[2]

[1]Department of Textile Technology, Bannari Amman institute of Technology, Sathyamangalam - 638 401, Erode District, Tamil Nadu

[2]Department of Textile Technology, PSG College of Technology, Coimbatore - 641 004, Tamil Nadu

E-mail: crktex@gmail.com

(Received on 06 December 2008 and accepted on 10 February 2009)

Abstract

The X-directional wrap yarn follows a theory behind Chinese puzzle principle, in which a braided finger size tube becomes tighter when a pulling force is being applied along with the longitudinal axis in an attempt to pull the tube off the finger. Compression force is being generated along with the wall of the Chinese puzzle when the puzzle is pulled. This Chinese puzzle phenomenon is analogous to the X- directional wrap yarn when used a dynamic processing.

Novel wrapping apparatus has been used to produce wrap yarns for some specific applications. The wrapping apparatus was developed by using two hollow spindles driven wrapping package holders'. These two wrapping package holders carry wrapper yarn and rotate opposite to each other to insert X directional twist to the core component.

XX- wrap yarns shows improvement in evenness and reduction in imperfection level over X-directional wrap yarns. Compactness of the wrap yarns improved due to wrapper filament and or yarn. Contra direction wrap yarns show improved tensile properties. Cotton yarn wrap multi filaments offer maximum elongation when it is fed as wrapper again. XX-wrapped cotton rove shows good contribution of staple fibres and elongation at break reduced considerably. Upper and lower wrap yarn holders influence on the tensile properties. HDPE multi-filaments wrapped with cotton yarns shows notable improvement in the tensile properties.

Keywords: *Fancy Yarns and High Performance Yarns, X- directional Wrap Yarns, XX- Directional Wrap Yarns*

1. INTRODUCTION

This paper describes the production and properties of X-directional wrap yarns through a novel wrapping apparatus. The X-directional wrap yarn follows a theory behind Chinese puzzle principle, in which a braided finger size tube becomes tighter when a pulling force is being applied along with the longitudinal axis in an attempt to pull the tube off the finger. Compression force is being generated along with the wall of the Chinese puzzle when the puzzle is pulled. This Chinese puzzle phenomenon is analogous to the X-directional wrap yarn when used a dynamic processing. The stress exerted on the X-directional wrap yarn during weaving / knitting will actually cause criss-cross filament wrap to tighten around the fibrous core and thus cause the yarn to become stronger rather than weaker [1]. The wrapping of twisted or twistless core yarns was done through a simple but simultaneously opposite rotating hollow spindles. Winding has to be done after wrapping. Wrapped yarns have many advantages such as high tenacity and regularity [2] and these kinds of spinning methods cater to the needs of fancy and high performance applications [3].

2. DIFFERENTIAL TWIST WRAPPED YARNS

Xin Li et.al [4] discussed on the differencial twist wrapped yarns production with wrap and plied wrap yarns (wrap yarns are combined and plied by conventional twister). False twist is inserted by hollow spindle to the core and that is removed when wrapper yarn is wrapped over it. Three natures of twists influence on the differencial twist wrap yarns. Those are self twist, wrapping twist and twisting twist.

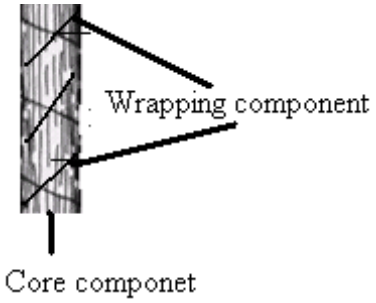

Fig. 1. a 'X' directional wrap yarn

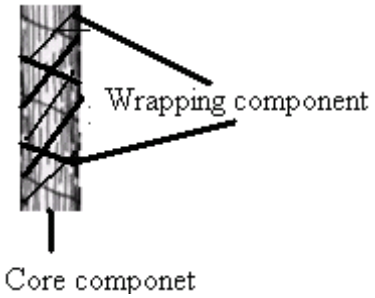

Fig. 1. b 'XX' directional wrap yarn

The self twists of core yarns and wrap yarns changes the wrap qualities. This difference leads to differential twist in wrapping strand. Wrapper yarn twist leads to wrapping and core yarns deformation due to torsion and bending.

A torque (ô) is a pseudovector [9] that measures the tendency of a force to rotate an object about some axis. Just as a force is a push or a pull, a torque can be thought of as a twist. The symbol for torque is ô, the Greek letter tau. Torque is a moment or moment force. The magnitude of torque depends on the force applied, the length of the lever arm [10, 11] connecting the axis to the point of force application; and the angle between the two. Torque has dimensions of force times distance and the SI unit of torque is newton meter (N m).

Bending (Flexural rigidity) is defined as the force couple required to bend a rigid structure to a unit curvature. It has SI units of Pa·m4 (which also equals to $N \cdot m^2$).

The curvature of two kinds of deformations is given by [4]

$$ô = â \, Sin \, â/R$$
$$k = Sin2 \, â/R.$$

where

ô = torsion
k = bending
R= radius of helical line in the yarn.
â= Helical angle when the helical radius is R.

Torsion deformation results from yarn relative turning in to its section that brings about the twist. The bending deformation makes the wrapping yarn wind on to the core yarn. Torsion deformation is in the twisting course while plying the wrap yarns by conventional twisting. This provides the core yarn with self twist while the wrapping yarn has both torsional and bending deformations. Torsional deformation of core induces self twist, while the wrapping yarn has both torsional and bending deformations. Its torsional deformation provides self twist and bending deformation that allow it to wind on core yarns.

The wrap yarns have four kinds of structures. i) Same directions of wrapping and twisting twist. ii) Opposite direction of wrapping and twisting twist. (With wrapper twist is greater than twisting twist.). iii) Opposite direction of wrapping and twisting twists (with wrapper twist is equal to the twisting twist). iv) Opposite direction of wrapping twist with twisting twist (with wrapping twist is lesser than twisting twist).

The first and second kind of twist structure assists for improvement in regularity and tenacity. When surplus yarn wrap over the core component, the structure becomes unstable [4].

2.1 Wrap Density and Core-wrapper Ratio

Unevenness, imperfections and mechanical properties are greatly influenced by both core-wrapper ratio and wrap density [5]. With increase in wrap density, the breaking extension, abrasion resistance and hairiness index decrease, whereas initial modulus, toughness and flexural rigidity increase. Initially, tenacity increases and then decreases with increase in wrap density.

Core-wrapper ratio will be selected according to the nature of utility. Normally the wrap yarns core % will be in the range of 80-98%. It may be increased depending on the yarn engineering. Different types of fibres, yarns and filaments (such as cotton, polyester, nylon, Kevlar,

glass, jute, acrylic, aramid, HDPE etc) can be used in the core and twisted staple fibres or filaments used as wrappers.

3. MATERIALS AND METHODS

3.1 Design and Development of Wrapping Apparatus

Novel wrapping apparatus has been used to produce wrap yarns for fancy and high performance applications [6-8]. The wrapping apparatus was developed by using two hollow spindles driven wrapping package holders'. These two wrapping package holders carry wrapper yarn and rotate opposite to each other to insert X- directional twist to the core component. The schematic diagram of the Novel wrapping apparatus is shown in the figure 2. A firm frame supports at top and bottom package holders' ensures vibration free rotation. Wrapping of yarns is performed with this device. Two For One (TFO) winding head is used to wind the wrap yarns. The X-directional; and XX- directional wrap yarns are shown in the figure 1.a and 1.b

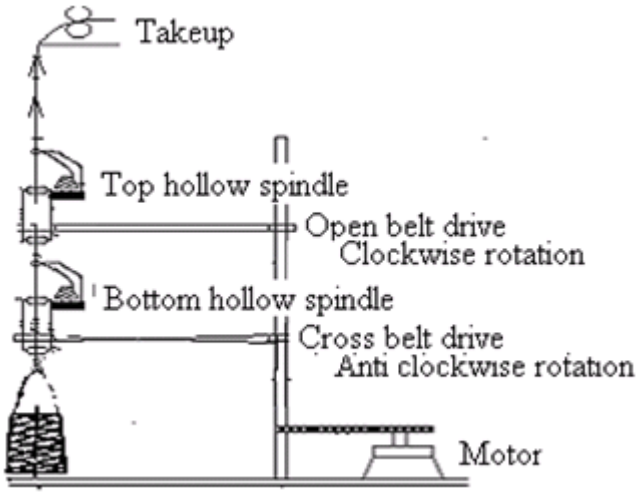

Fig. 2 Novel wrapping apparatus

The X-directional wrap yarn is a multi-component yarn which consists of three components, where core is wrapped by two filament yarns in counter and contra direction.The XX-directional wrap yarn has five components. It is produced by X-directional wrapping on X-directional wrap yarn. Hence, four filament yarns wrap over a core yarn. Out of four wrap yarns, two in counter and another two yarns in the contra direction. The proportion of core and sheath can be adjusted by varying the wraps per meter (wpm).

3.2 Production of Novel Wrap Yarns

By using this novel wrapping apparatus, eight fancy yarns and five high performance yarns are produced. The fancy yarns are produced by wrapping the 'S' and 'Z' twisted core yarns [6]. High performance yarns are produced by wrapping high performance core and sheath materials.

The wrapping package in the hollow spindle is rotated at 135 revolutions / minute to wrap the core component. The winding head speed is maintained at 6 meters/minute. For One wrapping, X and XX-directional wrapping, the wraps/meter is kept at 22.5, 45 and 90 wpm respectively. About 10% of breaking load is applied as pretension to the wrap yarns.

Table1 shows the specifications of novel wrap yarns. Yarns are produced with top hollow spindle wrapping, bottom hollow spindle wrapping, Counter wrapping, Contra wrapping, X-directional and XX-directional wrapping are made on core components separately and tested for its properties.

3.3 Yarn Testing

These novel yarns are tested for the linear density, tenacity, elongation, unevenness and imperfection. Premier Tensomax 7000 V 2.4 is used to test the tensile properties. About 25 samples are taken at a strain rate of 5000 mm/min for a yarn length of 500 mm. 0.50 cN/tex pretension is maintained. This instrument is working under the principle of Constant Rate of Elongation (CRE)

Unevenness test is performed with Star Yarn Evenness Tester I-B V5.09 (change in capacitance is used to detect mass variation). The test speed is set at 50 m/min for 10 minutes. Imperfections level is set to -50/50/200% (thick/thin/neps).

Table 1 Novel Wrap Yarns

Yarn	Resultant Count (Ne)	Wrap Yarns	Core Yarn Count	Wrap Yarn Count	Twist Direction of Wrap / Core
Y1	4.5	XX- Wrap yarn	80 Ne	Ne 20*4	Z/Z
Y2	14.7	One wrapping-Counter direction	30 Ne	Ne 30	Z/Z
Y3	14.2	One wrapping- Counter direction	33 Ne	Ne 30	S/Z
Y4	14.9	One wrapping- Contra direction	33 Ne	Ne 30	S/Z
Y5	14.9	One wrapping- Counter direction	33 Ne	Ne 33	S/S
Y6	16.0	One wrapping- Contra direction	33 Ne	Ne 33	S/S
Y7	15.6	One wrapping Counter direction (bottom hollow spindle)	30 Ne	Ne 30	Z/Z
Y8	14.9	One wrapping –Counter direction (top hollow spindle)	30 Ne	Ne 30	Z/Z
Y9	0.5	XX- Wrap yarn	1.0 Ne	150denier*4	-
Y10	3.7	X- wrap yarn	30 Ne	150denier*2	-/Z
Y11	0.5	XX- wrap yarn	600 d Spectra®	1.0*2, 150denier*2	-
Y12	4.0	XX- Wrap yarn	600 d Spectra®	30*2 and 80*2	-
Y13	0.8	XX- Wrap yarn	1.0 Ne	150denier*4	-

4. RESULTS AND DISCUSSION

4.1 Wraps/Meter for the Wrap Yarns

The false twist is inserted in both the hollow spindles along with the wrapping. Strength and elasticity of wrap yarns are found to be quite comparable with those of conventional yarns. These yarns are doubled in conventional ring-doubler machine and pliability of the wrapped yarns is found superior in terms of twist, Co-efficient of Variation % (CV %) of twist and evenness.

4.2 Effect of Yarn Evenness with Wrap Yarns

High wraps per meter improves evenness with reduced imperfection level. The results of evenness values of the wrap yarns are shown in the Table 2. XX-directional wrap yarns are found to have lower unevenness compare to X-directional wrap yarns due to four filaments wrapping and high wraps per meter. A test is made to wrap 30 Ne carded cotton yarn over 30 Ne carded cotton yarn. The imperfection levels declines significantly for XX-directional wrap yarn over X-directional wrap yarn (3.4 %). This is due to four filament wrapping. Similar to doubled yarn improvement is found in unevenness (U %) and total imperfections (thick, thin and nep/ kilo meter) due to decrement in yarn resultant count and more number of filaments in the yarn. Sharma et.al [4] state that in conventional yarns, neps and slubs tend to come to yarn surface but in wrapped yarns, they tend to stay in the centre, because of the absence of twist.

4.3 Effect of Wrapping on the Tensile Properties of the Yarn

With very increment in wraps/meter, the contributions to tensile load sharing by the wrapper filaments in the parallel direction of the yarn axis reduces, which results in decrease in tenacity [5].Wrap yarns tensile properties are shown in the Table 3. Tensile properties of the parent parallel yarns are tested for ANOVA and are found to have significant difference in tensile properties.

- Y1 yarns shows an improvement in the tensile properties compared to the parent yarns (Parent yarns means Core and wrapping components are subjected to tensile test in parallel form). Tenacity, elongation and work of rupture have significance and increment of 10%, 4.5% and 22.0% is observed.
- Lower hollow spindle (Y7) wrapped yarns are compared with upper hollow spindle (Y8) wrapped yarns. Y 7 yarns are found with high snarling tendency than the Y8 yarns due to high false twist effect.

Table 2 Evenness Values for Wrap Yarns

Yarn Specifications	Count Ne	U%	Thick Place/Km	Thin place/Km	Neps/Km	Total Imperfection /Km
Parent yarn	30	12	220	14	320	554
X- wrap yarn (30*2)	9.2	11.6	14	8	38	60
XX-wrap yarns (30*4)	5.5	11.2	4	7	19	30

- Counter and Contra direction wrapped yarns are produced form upper hollow spindle (Y2 and Y3 yarns). It is found that contra direction wrap yarns show improved tensile load (13.5%) and work of rupture (6.20%) due to compact wrapping and binding of core component by the wrap yarns and has offer good resiliency than the counter direction wrapping. The elongation at break is higher for the counter wrapped yarns (9.80% higher than the contra direction) due to less locking points than the contra direction and difference in wrap and core yarn twist direction. Same trend is observed in case of S directional twisted core yarns.
- Tenacity of Y13 is higher than the parent yarns and work of rupture is lesser (7.7 % elongation for wrap yarns against the filaments elongation 17.6%) due to the contribution of the cotton fibres in the wrap yarn.
- Y9 Yarn shows good elongation and work of rupture compared to the parent parallel rove and filament yarns (150 denier *4 and 1.0 Ne rove).
- Y11 yarns are tested in the 98 kilogram range load cell and found very high tensile properties. These yarns can cater to the high end applications in terms of cut resistance, bullet proof and some industrial applications. (Breaking force 10178 grams, Elongation at break 7.3% and work of rupture 17576 kgfm).

Table 3 Tensile Properties of Wrap Yarns

Yarn Code	Tenacity (gf/tex)	Elongation at break (%)	Breaking Work (kgfm)
Y1	11.36 (7.6)	6.0 (8.0)	2262 (13.9)
Y2	10.1 (14.5)	2.7 (22.8)	296 (32.9)
Y3	13.3 (4.8)	3.2 (7.3)	463 (8.7)
Y4	11.6 (9.7)	4.3 (7.1)	511 (15.8)
Y5	11.5 (8.2)	3.9 (9.5)	456 (15.9)
Y6	11.6 (14.7)	3.2 (21.2)	386 (35.6)
Y7	9.2 (6.0)	2.0 (9.5)	199 (15.4)
Y8	10.5 (6.5)	2.5 (10.6)	301 (15.9)
Y9	5.8 (17.6)	4.6 (17.2)	8369 (28.9)
Y10	16.0 (2.5)	18.3 (4.6)	13409 (8.1)
Y11	8.6 (15.9)	7.3 (27.7)	17576 (23.6)
Y12	79.3 (5.8)	3.2 (8.2)	17148 (13.1)
Y13	4.1 (12.2)	7.7 (23.0)	7751 (24.5)

Values within the parenthesis are CV%

5. CONCLUSION

A novel wrapping apparatus has been developed to produce high performance and fancy yarns for one wrapping, X and XX-directional wrapping. With 30 Ne yarn on 30 Ne yarn in X and XX-directional wrapping, the imperfection level has been found to decline 3.4 %. Lower hollow spindle (Y7) yarns are found with high snarling tendency.

Y9 Yarn shows good elongation and work of rupture compared to the parent parallel rove and filament yarns. Z twisted yarns have been compared based on counter or contra direction and found that contra direction wrapping shows, improved tensile load and work of rupture. The tenacity of Y13 yarn is higher than the parent filament yarns.

REFERENCES

[1] Gain L.Louis and Harold L.Salaun, "X Direction Filament-wrap Yarn", Textile Research Journal, Vol 56, 1986, pp161-163.

[2] R. Audivert, "Advantages of Staple-fibre Yarns Covered with a Filament", Textile Institute of India Vol.12, 1974, pp.271-272.

[3] H.S. Plummer, "Wrap Spinning-New Life", American Textiles, Vol.5, 1985, pp.45-49.

[4] Xin Li, Jianchun Zhng and Jiexin Li, "Differential Twist Wrapped Yarns Made on Hollow Spindle Spinning Machine", Textile Research Journal,Vol.72, February 2002, pp.181-185.

[5] I.C. Sharma, A. Mukhopadhyay and N.C. Ray, "Some Studies on Properties of Wrapped Jute/Acrylic (Parafil) Yarns", Indian Journal of Fibre & Textile Research, Vol.22, 1997, pp.89-93.

[6] Fritz Stahlecker, Bad Ueberkingen, US Patent 4519196, Wrapped Yarn Spinning Machine with Several Spinning Places, May 1985.

[7] A.Paul, S.Sawhney, Crig, C.Folk, George F.Rupenicker, "Production of Core/Wrap Yarns by Air Jet and Friction Spinning in Tandem", US Patent 5802826, September 1998.

[8] Fritz Stahlecker, Bad Ueberkingen, "Wrapped yarn Spinning Machine", US Patent 4481760,November 1984.

[9] R.A. Serway and J.W.Jr. Jewett, "Physics for Scientists and Engineers", 6th Ed. Brooks Cole. ISBN 0-53440-842-7.

[10] Tipler and Paul, "Physics for Scientists and Engineers: Mechanics, Oscillations and Waves, Thermodynamics (5th ed.)", W. H. Freeman. ISBN 0-7167-0809-4, 2004.

[11] SI brochure Ed. 8, Section 5.1, Bureau International Des Poids et Mesures, April 2007.

DESIGN OF CRYPTO ALGORITHMS FOR AN ENHANCED CRYPTO PROCESSOR TO THE SECURITY SYSTEMS

D. Sharmila[1] and R. Neelaveni[2]

[1]Department of Electronics and Communication Engineering, Bannari Amman Institute of Technology, Sathyamangalam - 638 401, Erode District, Tamil Nadu

[2]Department of Electrical and Electronics Engineering, PSG College of Technology, Coimbatore - 641 004, Tamil Nadu

Email: sharmiramesh@rediffmail.com, rn64asok@yahoo.co.in

(Received on 10 December 2008 and accepted on 18 February 2009)

Abstract

This paper presents an VHDL simulation of a crypto algorithms for the execution of encryption, decryption and key scheduling operations. Our crypto processor is enhanced by the addition of a crypto block which is hash algorithm. This crypto processor can be used for various security applications such as storage devices, embedded systems, network routers etc..The crypto processor consists of 32 bit RISC processor block and crypto blocks which are dedicated to secret key, public key and hash algorithms. AES, SEED, triple-DES, KASUMI are private key and ECC, RSA are public key algorithms while whirlpool-hashing core is hash algorithm. The 32-bit RISC processor block can be used to execute various crypto algorithms such as Hash and other application programs such as user authentication and IC card interface.

Keywords: *AES, KASUMI, RSA, SEED, Triple DES ECC, Whirlpool Hashingcore.*

1. INTRODUCTION

The expansion of the world wide communication network such as the internet and the increased dependency on digitized information in our society makes information more vulnerable to abuse. If there are security problems in these information systems, users will fear that information may be monitored and business secrets stolen. For these reasons it is important to make information systems secure by protecting data and resources. Cryptography algorithms are the core of such security systems.

Crypto processor has a RISC processor and coprocessor blocks dedicated to crypto algorithms. The dedicated crypto blocks of the crypto processor permit fast execution of encryption, decryption and key scheduling operations for AES, KASUMI, SEED, and triple DES secret key crypto algorithms and ECC and RSA public key crypto algorithm [1]. Compared to other block ciphers Whirlpool doesn't have same randomness related weakness as block ciphers usually tend to have. Overall structure of Whirlpool hash function has been shown to be resistant to the usual attacks on block-cipher-based hash codes. The 32 bit RISC processor block can execute other crypto algorithms including hash algorithms and control the dedicated crypto block and I/O buffers. Crypto algorithms can be programmed with out interrupting the host node work. The crypto processor is designed with the design philosophy of making reasonably high performance for other crypto algorithms. Various crypto algorithms can be programmed and executed in our crypto processor without interrupting the host node's work.

2. THE ENHANCED CRYPTO PROCESSOR ARCHITECTURE

The crypto processor has a PCI interface logic, dual port memory controller, register file, data path controller and dedicated crypto blocks for the AES, KASUMI, SEED, triple DES, ECC, RSA and whirlpool hashing core algorithms.

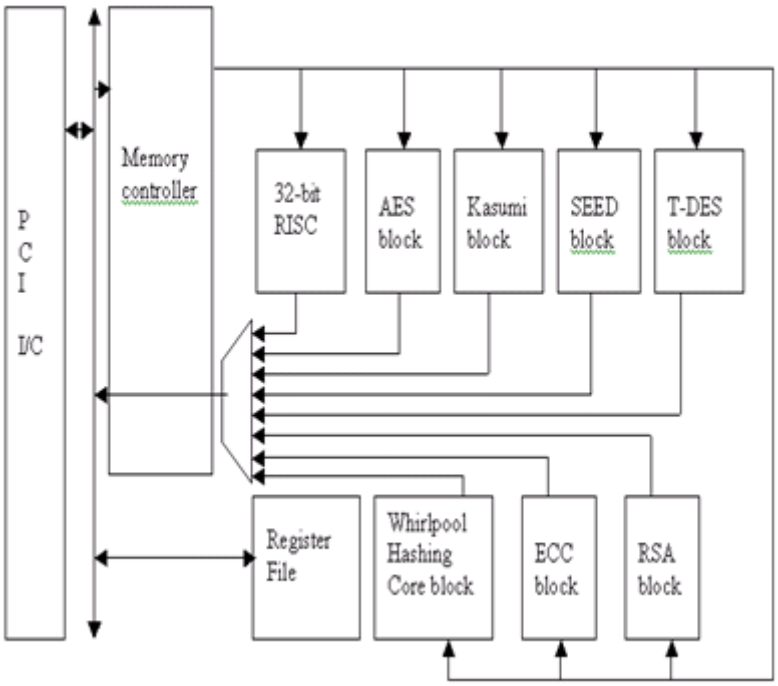

Fig. 1 Block diagram of the private and public key crypto processor.

The 32 bit RISC type controller controls the dedicated crypto block and performs the interface operations with external devices such as memory and I/O bus interface controller. The dedicated crypto block results in fast execution of the encryption, decryption and key scheduling operations for the AES, KASUMI,SEED and triple DES algorithms and enables fast scalar multiplication and exponentiation operation for the ECC and RSA crypto algorithms. Then PCI interface logic permits our crypto processor to be easily applied to practical environments.

3. THE 32-BIT RISC PROCESSOR BLOCK

In our crypto processor, we have used the ARM7TDMI processor, the 32 -bit RISC type processor block with a three-stage pipeline. It controls the operation of the dedicated crypto block during encryption, decryption and key scheduling and also performs the operations required to interface with external devices such as the input buffer, output buffer, memory and IC card interface logic. The RISC processor block is fully programmable; it can execute various crypto algorithms, protocols and application programs with a high degree of freedom.

The 32-bit RISC processor block has features such as barrel shifter, booth multiplier block, register file and a 16 bit and 32 bit data memory architecture that enable it to achieve high performance and savings in memory, when executing crypto algorithms. The 32 bit barrel shifter implements a shifty rotates of its input data by any amount to produce an output with in a fixed time period. The barrel shifter boosts the performance of crypto algorithms, such as most symmetric key crypto algorithms. The booth multiplier block assists in implementation of the multiply and multiply-and-add instructions.

4. AES CRYPTO BLOCK

The national institute of standards and technology (NIST) issued a request for possible candidates for a new advanced encryption standard to replace the DES. Then in October of 2000, NIST announced the cipher Rijndael, which is developed by Joan Daemen and Vincent Rijndael, is a block cipher using 128,192, 256 bit input/ output and keys. The sizes of data blocks and keys can be chosen independently. The number of rounds depends on both of these parameters.

In this paper 128 bits for both I/O block and user keys are assumed. Figure 2 shows the encryption and decryption structure of the AES algorithm. After the initial round key addition, N rounds of encryption are performed [2].

The first 1 N rounds are the same, with a small difference in the final round. As shown in Figure 2 (a), each of the first 1 N rounds consists of 4 transformations: Sub Bytes, Shift Rows, Mix Columns and AddRoundKey.

4.1 Sub Bytes

This transformation is performed on each byte of the State using a substitution table(S-box). The S-box is constructed of the compositions of two transformations: multiplicative inverse in GF(28) with irreducible polynomial m(x)=x8+x4+x3+x+1, and an affine mapping over GF(2).In the decryption process, the inverse S-box is used. The inverse S-box is constructed by first applying the inverse of the affine transformation and then computing the multiplicative inverse in Galois Field GF (2).

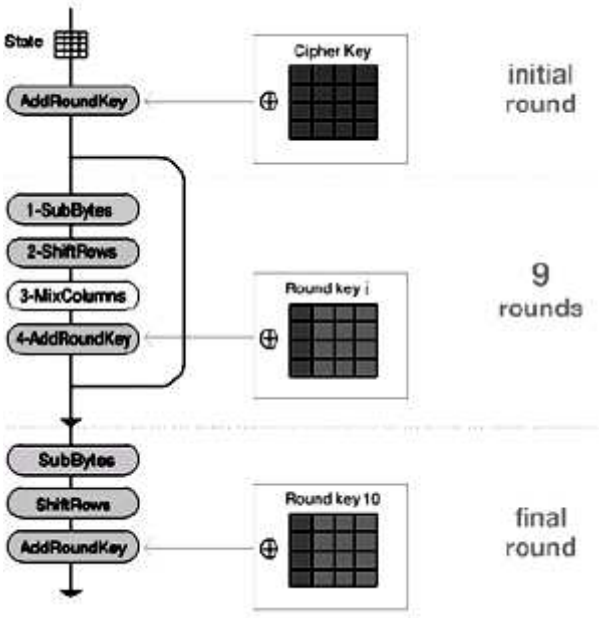

Fig.2 Structure of AES cipher

4.2 Shift Rows

In this transformation, the rows of the State shift cyclically to the left with different offsets. In the decryption process, the shifting offsets have different values.

4.3 Mix Columns

The MixColums transformation is performed on the State column-by-column. Each column is considered as a four-term polynomial over GF(28) and multiplied by a(x) modulo x4+1 ,
where a(x)={03}x3+{01}x2+{01}x+1 for encryption
and a(x)={0B}x3+{0D}x2+{09}x+{0E} for decryption.

4.4 AddRoundKey

In this transformation, a round key is added to the State using a bitwise Exclusive-OR(XOR) Operation. AddRoundKey is the same for the decryption process. The decryption algorithm uses a different ordering of the inverse forms of the transformations used in the encryption algorithm as shown in Figure2.

5. KASUMI CRYPTO BLOCK

KASUMI block cipher is used for the security part of many synchronous wireless standards that produces a 64-bit output from a 64-bit input under the control of a 128-bit key. KASUMI has a Feistel structure comprising eight rounds, operates on 64-bit data blocks, and the processing is controlled by a 128-bit encryption key K.

Additionally, KASUMI has the following features derived from its Feistel nature: input plaintext is the input to the first round, cipher text is the last round's output, the encryption key is used to generate a set of round keys {KLi, KOi, KIi} for each round i, each round computes a different function as long as the round keys are different, and the same algorithm is used both for encryption and decryption.[3] For odd rounds the round-function is computed by applying the FL function followed by the FO function. For even rounds the FO function is applied before FL. FL is a 32-bit function made up of simple AND, OR, XOR and left rotation operations. FO is also a 32-bit function having a three round Feistel organization which contains one FI block per round. FI is a non-linear 16-bit function having itself a four-round Feistel structure. It is made up of two nine bit substitution boxes (S-boxes) and two seven-bit S-boxes [4].

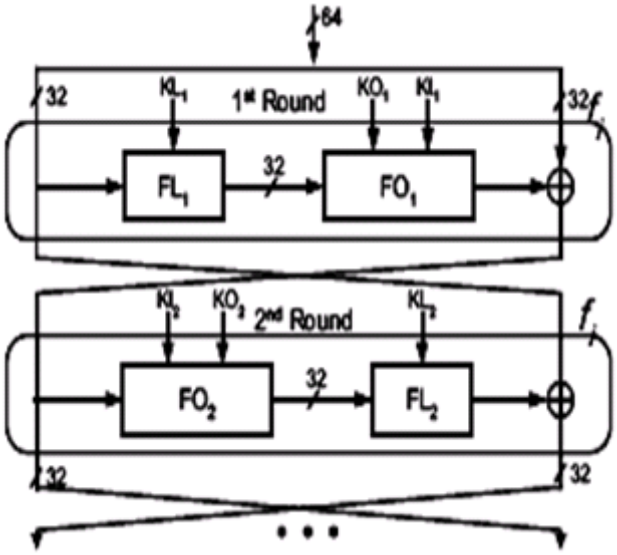

Fig.3. Block diagram of the KASUMI crypto algorithm

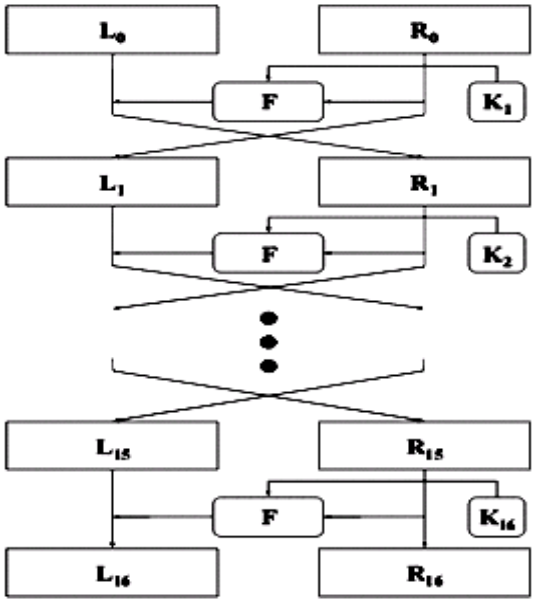

Fig.4 Structure of SEED

Figure 3 shows that data in the FI function flow along two different paths: a nine-bit long path (thick lines) and a seven bit path (thin lines). Notice that in Feistel structures, such as the ones used in this algorithm, each round's output is twisted before being applied as in put to the following round. After completing eight rounds KASUMI produces a 64-bit long cipher text block corresponding to the plaintext input block.

6. SEED CRYPTO BLOCK

SEED is designed to utilize the S-boxes and permutations that balance with the current computing technology. Figure 4 shows the Feistel structure with 16 rounds, and is strong against differential cryptanalysis and linear cryptanalyst is balanced with security/efficiency trade-off. [5]

This section specifies a complete decryption of the encryption algorithm. SEED, which is a secret key cipher with 128-bit data block and 128-bit secret key. The abstract features of SEED are outlined as follows

- Feistel structure with 16 rounds
- 28-bit input-output data block size
- 28-bit key length
- Two 8× 8 S-boxes
- Mixed operations of exclusive OR and modular addition.

7. T-DES CRYPTO BLOCK

The Data Encryption Standard (DES) shall consist of the following Data Encryption Algorithm (DES) and Triple Data Encryption Algorithm (TDEA). These devices shall be designed in such a way that they may be used in a computer system or network to provide cryptographic protection to binary coded data. Triple DES is simply another mode of DES operation. Fig.5 shows the block diagram of T-DES algorithm, with three 64-bit keys, for an overall key length of 192 bits. In Private Encryptor, you simply type in the entire 192-bit (24 character) key rather than entering each of the three keys individually. The Triple DES DLL then breaks the user provided key into three sub keys, padding the keys if necessary so they are each 64 bits long. The procedure for encryption is exactly the same as regular DES, but it is repeated three times.

Hence the name Triple DES. The data is encrypted with the first key, decrypted with the second key, and finally encrypted again with the third key.

The procedure for decrypting something is the same as the procedure for encryption, except it is executed in reverse. Like DES, data is encrypted and decrypted in 64-bit chunks. Unfortunately, there are some weak keys that one should be aware of: if all three keys, the first and second keys, or the second and third keys are the same, then the encryption procedure is essentially the

same as standard DES. The least significant (right-most) bit in each byte is a parity bit, and should be set so that there are always an odd number of 1s in every byte. These parity bits are ignored, so only the seven most significant bits of each byte are used, resulting in a key length of 56 bits. This means that the effective key strength for Triple DES is actually 168 bits because each of the three keys contains 8 parity bits that are not used during the encryption process

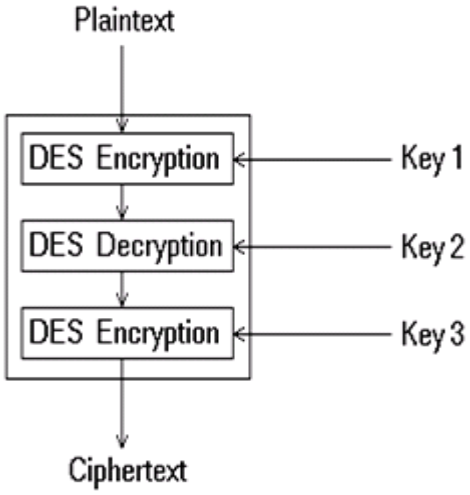

Fig. 5 Block diagram of T-DES crpyto algorithm

7.1 Triple ECB (Electronic Code Book)

This variant of Triple DES works exactly the same way as the ECB mode of DES. Triple ECB is the type of encryption used by Private Encryptor. This is the most commonly used mode of operation.

7.2 Triple CBC (Cipher Block Chaining)

This method is very similar to the standard DES CBC mode. As with Triple ECB, the effective key length is 168 bits and keys are used in the same manner, as described above, but the chaining features of CBC mode are also employed. The first 64-bit key acts as the Initialization Vector to DES. Triple ECB is then executed for a single 64-bit block of plaintext. The resulting cipher text is then XORed with the next plaintext block to be encrypted, and the procedure is repeated. This method adds an extra layer of security to Triple DES and is therefore more secure than Triple ECB, although it is not used as widely as Triple ECB.

8. WHIRLPOOL HASHING CORE

Fig.6 shows the Whirlpool algorithm based on a dedicated block cipher W that operates on 512-bit data blocks (ni) using a 512-bit key (Hi”1). Initially, the key input (H0) is a string of zeroes. The hash function is constructed from a compression function using the Merkle- Damgård method. The compression function has been built from the internal block cipher with the Miyaguchi- Preneel construction. Before the message is subjected to hashing operation, a specific padding is appended to the message. The block cipher W is composed of ten identical rounds of transformations. All basic operations are performed on 8-bit bytes and each byte are interpreted as a polynomial in the Galois Field GF (28). The cipher operates on a 512-bit hash state using a chained 512-bit key state, derived from the data input and the key input respectively. The states are internally viewed as 8-by-8 matrices of bytes.

The data path and the key schedule of W and the sequences of the round transformations. The operations are performed in the data path as well as in the key schedule during a round are defined as follows: The non-linear layer ã is a byte substitution operation. The substitute values for the bytes of the state are derived from the substitution box (S-box) S individually The key schedule expands the initial 512-bit cipher key into a sequence of 11 round keys K0, K1, K10, i.e. key states. Before the transformations of the first round, the input message block ni is XORed with the first round keyK0, which equals to the input Hi”1. In the key addition phase of the key schedule, an iteration-round-dependent constant matrix cr is XORed to the key state.

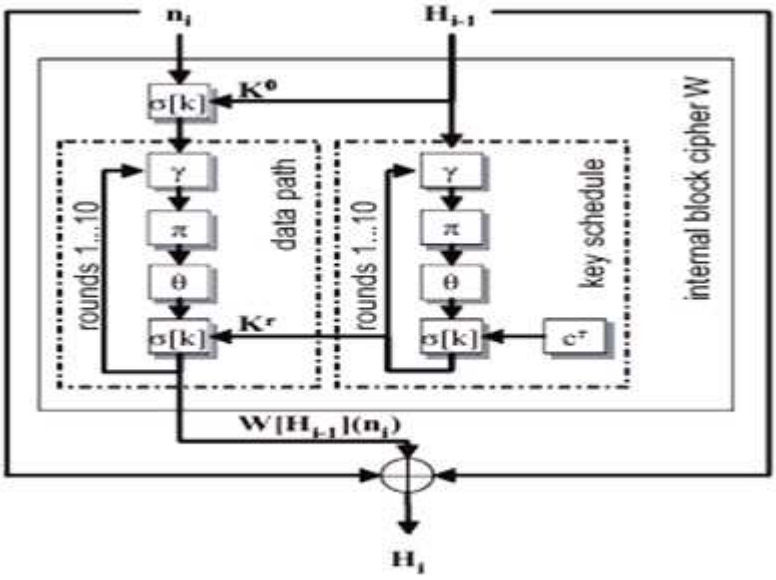

Fig. 6 Block diagram of whirlpool hashing core

8.1 Substitution Box

The non-linear layer transformation ã makes use of the S-box S that has 256 8-bit entries. It can directly be implemented as combinatorial logic or ROM. However, due to the internal structure of S, it can also be constructed from 16-entry mini-boxes E, E"1, and R. The contents of the boxes are given in [1]. Each mini-box can be implemented by using only four 4-input Look-Up-Tables (LUT), which typically are the basic building blocks of FPGA devices. Since each XOR gate consumes one 4-input LUT, the total resource consumption for a mini-box-based S-box is 32 4-input LUTs.

8.2 Diffusion Unit

The constant polynomial coefficients of C in the diffusion layer transformation è have been chosen so that they contain as few terms as possible. The needed basic operation for the matrix multiplication is a finite field multiplication in GF(28) with the polynomial 02x. The multiplications by 04x and 08x can be calculated by successively applying the multiplication with 02x, since $04x \cdot d = 02x \cdot 02x \cdot d$ and $08x \cdot d = 02x \cdot 04x \cdot d$.

Similarly, the multiplications with 05x and 09x can be performed by using previously computed values and one addition (which is simply an XOR operation). The complete circuit that computes all the required multiplications for a state byte, requires 25 XOR gates in total. The multiplier unit exploits the circulant property of the multiplicand matrix in the same way as in the implementation of the AES algorithm. Data are fed to the unit's input (d_in) byte by byte and the intermediate results are maintained in the eight registers. During the first eight cycles of the operation, the multiplication operation is performed by adding and cyclically shifting the intermediate results in the unit.

8.3 Cyclical Permutation

Since the states are stored in memories, the permutation ð can be performed with addressing logic. The data elements of the states remain at the same memory locations during the round operations but the addressing sequence differs from round to round. After the bytes of a row are processed, they are written back to the same memory locations. The 64-entry DPRAMs are organized so that the three most significant bits of a memory address indicate the row of a state matrix and the three least significant bits indicate the column.

Initially, before the first round, the bytes of the state s are organized so that the element sij is located in the memory location [i, j] (the notation [i, j] refers to the memory location (8i+j). It can be seen from (1) that during the first round of operation the jth element of the row i must be read from the location

[(i - j) mod 8, j].

Similarly, since the bytes are stored back in the same locations, the read address for the second round is [((i - j) mod 8 - j) mod 8, j] = [(i -2j) mod 8, j].

This can be generalized for the round r, for which the address location for the jth element of the row i is [(i - rj) mod 8, j].

The addressing logic satisfying this is implemented with three 3-bit counters i, j, and r and a small amount of combinatorial logic.

9. RSA CRYPTO BLOCK

The RSA public key crypto system was invented in 1978 by Rivest et al. and it is now the most widely deployed public key crypto system. It is used for securing web traffic and e-mail in the SSL protocol. The security of the RSA cryptosystem depends on the difficulty of factoring a large integer, the published modulus value. [6]

RSA is a cipher in which the plaintext and the cipher text are integers between 0 and 'n-1', for some valued 'n'. For a long message, the message is broken into blocks. These blocks are log2n bits long. Two high-value prime numbers are multiplied to get 'n' so that extracting the value of 'n' becomes very difficult. As the public and private keys are dependent on the value of 'n', guessing this value is very difficult. Encryption and decryption make use of modular arithmetic. The RSA algorithm for plaintext block M and cipher text block C with keys 'e' and 'd' is given below: Key generation

Select p, q p and q are both prime

Calculate n = p x q

Calculate f(n) = (p-1)(q-1)

Select integer e gcd(f(n),e)=1; 1<e<f(n)

Calculate d d=e-1 mod f (n)

Public Key KU = {e,n}

Secret key KR = {d, n}

Encryption

Plaintext: M<n

Cipher text: C = M(modn)

Decryption

Cipher text: C

Plaintext: M = C(mod n)

The RSA Algorithm

C = Me mod n

M = Cd mod n = (Me)d mod n = Med mod n

Both sender and receiver must know the value of 'n' and 'e'; whereas only the receiver knows the value of d. Thus, this is a public-key encryption algorithm in which the public key is {e,n} and the private key is {d,n}. For public-key encryption, this algorithm will be satisfactory if the following conditions are fulfilled:

- Values of e, d, and n exist such that M = Med mod n, for all M < n.
- It should be relatively easy to calculate Me and Cd for all values of M < n.
- It should be unfeasible to determine d, even if the values of e and n are known.

10. ECC CRYPTO BLOCK

ECC crypto system was proposed independently in 1985 by Vitor Miller and Neal Koblitz. The ECC crypto system is based on the difficulty of solving the discrete logarithm problem. In general, ECC has advantages over RSA in that ECC has higher security per key bit, higher speed, lower power consumption, and better storage efficiencies than RSA. For these reasons, ECC is particularly beneficial in applications with bandwidth, processor capacity, power availability, or storage constraints such as IC cards, mobile devices, etc. [7].

The elliptic curve used in our crypto processor is defined by Weierstrass equations. Since the ECC over a normal basis is efficient in hardware implementations; we have chosen a curve such as GF (2146) over a normal basis.

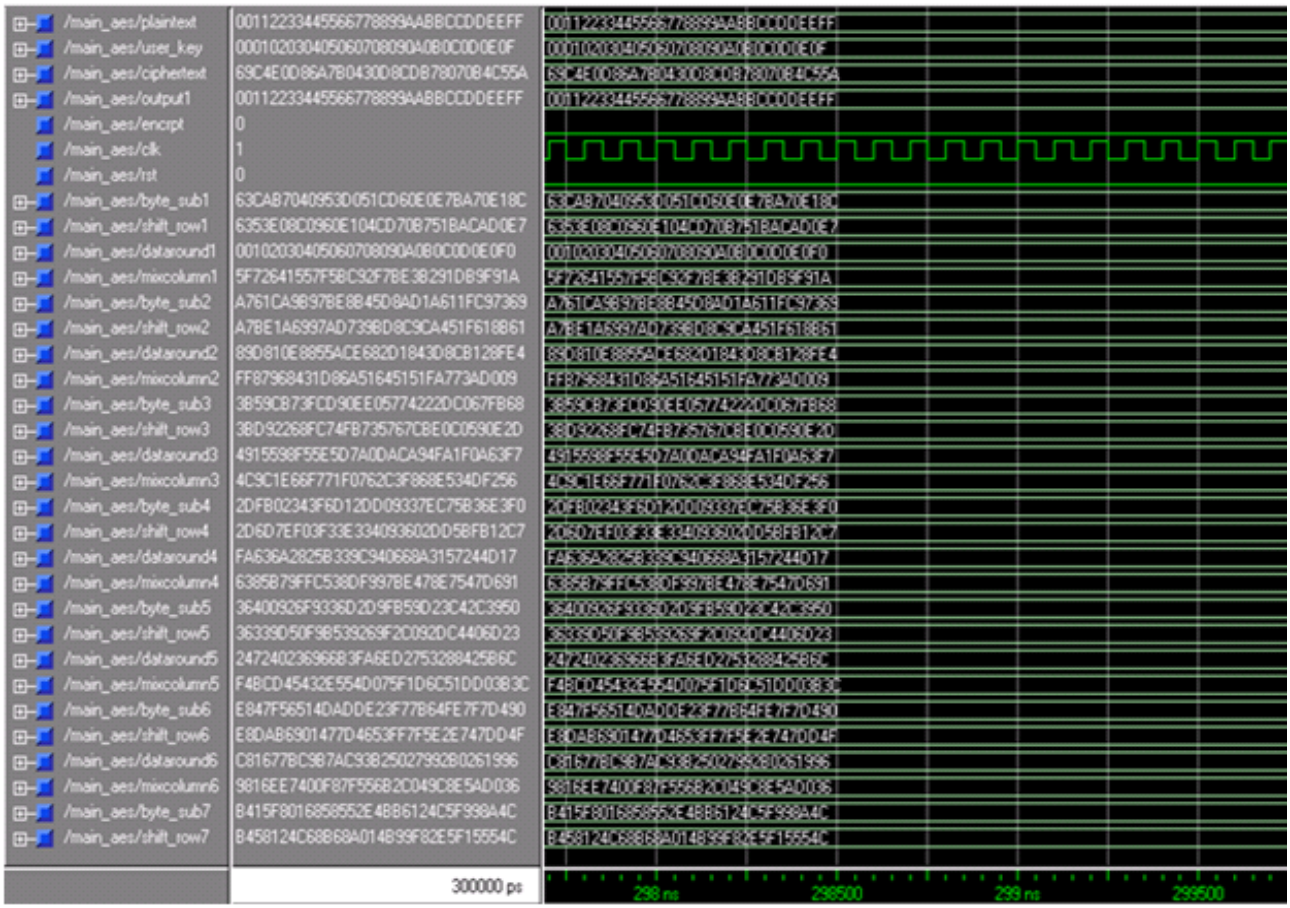

12.2 Simulation Result for KASUMI Algorithm

The simulation results employing encrypted and decrypted output of 64 bit data with 128-bit key and shows the output data for each round.

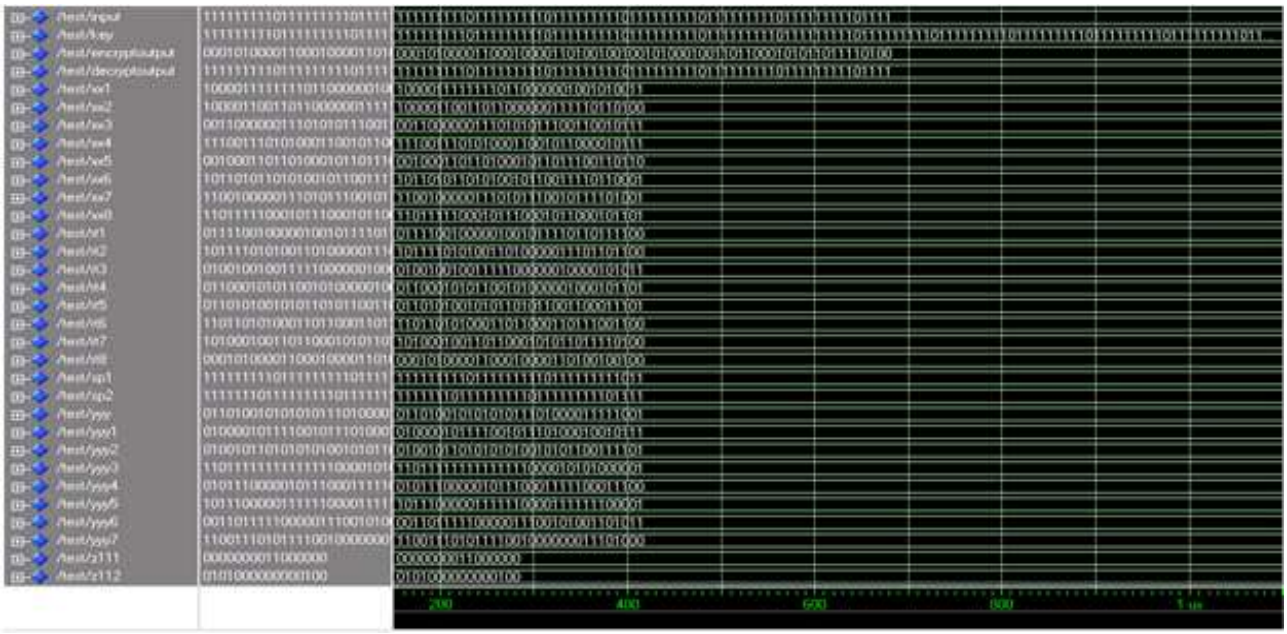

12.3 Simulation Result for SEED Algorithm

Displays the encryption and decryption results of 128 bit data with the round keys

12.4 Simulation Result for T-DES Algorithm

Shows the simulated output of T-DES algorithm employing the encryption and decryption data with the scheduling of three keys.

12.5 Simulation Result of Whirlpool Algorithm

12.5(i) Simulation Result of s-box

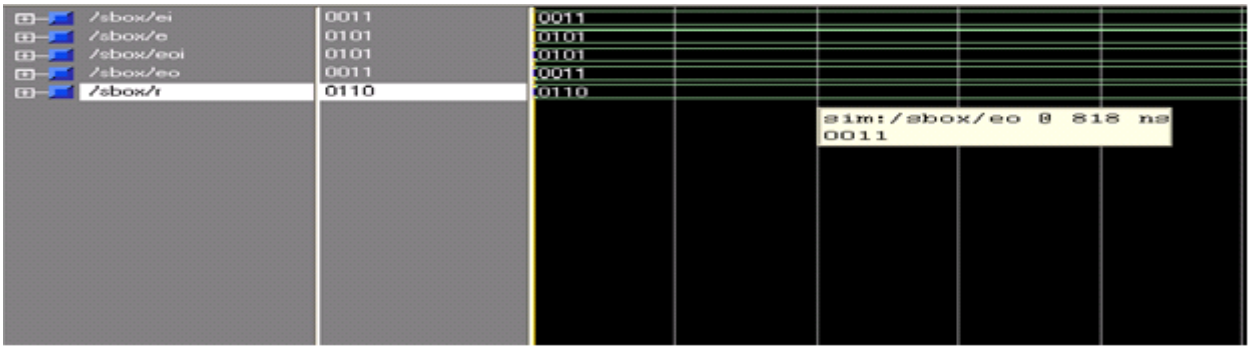

12.5(ii) Simulation Result of Diffusion Unit

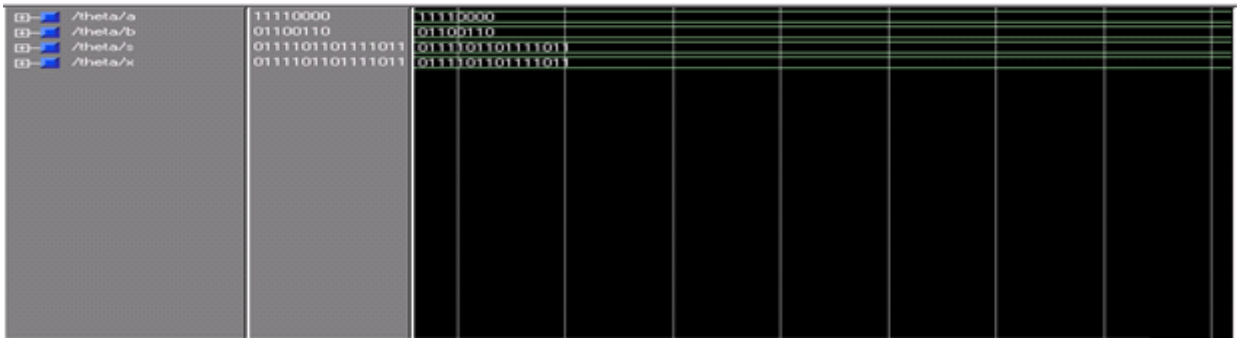

12.6 Simulation Result for RSA Algorithm

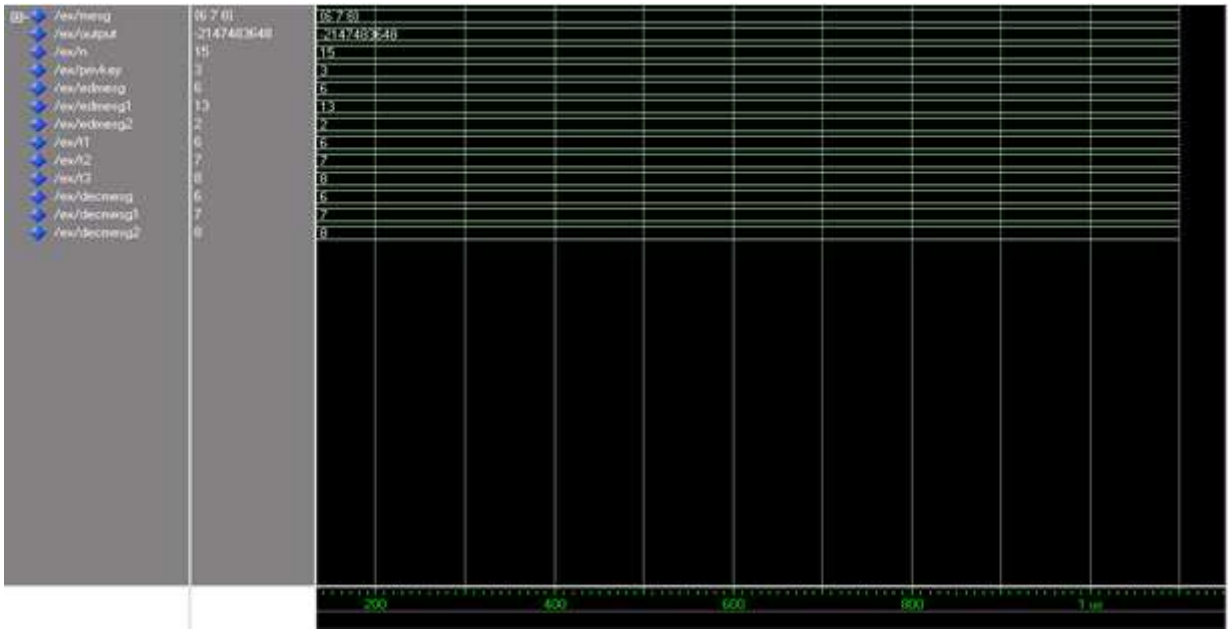

REFERENCES

[1] HoWon Kim and Sunggu Lee, "Design and Implementation of a Private and Public Key Crypto Processor and its Application to a Security System", IEEE Transactions on Consumer Electronics, Vol.50, No.1, February 2004.

[2] Xinmiao Zhang and Keshab K.Parhi, "Implementation Approaches for the Advanced Encryption Standard Algorithm", IEEE Circuits and Systems Magazine, Vol.2, No.4, pp.24-46.

[3] ETSI/SAGE, Specification of the 3GPP Confidentiality and Integrity Algorithms, Document 2: KASUMI Specification December 1999.

[4] H. W. Kim, Y. J. Choi, M. S. Kim, and H. S. Ryu, "Hardware Implementation of 3GPP KASUMI Crypto Algorithm", ITC-CSCC, Phuket, Thailand, Vol. 1, July 16 -19, 2002, pp.317-320.

[5] TTA, 128-bit Symmetric Block Cipher (SEED), Telecommunications Technology Association (TTA), Seoul, Korea, June 1999.

[6] R. L. Rivest, A. Shamir and L. Adleman, "A Method for Obtaining Digital Signatures and Pubic-key Cryptosystems" , Commun. ACM, Vol.21, No.2, 1978, pp. 120-126.

[7] F. Blake, G. Seroussi and N.P. Smart, "Elliptic Curves Cryptography", London Mathematical Society Lecture Notes, C Cambridge University Press, Cambridge, 2000.

[8] H. W. Kim, Y. J. Choi, M. S. Kim, and H. S. Ryu, "Hardware Implementation of 3GPP KASUMI Crypto Algorithm" , ITC-CSCC, Phuket, Thailand, Vol.1, July 16-19, 2002, pp.317-320.

[9] Don B. Johnson, Alfred J. Menezes and Scott Anstone, "Elliptic Curve Digital Signature Algorithm (ECDSA)", available at http://www.certicom.com.

[10] Konstas Marinis, Nikos K. Moshopoulos, Foris Karoubalis and Kiamal Z. Pekmestzi, "On the Hardware Implementation of the 3GPP Confidentiality and Integrity Algorithms", ISC 2001, Lecture Notes in Computer Science, 2001.

[11] National Institute of Standards and Technology, FIPS Publication 46-2: Data Encryption Standard, National Institute for Standards and Technology, Gaithersburg, MD, USA, December 1993.

[12] Alfred J. Menezes, Paul C. Van Oorschot and Scott A.Vanston, Ed., "Handbook of Applied Cryptography", CRC Press, 1996.

[13] Mitsuru Matsui, "New Block Encryption Algorithm MISTY," Fast Software Encryption '97, Vol. 1267 of LNCS, Springer-Verlag, 1997, pp.54-68.

COMPARATIVE STUDY OF CADMIUM SULPHIDE AND ALUMINIUM DOPED CADMIUM SULPHIDE FILMS PREPARED BY SPRAY TECHNIQUE

R. Thiyagarajan[1], M. Anusuya[2] and M. Mahaboob Beevi[3]
[1]Department of Physics, Urumu Dhanalakshmi College, Trichy - 620 018, Tamil Nadu
[2&3]Department of Physics, Trichy Engineering College, Trichy - 621 132, Tamil Nadu
E-mail: anu51069@yahoo.com
(Received on 15 December 2008 and accepted on 27 February 2009)

Abstract

Thin films of Cadmium Sulphide and Aluminum doped Cadmium Sulphide were deposited on glass substrates at 2500C using chemical spray pyrolysis technique from the aqueous solution of Cadmium acetate, Thiourea and Aluminium acetate along with the Complexing agent. Investigation of the optical properties of the film was carried out using computer controlled spectrophotometer. Energy band gap (Eg) of these films was found by plotting a graph between hv and (áhv)1/2 and it is in the range of 2.05eV to 2.25eV. These films shows low transmittance (below 50 %) in the visible region while exhibiting high absorbance in the same region therefore they could be used for window layer material. X- ray diffraction (XRD) studies reveal that the films are polycrystalline in nature with grain size in the order of nanometers and it is confirmed with SEM results.

Keywords: *Band Gap, Structural Properties, Spray Pyrolysis,Thin Film*

1. INTRODUCTION

Thin film science has received tremendous attention during the last few decades because of its numerous applications in various fields. Thin film coatings of ceramic material are widely used as a protective layer against corrosion, antireflection coating and for special electrical functions. Due to thermal and chemical stability of cadmium, it found extensive application in optical coating [1], and optoelectronic devices [2,3]. In the recent past cadmium is attracting continuously with increasing interest as a dielectric, with relatively wide band gap and high refractive index. For large area deposition the techniques requiring vacuum system may not be suited for meeting the goal of a low cost production technology. Chemical spray pyrolysis can be one of the techniques, which may be suitable for this purpose.

Chemical Spray Pyrolysis is a low equipment cost technique for depositing thin polycrystalline films of oxides, binary and ternary chalcogenides and superconducting oxide films [4]. Physical quantities are usually influenced by the chemical composition, micro structure, and substrate morphology which are dependent on the deposition condition and preparation methods.

2. EXPERIMENTAL

Cadmium Sulphide thin films were prepared from the precursor solutions, containing salts of Cadmium acetate (Cd (CH3COO)2.2H2O) (0.1M), and Thiourea (CH4N2S) (0.1M) in double distilled water along with the complexing agent Ethylene-Diamine-Tetra-Acetic acid (EDTA) C10H16N2O8 of 0.1M is chosen to stabilize the grain size. The amount of solution was made together as 50 ml. In the same way Aluminium doped Cadmium Sulphide thin films were prepared from the precursor solutions; containing salts of Cadmium acetate (0.1M), Thiourea (0.1M) and Aluminum acetate (CH3CO2)2AlOH (0.05M) in double distilled water along with the complexing agent Ethylene-Diamine-Tetra-Acetic acid (EDTA) of 0.1M is chosen to stabilize the grain size.

The Spray Pyrolysis setup consists of a substrate heater, spray gun, air compressor, solution reservoir and a gas exhaust unit. Details of this setup have been published elsewhere [5]. The air pressure is kept around 1.1 bar, the solution flow rate is fixed to 2 ml per minute and the spraying time is ranged between 1-2 seconds. The aqueous solution was then sprayed on the preheated glass substrate kept at 2500C compressed dry air at a pressure of 12 kg/cm2 from an air compressor via an air

filter cum regulator was used as the carrier gas and spray rate of the solution was maintained at 3ml/min. The distance between the spray nozzle and the substrate is 35cm. The spray time was maintained constant about one second throughout the deposition. An increase in spray time causes thermal shock of the substrate due to excessive cooling. A two minute waiting time is allowed between each spray to maintain the substrate temperature and enable to decompose the starting material completely. Total time is forty five minute for all deposition. Film obtained due to endothermic thermal decomposition that takes place at the hot surface of the substrate. The terminal thickness of the films was measured by gravimetric technique and it is found to be in the order 800-900 nanometers. The measured thickness of the films is verified by the cross sectional view of the Scanning Electron Microscope.

3. RESULT AND DISCUSSION

3.1 Optical Studies

A computer controlled ELICO make (SL 159 UV - VIS) Spectrophotometer was used to obtain optical properties of CdS and CdS: Al films over a wide wavelength range of 400 nm to 1000 nm. The obtained absorbance and transmittance spectra of films in visible region are shown in Figure 1 and Figure 2. It is found that transmittance decreases due to the Aluminium dopant in CdS. This decrease in transmittance is due to the increase in absorption and reflection at the surface. It is also observed that the increase in transmittance with increase in wavelength for the film is not sharp.

This indicates that the transitions in the studied films are due to direct and indirect transition. The transmission spectrum of both the films reveals that films exhibits poor transmittance between 20 to 35% in the visible region. This property of low transmittance of the film throughout the visible region makes it a good material for window layer application.

The transmittance of the film is also influenced by a number of minor effects which include surface roughness and optical inhomogeneous in the direction normal to the film surface.

The absorption co-efficient (á) is calculated using Lamberts law and it is found in the order of 104 m-1.

$$á = 2.303A/t \quad (1)$$

'A' is the absorbance and 't' is the thickness of the film, neglecting the reflection co-efficient which is negligible and insignificant near the absorption edge. The optical band gap Eg was calculated using Tauc's plot (áhí)2 Vs hí. The photon energy at the point where (áhí)2 is zero represents Eg, which is determined by extrapolation. The typical plots of (áhí)2 versus hí for CdS and CdS: Al thin films deposited on glass substrate is shown in Figure (3).

It was observed there is a slight shrinkage in optical band gap (2.25eV-2.05eV) due to the doping of Aluminium in CdS.

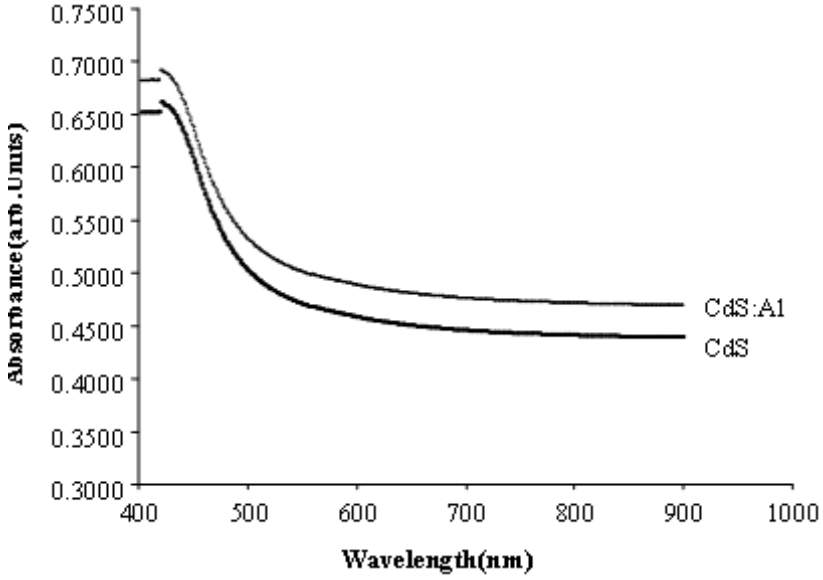

Fig.1 Absorbance spectra of CdS and Al doped CdS films

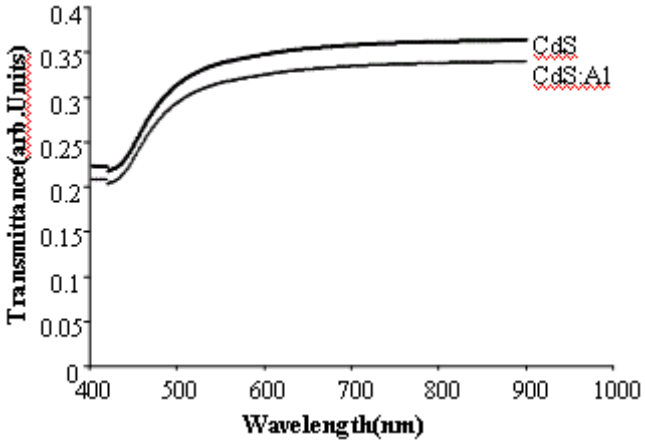

Fig. 2 Transmittance spectra of CdS and Al doped CdS films

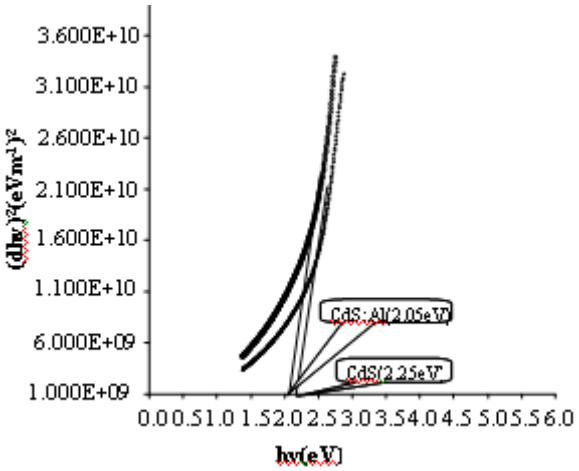

Fig.3 Tauc's plots of CdS and Al doped CdS films

The Optical band gap widening and shrinkage was generally attributed to Moss-Burstein shift [6], it is due to the optical band filling effect. The optical shrinkage is due to the electron to electron interaction at higher carrier concentration. The difference in band gap between undoped CdS [7,8] and Al doped CdS films, may be a particle size effect (grain size), and it is also corroborated by XRD and SEM analysis. From XRD and SEM results, the grain size of Aluminium doped CdS is smaller than undoped CdS. It can be attributed that grain size decreases, the band gap also decreases of as deposited films [9].

3.2 XRD Studies

XRD pattern of the deposited films were studied at room temperature by using (model RAD II A) with CuKá radiation (1.5418Å) where other radiations are suppressed using Ni filter. The data were recorded at a scan rate of 0.20 /min and in the range of 200<2è<800. The crystalline pattern of as deposited films on clean glass substrate prepared at 2500C is as shown in Figure (4). The film surface found to be smooth, homogeneous and adherent to the substrate with no signature for impurity phases. The observed peaks in all the diffractograms confirm the nanocrystalline nature of the film. The XRD pattern of the films also reveals that the film is polycrystalline with cubic crystal structure with preferential orientation along (111) [10, 11] plane.

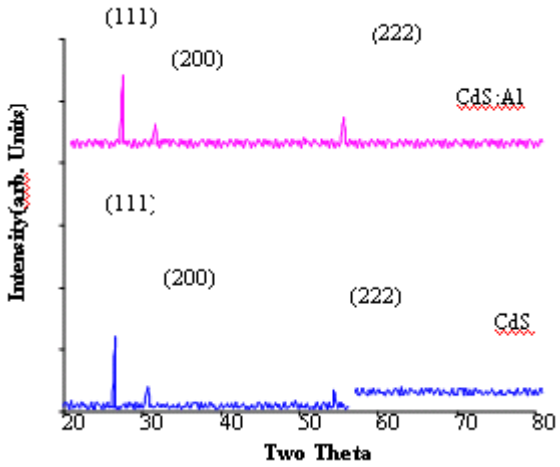

Fig.4 XRD pattern of CdS and Al doped CdS films

The absence of the additional peaks in the XRD results of Aluminum doped Cadmium Sulphide thin film samples indicates the formation of single phase CdS. No phase corresponding to Aluminum / Aluminum Sulphide or other Aluminum compounds was detected in the XRD. The films exhibited an intense peak oriented along the (111) lattice plane parallel to the substrate. The other strong peaks observed from the XRD spectra correspond to the (200) and (222) orientations. The diffraction peaks appear in the spectrum has been identified at 26.55 0, 30.75 0 and 54.680 are verified with the known patterns of standard X-Ray Diffraction data file (JCPDS file No: CdS- 80-0019) [12] While comparing the X-ray diffraction (XRD) pattern it is found due to Aluminum dopant in the film, the position of the Bragg peaks in XRD pattern, shift towards higher angle. It may be attributed to the change in grain size and strain in the film. The mean grain size of CdS calculated using Scherrer's equation is 45 nm and for Aluminium doped CdS is found to be

38nm. It was found that the grain size decreases due to Aluminium in the films. The above result is in good agreement with SEM results.

3.3 SEM Studies

The SEM micrograph of the thin film deposited on a clean glass slide at 2500C, is taken using cold field emission of SEM (JEOL, JSM 6701F, Japan). Prior to the observation, using an auto sputter fine coater (JFC 1600, JEOL Japan) about 50A0 gold was sputtered on the thin film surface for better contrast and to avoid charge accumulation. SEM micrograph of the undoped Cadmium Sulphide thin film and Aluminium doped Cadmium Sulphide thin film deposited at 2500C is taken to support the XRD observations. Fig. (5) & (6) shows the SEM micrographs of surface topography of the deposited films. The films doped with Al (fig. 6) have smaller particle size of than that undoped CdS (Fig. 5).

A decrease in crystallite size could be attributed to the increasing number of nucleation centers during incorporation of dopant into the host material. The grains are closely placed with some pinhole. The undoped Cadmium Sulphide thin films showed compact distribution over the surface and good connectivity between grains. From the micrographs it is clearly seen that the grain size is in the nanometer range and they are spherical in shape. The fluffy mass was present in cluster form and they were not uniformly distributed.

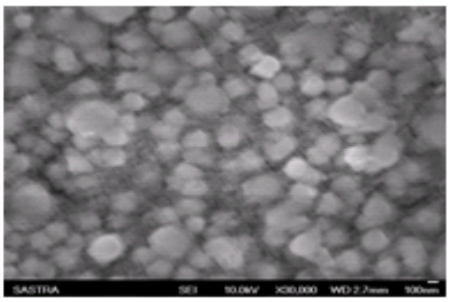

Fig.5 SEM image of CdS

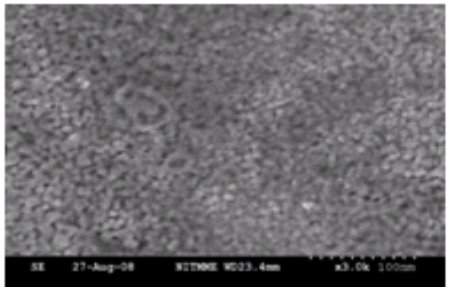

Fig.6 SEM image of Al:CdS

The films showed compact distribution over the surface and good connectivity between grains. From the micrographs it is clearly seen that the grain size is in the nanometer range and they are spherical in shape

4. CONCLUSION

Thin films of undoped CdS and Aluminium doped CdS on glass substrate were prepared by spray pyrolysis technique at 250°C. The absorption coefficient and optical band gap were determined from the absorbance spectra recorded in the wavelength range of 400-1000nm.

It was found that the absorbance of the Aluminium doped CdS thin films increases slightly due to deponent of Aluminium. Optical energy band gap value of CdS and Al doped CdS were found to be 2.25eV, 2.05eV respectively. The properties of low transmittance CdS: Al film throughout the visible region makes it a suitable material for window layer application. The XRD pattern of the both CdS and Aluminium doped CdS are polycrystalline in nature having a cubic crystal structure of visualize an intense peak oriented along the (111) plane and grain size found to be in the order of nanometer which is confirmed with SEM results.

REFERENCES

[1] S.M. Edlou, A.Smajkiewicz and G.A. Al- Jumaily, "Optical Properties and Environmental Stability of Oxide Coatings Deposited by Reactive Sputtering", Applied Optics, Vol.32, 1993, pp.5601.

[2] O.V. Salata, P.J. Dobson and S.Sabesan "Preparation of Cds Films Suitable for Opto-electronic Device Applications", Thin Solid Films, Vol.28, 1996, pp.235.

[3] H.Derin and K.Kantarli, "Structural and Optical Characterization of Thermally Evaporated CdS Thin

Films", Surface and Interface Analysis, Vol.41, 2008, pp.61.

[4] P. S.Patil, "Versatility of Chemical Spray Pyrolysis Technique," Material Chemistry Physics, Vol.59, 1999, pp.185.

[5] R.Thiyagarajan, M. Mahaboo Beevi and M.Anusuya, "Preparation and Characterization of Aluminium Doped Zirconium Sulphide Thin films", The Pacific Journal of Science and Technology, Vol.10, No.1, May 2009 (Spring).

[6] J.S.Bhat and K.I.Maddani, " Influence of Zn Doping on Electrical and Optical Properties of Multilayered Tin Oxide Thin Films" Bulletin Materials Science, Vol.29, No.3, 2006, pp.331.

[7] Udaya S.Ketipearachchi, David W.Lane, Keith D.Rorgers, Jonathan D.Painter and Michael A. Cousins, "Bath pH Dependence on the Structural and Optical Properties of Chemical Bath Deposited CdS Thin Films" Materials Research Society.

[8] N.B.Chauve, S.Borads, A.P.Samantilleke, S.N.Chaure, J.Haigh and M.Dharmadas, "Investigation of Electronic Quality of Chemical Bath Deposited Cadmium Sulphide Layers Used in Thin Film Photovoltaic Solar Cells", Thin Solid Films, 2003, Vol.43, No.1-2, pp.10-17

[9] Palash K Bashu, E.Bontempi, S.Maji, H.Saha and Sukumar Basu, "Variation of Band Gap in Anoidcally Grown Nanocrystalline Zno Thin Films at Room Temperature-effect of Electrolyte Concentrations", Journal of Materials Science:Materials in Electronics, Feb 2009.

[10] Figen Kadirgan, Duli Mao, Wenjie Song, Tim Ohno and Brian McCandless, "Properties of Electrodeposited Cadmium Sulphide Films for Photovoltaic Devices with Comparison to CdS Films Prepared by Other Methods", Turkey Journal of Chemistry, Vol.24, 2000, pp.21-33.

[11] H.Moualkia, S.Hariech and M.S.Aida, "Structural and Properties of CdS Thin Films Grown by Chemical Bath Deposition", Thin Solid Films, Article in press, May 2009

[12] P.P.Hankare, P.A.Chafe and D.J.Sathe, "CdS Thin Film: Synthesis and Characterization", Solid State Sciences, Vol.11, No.7, 2009, pp.1226-1228.

COST COMPARISON OF TWO TYPES OF HYPERBOLIC PARABOLOID SHELL ROOFS

N. Arunachalam and V. Preetha
Department of Civil Engineering, Bannari Amman Institute of Technology, Sathyamangalam-638 401, Erode District, Tamil Nadu
Email: drnarunachalam@yahoo.co.in, preethacivil@yahoo.co.in
(Received on 27 December 2008 and accepted on 03 March 2009)

Abstract

In order to study the relative cost involved to cover a given area by doubly curved shells, the following two types of doubly curved shell roofs are analyzed, designed and the costs of construction to cover unit floor area have been estimated. 1. Inverted umbrella type of hyperbolic paraboloid shell roof, 2. Hipped type of hyperbolic paraboloid shell roof. The sizes of the areas to be covered by the shell roofs selected in this investigation are 20m x 20m to 40m x 40m. All the designs have been carried out by incorporating the recommendations of I.S 2210 – 1988 code and I.S 456 -2000 code. Computer Programmes in "C" language have been developed and used for the analysis and design of both the types of shell roofs. The cost of roof to cover unit area has been estimated in all the cases and compared.

Keywords: *Gaussian curvature, Hyperbolic Paraboloid, Inverted umbrella*

1. INTRODUCTION

Shells or skin space roofs are preferable to plane roofs since they can be used to cover large floor spaces with economical use of materials of construction. The use of curved space roofs requires 25 to 40% less materials than that of the plane elements. Structurally the shell roofs are superior since the whole cross section is uniformly stressed due to direct forces with negligible bending effects. Due to this aspect the thickness is usually very small in the range of 75mm to 150mm.

Hyperbolic Paraboloid, generally known as hypar shell is a doubly curved anticlastic shell of translation. Hypar shell is widely used for variety of structures like exhibition halls, swimming pools, cycle stands in modern monumental and industrial architecture. The main advantages of hypar shell are

- Its surface can be generated by two systems of straight lines so that the formwork is provided by straight boards, warped only slightly over their length.
- It can be used for roofs as well as foundation where the safe bearing capacity of the soil is very low.

2. CHARACTERISTICS OF HYPERBOLIC PARABOLOID SURFACE

- It is a Doubly Curved Surface.
- It is an anticlastic surface, so non-developable.
- It is a ruled surface.
- It's surface equation is hyperbolic type.
- It's Gaussian curvature is negative.
- It can not be described as a surface of revolution.

3. OBJECTIVE OF THE INVESTIGATION

The main objective of this investigation is to know the relative cost involved in the above two types of hyperbolic Paraboloid shell roofs.

4. SCOPE OF THIS INVESTIGATION

The sizes of the areas to be covered by the shell roofs selected in this investigation are 20m x 20m to 40m x 40m. The provision of IS: 2210-1988 (Criteria for design of reinforced concrete shell structures and folded plates) and IS 456-2000 (Code of practice for plain and reinforced concrete) are made use of wherever required. Concrete of grade M20 and Steel of grade Fe 415 are used throughout the investigation.

5. METHODOLOGY

Analysis and design of hyperbolic paraboloid shells to cover various areas have been carried out with the help of software developed using C-Programming language. The cost of roof to cover unit area has been estimated in all the cases and compared.

6. GEOMETRY OF HYPAR SHELL

The generation of hypar shell surface is shown in Figure 1. Consider a plane rectangle OXBY. If B is now elevated by an amount BB'=h, the warped surface OXB'Y is an hyperbolic paraboloid. Each pair of opposite sides are divided into equal parts and the corresponding points joined by straight lines to obtain the hypar surface. The surface between X and Y is parabolic (Convex parabola) and is well suited to resist compressive forces similar to that of arch elements. The surface between O and B' is an inverted parabola (Concave parabola or catenary) and is well suited to take tensile forces much similar to that of a catenary.

The hypar surface combining these shapes has a great stiffness and resistance to buckling and except for secondary bending effects ,normal applied loads are carried by membrane or direct forces within the thickness of shell. The shear forces within the shell gather along the four edges transferring the applied loads to the positions where support is provided.

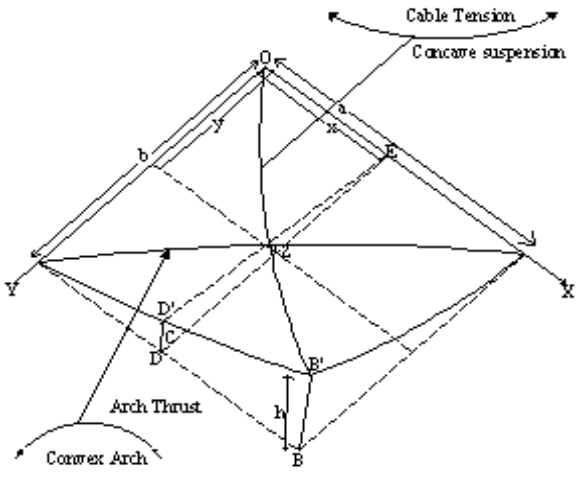

Fig.1 Geometry of hypar shell

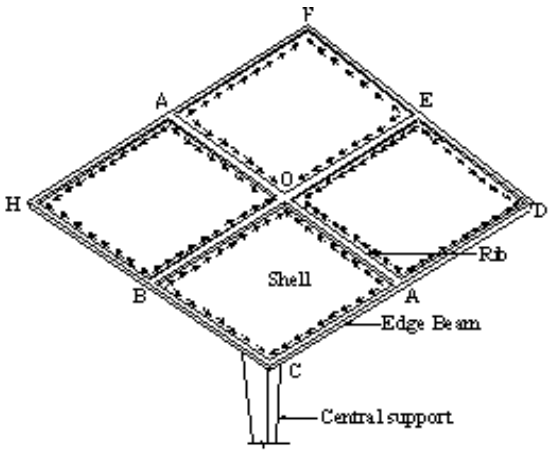

Fig. 2 Inverted umbrella type of hyperbolic paraboloid shell roof

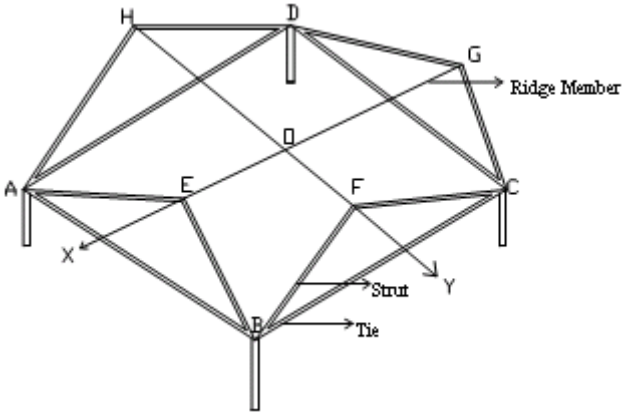

Fig.3 Hipped type of hyperbolic paraboloid shell roof

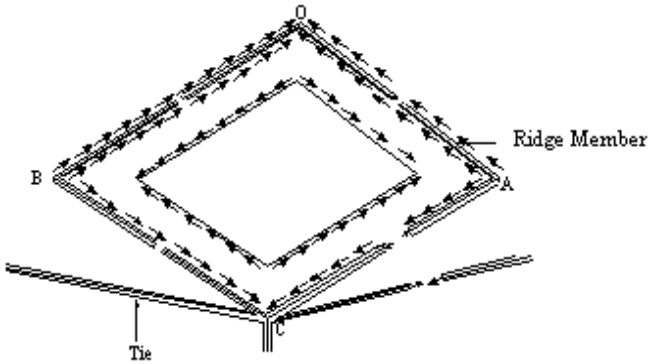

Fig.4 Direction of forces in a shell

7. COST COMPARISON OF TWO TYPES OF HYPERBOLIC PARABOLOID SHELL ROOFS

For the purpose of cost comparison, the rates are adopted as per the prevailing ones at Sathyamangalam are given below:

Rate of concrete : Rs.4500 per m^3
Rate of steel : Rs.35 per kgf

The effect of cost of two types of hyperbolic paraboloid shell roofs are studied through Figure 5 to 7. It may be noted that, as area to be covered increases, cost also increases. From Table.1 Total Cost (Rs)/Sqm covered for two types of shells has been studied.the design of all the shells has been made as per the first reference book.

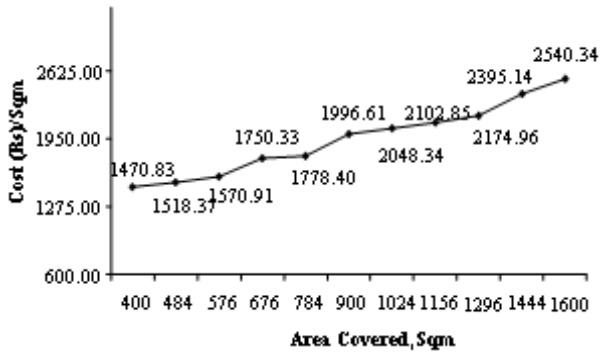

Fig.5 Variation of cost for inverted umberella type shell roof

Table 1 Total Cost (Rs) / Sqm Covered for Two Types of Hyperbolic Paraboloid Shell Roof

Area (Sqm)	Total Cost (Rs)/Sqm	
	Inverted Umbrella Type	Hipped Hypar Type
400	1470.83	1805.11
484	1518.37	1943.76
576	1570.91	2008.51
676	1750.33	2207.14
784	1778.40	2265.20
900	1996.61	2396.18
1024	2048.34	2523.17
1156	2102.85	2590.35
1296	2174.96	2844.71
1444	2395.14	2919.69
1600	2540.34	3102.93

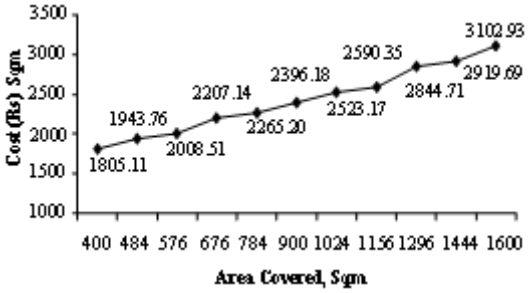

Fig.6 Variation of cost for hipped hypar type

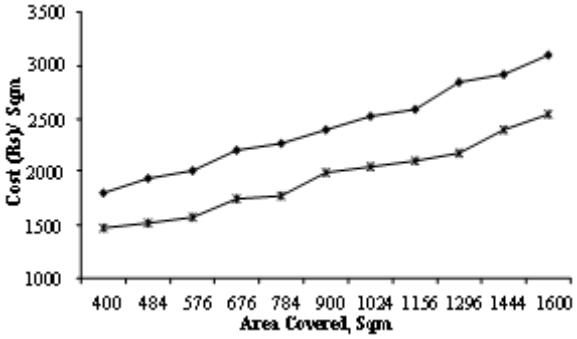

Fig.7 Cost comparision of two types of hyperbolic paraboloid shells

8. CONCLUSION

To cover a given area, as the area increases cost per unit area also increases. From Fig: 7, it is observed that by comparing the two types of shell roofs to cover a given area, cost will be lower when inverted umbrella type shell is used. Cost of hipped hypar shell roofs is nearly 20 percent higher than that required for inverted umbrella type shell roofs.

REFERENCES

[1] N. Krishnaraju," Advanced Reinforced Concrete Structures", CBS Publishers and Distributors, 1986.
[2] G. S. Ramasamy "Design and Construction of Concrete Shell Roofs", CBS Publishers & Distributors, (First Edition) 1986.
[3] I.S 2210 – 1988 Criteria for Design of Reinforced Concrete Shell Structures and Folded Plates (First Revision).
[4] I.S 456 -2000, "Plain and Reinforced Concrete", Code of Practice (Fourth Revision).

Indian Journal of Engineering, Science, and Technology (IJEST)

(ISSN: 0973-6255)
(A half-yearly refereed research journal)

Information for Authors

1. All papers should be addressed to The Editor-in-Chief, Indian Journal of Engineering, Science, and Technology (IJEST), Bannari Amman Institute of Technology, Sathyamangalam - 638 401, Erode District, Tamil Nadu, India.
2. Two copies of manuscript along with soft copy are to be sent.
3. A CD-ROM containing the text, figures and tables should separately be sent along with the hard copies.
4. Submission of a manuscript implies that : (i) The work described has not been published before; (ii) It is not under consideration for publication elsewhere.
5. Manuscript will be reviewed by experts in the corresponding research area, and their recommendations will be communicated to the authors.

Guidelines for submission

Manuscript Formats

The manuscript should be about 8 pages in length, typed in double space with Times New Roman font, size 12, Double column on A4 size paper with one inch margin on all sides and should include 75-200 words abstract, 5-10 relevant key words, and a short (50-100 words) biography statement. The pages should be consecutively numbered, starting with the title page and through the text, references, tables, figure and legends. The title should be brief, specific and amenable to indexing. The article should include an abstract, introduction, body of paper containing headings, sub-headings, illustrations and conclusions.

References

A numbered list of references must be provided at the end of the paper. The list should be arranged in the order of citation in text, not in alphabetical order. List only one reference per reference number. Each reference number should be enclosed by square brackets.

In text, citations of references may be given simply as "[1]". Similarly, it is not necessary to mention the authors of a reference unless the mention is relevant to the text.

Example

[1] M.Demic, "Optimization of Characteristics of the Elasto-Damping Elements of Cars from the Aspect of Comfort and Handling", International Journal of Vehicle Design, Vol.13, No.1, 1992, pp. 29-46.

[2] S.A.Austin, "The Vibration Damping Effect of an Electro-Rheological Fluid", ASME Journal of Vibration and Acoustics, Vol.115, No.1, 1993, pp. 136-140.

SUBSCRIPTION

The annual subscription for IJEST is Rs.600/- which includes postal charges. To subscribe for IJEST a Demand Draft may be sent in favour of IJEST, payable at Sathyamangalam and addressed to IJEST. Subscription order form can be downloaded from the following link http:// www.bitsathy.ac.in./ ijest.html.

For subscription / further details please contact:

IJEST
Bannari Amman Institute of Technology
Sathyamangalam - 638 401, Erode District, Tamil Nadu Ph: 04295 - 221289
Fax: 04295 - 223775 E-mail: ijest@bitsathy.ac.in Web:www.bitsathy.ac.in/ijest.html

Published by

BANNARI AMMAN INSTITUTE OF TECHNOLOGY
Sathyamangalam - 638 401 Erode District Tamil Nadu India
Ph: 04295-221289 Fax: 04295-223775
www.bitsathy.ac.in E-mail: ijest@bitsathy.ac.in

BANNARI AMMAN INSTITUTE OF TECHNOLOGY
Stay Ahead

TÜV CERT EN ISO 9001 Certificate : 3410021309
RWTÜV